Observation Based Budget and Lifetime of Excess Atmospheric Carbon Dioxide

Stephen E. Schwartz

Environmental and Climate Sciences Department, Brookhaven National Laboratory, P. O. Box 5000, Upton NY 11973 USA

5 *Correspondence to*: Stephen E. Schwartz (ses@bnl.gov)

Abstract, The global budgets of CO_2 and of excess CO_2 (*i.e.*, above preindustrial) in the biogeosphere are examined by a top-down, observationally constrained approach. Global stocks in the atmosphere, mixed-layer and deep ocean, and labile and obdurate terrestrial biosphere, and fluxes between them are quantified; total uptake of carbon by the terrestrial biosphere is constrained by observations, but apportionment to the two terrestrial compartments is only weakly constrained, requiring

10 examination of sensitivity to this apportionment. Because of near equilibrium between the atmosphere and the mixed-layer ocean and near steady state between the atmosphere and the labile biosphere, these three compartments are tightly coupled. For best-estimate present-day anthropogenic emissions the turnover time of excess carbon in these compartments to the deep ocean and obdurate biosphere is 67 to 158 years. Atmospheric CO_2 over the Anthropocene is accurately represented by a five-compartment model with four independent parameters: two universal geophysical quantities and two, specific to CO_2,

15 treated as variable. The model also accurately represents atmospheric radiocarbon, particularly the large increase due to atmospheric testing of nuclear weapons and the subsequent decrease. The adjustment time of excess atmospheric CO_2, evaluated from the rate of decrease following abrupt cessation of emissions, is 78 to 140 years, consistent with the turnover time, approaching a long-time floor of 15-20 % of the value at the time of cessation. The lifetime of excess CO_2 found here, several-fold shorter than estimates from current carbon-cycle models, indicates that cessation of anthropogenic emissions

20 atmospheric would result in substantial recovery of CO_2 toward its preindustrial value in less than a century.

Short Summary

Carbon dioxide is central to anthropogenic climate change, but the response of CO_2 to potential reductions in emissions is quite uncertain. Current model estimates of the lifetime of excess atmospheric CO_2 above preindustrial range from about 150 years to upwards of 500 years. Based on a global budget and a compartment model this lifetime is constrained here to

25 110 ± 30 years. These results demonstrate that reduction of CO_2 emissions could yield tangible results within a human lifespan.

1 Introduction

About 250 years ago humankind initiated what has been characterized (Ramanathan, 1988) as an inadvertent global experiment to change Earth's climate by emitting carbon dioxide, CO_2, into the atmosphere in conjunction with combustion

30 of fossil fuels, mainly for energy, other industrial activities, and changes in land use. Anthropogenic CO_2, the amount in excess of preindustrial (PI), affects Earth's radiation budget, with present radiative forcing relative to preindustrial about 2 W m^{-2}, and acidifies the ocean, with the present decrease in pH of the surface ocean relative to preindustrial about 0.14. The present paper examines the extent to which and the rate with which that experiment might be reversed by cessation of anthropogenic emissions of CO_2. Despite the central importance of anthropogenic CO_2, the response of atmospheric CO_2 to

35 potential reductions in emissions is quite uncertain. Here as an example attention is called to Figure 4.39 of the Sixth Assessment Report (AR6) of the Intergovernmental Panel on Climate Change (IPCC), which shows considerable variation in the rate and extent of atmospheric CO_2 mixing ratio over the initial 100 years following abrupt cessation of emissions, specifically a factor of 2 range in the decrease of mixing ratio (Lee et al., 2021).

In principal a single measure of the rate of response of atmospheric CO_2 to change in emissions is the lifetime of excess

40 atmospheric CO_2. However present estimates of this lifetime vary enormously, from a few years to a few tens of years to tens of thousands of years. In part this range is due to differing definitions and ways of evaluating this lifetime, However even if a suitable definition of lifetime is agreed to, the spread is quite large in recent assessments of the budget of CO_2 in the coupled active compartments that control this budget – the atmosphere, the ocean, and the terrestrial biosphere. Here this budget is re-examined, as constrained by observations, and a simple, transparent model is developed to describe the stocks of

45 carbon in the several active compartments and the fluxes between these compartments, the parameters of which are likewise constrained by observation. The guiding principle here is to minimize the number of parameters, the better to constrain them. A key objective of this examination is to determine observationally constrained bounds on the lifetime of excess CO_2.

Recent estimates of the rate at which excess atmospheric CO_2 would decrease in response to hypothetical abrupt cessation of emissions range over more than an order of magnitude. **Figure 1a** compares the fraction $f(t)$ of excess CO_2 that would

50 remain in the atmosphere as a function of time t subsequent to such a hypothetical cessation of emissions, as determined by several carbon-cycle (CC) and compartment models. Although this set of curves is an ensemble of opportunity assembled from studies which calculated atmospheric CO_2 after abrupt cessation of emissions or which provided impulse response functions permitting such calculation, at varying conditions such as CO_2 amount at the time of cessation x_{CO2}^0, the bulk of the spread of the curves results from differing treatments of the processes governing CO_2 decay. The spread of x_{CO2}^0 was

55 greatly reduced, to 508–571 ppm, in the intercomparison of decrease of CO_2 mixing ratio following abrupt cessation as calculated by current Earth system models that incorporate CC models (Zero Emissions Commitment Model Intercomparison Project, ZECMIP; MacDougall et al., 2020). However, even with that rather narrow range in x_{CO2}^0, there is

still substantial spread in the decay curves following abrupt cessation, **Fig. 1c**, indicative of differing treatment of the processes governing decrease of atmospheric CO_2 in the different models. The instantaneous adjustment time, the inverse of the fractional rate at which excess CO_2 would decrease in the absence of anthropogenic emissions, ranges from 70–100 years to more than 700 years, as can be inferred from comparison of the slopes of the several curves with those of the dotted black lines, a straight line on the semi-logarithmic plot denoting a constant adjustment time (exponential decay with indicated time constant). The wide range in the corresponding adjustment time characterizing the decay of excess CO_2 over the time horizon t subsequent to cessation (equivalent $1/e$ lifetime $\tau_E(t) = -t / \ln f(t)$, **Sect. 2**, is explicitly displayed in **Fig. 1**.

The 12 models that participated in the abrupt cessation intercomparison described by Zickfeld et al. (2013; Figure 6, RCP 6) showed decrease of excess CO_2 by only 7 to 14 % (multimodel mean 10 %) with $\tau_E(100 \text{ yr})$ of the multimodel mean equal to 920 years. At the other extreme, prior observationally based, top-down assessments of the lifetime of excess atmospheric CO_2 (Moore and Braswell, 1994; O'Neill et al., 1994, 1997; Jacobson, 2005) have yielded values as low as about 30 to 60 years, but that approach has been strenuously criticized (Tans, 1997; Archer et al, 2009; Joos et al., 2013b). A simple model employed by Allen et al. (2009) shown at the top of **Fig. 1a** shows essentially no decrease of CO_2 in the first century following cessation. Hybrid observational-model studies (Gloor et al., 2010, Raupach, 2013; Raupach *et al.*, 2014) have yielded lifetimes of 40 to 200 years. It is this situation of enormous variation in estimates of the rate of decrease of excess atmospheric CO_2 following abrupt cessation of emissions that has motivated the present study.

Also shown, by the thicker dashed curve in **Fig. 1a**, is the decay curve obtained for the mean of multiple models participating in the model intercomparison of Joos et al. (2013) widely used for projecting the consequences of prospective reduction of CO_2 emissions. A more rapid decay would imply a greater response of atmospheric CO_2 to such reductions in emissions, highlighting the importance of knowledge of such decay for policy purposes. The multi-model mean of Joos et al. is also widely used in calculation of so-called global warming potentials (GWPs) of non-CO_2 greenhouse gases that permits comparison of their integrated forcings with that of CO_2; an increased decay rate of atmospheric CO_2 would result in an increase in the GWPs of other greenhouse gases, further highlighting the importance of accurate knowledge of the lifetime of atmospheric CO_2 for policy purposes.

The hundred-year time frame that is the focus of this study assumes great importance in anticipating responses of Earth's climate system to prospective reductions in anthropogenic CO_2 emissions. The time scale of response of global mean surface temperature to change in forcing is rapid, five to 10 years, as established by multiple energy-balance models and GCM calculations (Schneider and Thompson, 1981; Brasseur and Roeckner, 2005; Gregory, 2000; Schwartz, 2008; Held et al., 2010; Boucher et al., 2012, Geoffroy et al., 2013); hence it is the time scale of response of excess atmospheric CO_2 to changes in emissions that governs the overall time scale of climate response to such changes.

The objectives of this study are 1) to provide a top-down budget, constrained by observations, chemical equilibria, and the requirement of preindustrial steady state, for CO_2 in the atmosphere and the coupled ocean and biosphere compartments, for

90   preindustrial and present conditions, the anthropogenic perturbation obtained by difference; 2) to use this budget to infer the turnover time pertinent to excess atmospheric CO_2; 3) to use this budget to construct a simple, transparent global-scale numerical model for atmospheric CO_2 and carbon in compartments that are coupled to the atmosphere, and 4) to use this model to determine the adjustment time and other measures of the lifetime of excess atmospheric CO_2 on the time scale over which, in the absence of anthropogenic emissions, CO_2 would be expected to recover substantially toward its preindustrial

95   value. Like any model, the model developed here might appropriately be viewed as a hypothesis that is to be tested against observations.

The approach of this study is to develop a parsimonious yet accurate picture of the global CO_2 budget based on observations of present and preindustrial atmospheric CO_2 and its present annual increase, well established solubility properties of CO_2 in ocean water, and independently determined coefficients describing the rates of material transfer between the several

100   compartments, together with emissions determined by inventories. This picture is used to provide values of the parameters needed to represent this budget in a simple transparent model that apportions anthropogenic carbon into the atmosphere (atmospheric compartment, AC) and compartments that are coupled to the atmosphere on time scales up to several centuries: two ocean compartments, the mixed layer ocean (ML), the deep ocean (DO); and two terrestrial biosphere (TB) compartments, a labile biosphere (LB) that is closely coupled to the atmosphere by photosynthesis and respiration, and an

105   obdurate biosphere (OB) that exhibits a turnover time of multiple centuries; TB refers to the sum of LB and OB. While the ML and DO compartments can be rather confidently distinguished on physical grounds, the same cannot be said for demarcation between the biosphere compartments LB and OB, and indeed apportionment of the uptake of anthropogenic CO_2 by the TB into even so few as two compartments is underconstrained by observations. For this reason this apportionment is examined by varying two unconstrained parameters that govern the amount of uptake of carbon by the

110   labile biosphere, specifically, the amount of carbon in the preindustrial labile biosphere and a fertilization exponent characterizing the dependence of global primary production (GPP) on the amount of atmospheric CO_2. The model is exercised over a range of these parameters to calculate the time evolution of atmospheric CO_2 over the Anthropocene and of atmospheric and oceanic radiocarbon (^{14}C) response to emissions due mainly to weapons testing in the late 1950's and early 1960's. Comparison of model results with observations considerably limits the domain of the unconstrained parameters,

115   thereby providing a rather narrow range of parameter values and lifetime consistent with observations. This model so developed was used to calculate the decay profiles of excess CO_2 subsequent to abrupt cessation of emissions shown in **Fig. 1**, which bound the range consistent with observations, and other measures of the lifetime of excess CO_2 presented here.

This paper is organized as follows. **Section 2** presents expressions for multiple measures of the lifetime of excess CO_2 that are evaluated using the budget and model that are developed later in the paper. **Section 3** summarizes the budgets of preindustrial and anthropogenic CO_2 presented in detail in **Appendix A** and compares to recent IPCC assessments. **Section 4** identifies and quantifies the transfer coefficients that characterize the rates of transport of CO_2 between the several compartments of the biogeosphere pertinent to evolution of excess CO_2 on the centennial time scale. **Section 5** identifies the several characteristic times pertinent to CO_2 in the biogeosphere and quantifies these based on the budget. The transfer coefficients are inputs to a simple, transparent model described in **Section 6**. In **Section 7** the model is exercised for historical emissions over the Anthropocene and for hypothetical abrupt cessation commencing in 2017 and for radiocarbon over the Anthropocene, with focus on the period surrounding peak emissions from atmospheric weapons testing. That section also compares results of the model runs for historical emissions to measurements and to CC model results. **Section 8** discusses the present results and compares to previous studies. **Section 9** presents conclusions and some implications of the present findings.

In view of the large difference in the rate of decrease of atmospheric CO_2 following abrupt cessation found with the model developed here and results from current CC models, and in view also of the societal importance of the response of atmospheric CO2 to prospective changes in emissions, the intent here is to fully describe the approach, the data, and the findings, all of which are presented in six Appendices, seven sections of Supporting Information text, and one Excel Workbook consisting of six Data Tables. The appendices are as follows:

Appendix A: Budget of CO_2 in the biogeosphere.

Appendix B. Rate of transfer of CO_2 between the atmosphere and the ocean mixed layer.

Appendix C. Dependence of gross primary production on CO_2 mixing ratio.

Appendix D. Equilibrium–steady-state (ESS) model.

Appendix E. Application to anthropogenic radiocarbon.

Appendix F. Arguments against determination of the lifetime of excess CO_2 by top-down observations, and rebuttals

Supporting Information text consists of the following sections:

S1. Abrupt cessation profiles shown in **Fig. 1**.

S2. Relating stocks and concentrations.

S3. Equilibrium solubility of incremental CO_2 in ocean surface water.

S4. Anthropogenic emissions of CO_2.

S5. Annual increment in atmospheric stock.

S6. Dependence of adjustment time on functional form of CO_2 emission rate.

S7. Numerical modeling.

Notation. S_i denotes stock of CO_2, of dissolved inorganic carbon DIC, or of organic carbon, as mass of carbon, C (not CO_2)

150 in Pg (10^{15} g), in a given compartment i denoted by subscripts a, m, d, l, o, for the AC, ML, DO, LB, and OB, respectively, or in two or more compartments, e.g., S_{am} for the sum of $S_a + S_m$. ΔS_i, in Pg yr^{-1}, denotes the present annual increment in S_i. F_{ij}, in Pg yr^{-1}, denotes gross flux from compartment i to compartment j; $F_{ij,net}$ denotes net flux from compartment i to j and is equal to $F_{ij} - F_{ji}$. Radiocarbon stocks and fluxes are denoted R_i and G_i, respectively, with units atoms and atoms per year, respectively. The term "ordinary carbon" is used where necessary to distinguish total carbon from radiocarbon.

155 Transfer coefficients k_{ij}, yr^{-1}, denote flux F_{ij} per stock of leaving compartment S_i; k_{ij}^* is used for radiocarbon where different from k_{ij}. Q_{ant}, in Pg yr^{-1}, denotes anthropogenic emission rate; Ω_{ant}, in Pg, denotes total integrated anthropogenic emission (1750 to 2016) or as a function of time over the Anthropocene $\Omega_{ant}(t)$; similarly Q_R and Ω_R for radiocarbon. The subscripts ff and lu denote emissions from fossil fuel combustion and other industrial activities, and from land use changes, respectively; the subscript pc denotes the gravitational flux of particulate carbon from the ML to the DO. Subscripts or

160 superscripts pi, pd, and ant denote, respectively, the preindustrial, present-day, and anthropogenic component of a stock or flux. Superscripts to and adj denote turnover time and adjustment time, respectively.

2. Alternative measures of lifetime

Much attention has been paid, in the environmental literature and more broadly in societal considerations, to a quantity that is qualitatively denoted the "lifetime" of a substance, a quantity that characterizes the duration of persistence of that

165 substance subsequent to its introduction into a reservoir. However there is much difficulty in precisely defining such a lifetime, especially for substances that exchange among multiple compartments, as is the case with CO_2. Numerous investigators have introduced a variety of terminologies that are not consistent, as discussed, perhaps most recently, by Sierra et al. (2017). This situation necessitates careful attention to definition of suitable quantities to characterize the lifetime of excess CO_2. This section examines alternative measures of lifetime with specific reference to excess atmospheric CO_2 and

170 presents explicit definitions of quantities that may be evaluated based directly on observations or from model output.

As stressed by Archer et al., (2009), "There are rival definitions of a lifetime for anthropogenic CO_2." Archer et al. continue:

One is the average amount of time that individual carbon atoms spend in the atmosphere before they are removed, by uptake into the ocean or the terrestrial biosphere. Another is the amount of time it [would take] until the CO_2 concentration in the air recovers substantially toward its original concentration [in the absence of anthropogenic

175 emissions]. The difference between the two definitions is that exchange of carbon between the atmosphere and other reservoirs affects the first definition, by removing specific CO_2 molecules, but not the second because exchange does not result in net CO_2 drawdown. The misinterpretation that has plagued the question of the atmospheric lifetime of CO_2 seems to arise from confusion of these two very different definitions.

This situation led Archer et al. (2009) to observe that the rival definitions of the lifetime of anthropogenic CO_2 could lead to estimates as short as a few years (the average amount of time that individual carbon atoms spend in the atmosphere before they are removed, by uptake into the ocean or the terrestrial biosphere) or as great as tens of thousands of years (mean lifetime of the elevated CO_2 concentration of the atmosphere resulting from fossil fuel combustion). As Archer et al. (2009) make clear, the rate of exchange of individual molecules characterized by the opposing and essentially equal fluxes between the atmosphere and the terrestrial biosphere and between the atmosphere and the mixed-layer ocean results in no net drawdown, and hence the first definition (average time that individual CO_2 molecules spend in the atmosphere until they are first removed), about 3 years, **Sect. 5.1**, must be rejected as a measure of the lifetime of excess atmospheric CO_2. To this it should be added that processes taking place over millennia after atmospheric CO_2 has substantially recovered to its preindustrial value are of little consequence to the response of atmospheric CO_2 to emissions reductions on the time scale over which that substantial recovery occurs, which is the time scale that is of great societal interest and is the focus of this study.

Broadly speaking, the lifetime of a constituent in a reservoir can be characterized by two distinct classes of quantities. The first, is denoted *turnover time*, where the turnover time of a substance in a reservoir is *the quotient of the stock in the reservoir upon the net or gross leaving flux*,

$$\tau_i^{\text{to}} = \frac{S_i}{\sum_{j \neq \text{a}} F_{ij}} \,. \tag{2.1}$$

For substances that exit a compartment irreversibly, then the receiving compartment is usefully considered a sink, and the turnover time so determined serves as an accurate measure of the lifetime of the substance in the compartment (e.g., Bolin and Rodhe, 1973; Schwartz, 1979; O'Neill et al., 1994, 1997; Planton, 2013). However a definitional problem arises if the substance in question returns to the leaving compartment. If the return flux from the sink compartment is appreciable relative to the leaving flux, as is the case for atmospheric CO_2, then a turnover time so determined must be interpreted with caution. At the other extreme, if there is rapid exchange between the reservoir of interest and some other compartment or compartments, then the turnover time characterizing this rate of exchange is not a useful measure of the lifetime of interest. In this situation those tightly coupled compartments are usefully considered a single compartment, as the time constant(s) for establishing steady state among them are short compared to the overall lifetime of the substance of interest in the combined set of compartments against removal to long-term sink; this situation is particularly applicable to CO_2 which exhibits rapid exchange between the atmosphere and the ML and between the atmosphere and the labile terrestrial biosphere, as is examined in **Sect. 7.7** using results obtained with the model developed here. For a substance for which there is a natural source and a corresponding natural amount in the reservoir(s) of interest the turnover-time concept is readily extended to the perturbations in stock and exiting flux, and thus a turnover time may be defined for both the natural substance and for the

perturbation. If the system is linear, the turnover time pertinent to the perturbation is the same as that pertinent to the

210 unperturbed system. However, if the system is nonlinear, as is the case for CO_2 in the atmosphere and coupled reservoirs, these quantities would be expected to differ, perhaps substantially. All of these considerations of identification of what constitute the pertinent reservoirs and sink processes contribute to differences (some small, some quite large) in reported turnover times for atmospheric CO_2.

A second problem specific to CO_2 arises from the possible long tail of excess atmospheric CO_2 resulting from

215 anthropogenic emissions that might result in the average lifetime of excess CO_2 greatly exceeding the time required for excess CO_2 to decrease substantially relative to its value at the time of cessation of emissions. Indeed, if even a small fraction of excess CO_2 were to remain in the atmosphere indefinitely, this long tail would result in the average lifetime of excess CO_2 being infinite. This situation that has led some investigators, noting that anthropogenic CO_2 would never entirely leave the system until subsumed by long-term geological processes, would argue that the average lifetime is upwards

220 of tens of thousands of years (Archer, 2005; Archer et al., 2009), or that the lifetime concept simply does not apply to anthropogenic CO_2 (Tans, 1994). Alternatively, others, e.g., Moore and Braswell (1994), have avoided that problem by defining the adjustment time of excess CO_2 relative not to excess CO_2 above preindustrial but, rather, to the excess above the infinite-time value of this excess, which those investigators took to be a substantial fraction of the initial perturbation. Here the argument is made that the time scale of interest is that of substantial recovery of atmospheric CO_2 to its

225 preindustrial value, thereby avoiding the issue of the small long tail.

As developed in **Sect. 5**, and **Sect. 7.7**, based on the rapid exchange, with time scale of a few years, between the atmosphere, labile terrestrial biosphere, and mixed-layer ocean compartments, it is useful to define the reservoir for anthropogenic CO_2 pertinent to the turnover time as the sum of the stocks in the three compartments, with stock $S_{\text{alm}}^{\text{ant}} = S_{\text{a}}^{\text{ant}} + S_{\text{l}}^{\text{ant}} + S_{\text{m}}^{\text{ant}}$, and with leaving flux the sum of the net anthropogenic fluxes into the obdurate biosphere and the deep ocean, $F_{\text{ao,net}}^{\text{ant}} + F_{\text{md,net}}^{\text{ant}}$,

230 yielding turnover time

$$\tau_{\text{alm}}^{\text{to}}(t) = \frac{S_{\text{alm}}^{\text{ant}}(t)}{F_{\text{ao,net}}^{\text{ant}}(t) + F_{\text{md,net}}^{\text{ant}}(t)} , \tag{2.2}$$

where the stocks and fluxes can be determined either from observations, **Sect. 3**, and **Sect. 5**, or from model calculations, **Sect. 7.6**. In **Eq 2.2** the turnover time is explicitly denoted as a function of time, as the pertinent quantities on the RHS can vary with time. These quantities can be evaluated, from observations at present, as in **Sect. 4**, and at prior times. Importantly,

235 turnover times so evaluated can be compared with time constants for establishing steady state between compartments that are treated as a single compartment, specifically, between the AC and the ML and between the AC and the LB, to assess treating them as a single compartment, **Sect. 5.3 and Sect. 5.7**.

A second class of lifetimes is denoted *adjustment times*, measures of the period of time over which the amount of the substance in the reservoir(s) of interest, or of the amount in excess above the natural amount, would decrease subsequent to

240 cessation of the source of the substance, or of the perturbation in the source. In contrast to turnover times, which can be determined from observed stocks and flows, determining adjustment times requires a numerical model that describes future behavior of the system in response to the putative change in emissions. One measure of the adjustment time would thus characterize the fractional rate of decrease of excess CO_2 following cessation of emissions shown in **Fig. 1**. As for turnover times, differences in definition can lead to differences in the value of the adjustment time, depending, on whether the it is

245 evaluated as a local, instantaneous quantity or over an extended time period and depending how averages or other measures of determining the quantity over an extended period are defined.

An unambiguous measure of the instantaneous adjustment time is given, for excess CO_2, as the quotient of the excess amount of the substance in a reservoir of interest upon the rate of removal of the substance from the reservoir in the absence of anthropogenic emissions, both a function of time t. For atmospheric CO_2 this adjustment time is

$$250 \quad \tau_{CO2}^{inst}(t) = \frac{S_a^{ant}(t)}{\left(-\dfrac{dS_a^{ant}}{dt}(t)\right)} = \frac{x_{CO2}^{ant}(t)}{\left(-\dfrac{dx_{CO2}^{ant}}{dt}(t)\right)} = \left(-\frac{d\ln x_{CO2}^{ant}}{dt}(t)\right)^{-1}, \qquad (2.3)$$

where the second equality simply follows from the stock S_a^{ant} being proportional to the mixing ratio x_{CO2}^{ant} and where the third equality shows that $\tau_{CO2}^{inst}(t)$ is equal (apart from a factor of ln 10) to the negative inverse of the slopes of the curves shown in **Fig. 1a**. The decrease in slopes of the several curves is indicative of an increase in $\tau_{CO2}^{inst}(t)$ over this period as calculated by the several models.

255 In recognition of the objective of characterizing the lifetime of excess atmospheric CO_2 over the time scale pertinent, in the absence of anthropogenic emissions, to substantial recovery toward the unperturbed state, O'Neill et al. (1997) defined what they denoted a "past commitment lifetime" which examines the question "if emissions were significantly reduced or stopped, how long would it take for the world to return to 'normal'?". Similarly, as noted above, Archer et al. (2009) proposed defining the lifetime of CO_2 as the time it would take in the absence of anthropogenic emissions "until the CO_2

260 concentration in the air recover[ed] substantially toward its original concentration." This objective of characterizing the time scale of such substantial recovery prompts the careful examination here of such measures of adjustment time pertinent to the time periods over which this recovery would occur.

A first such measure of adjustment time would be a simple time-average of the instantaneous adjustment time over period of time T, often denoted time horizon, subsequent to the time of cessation of anthropogenic emissions T_c,

265 $$\tau_{\text{CO2}}^{\text{t-avg}}(T) = \frac{\int_{T_c}^{T_c+T} \tau_{\text{CO2}}^{\text{inst}}(t)dt}{\int_{T_c}^{T_c+T} dt} = \frac{1}{T} \int_{T_c}^{T_c+T} \tau_{\text{CO2}}^{\text{inst}}(t)dt$$ (2.4)

A concern with this quantity is that it equally weights values of $\tau_{\text{CO2}}^{\text{inst}}(t)$, at short times when the amount of excess CO_2 is large and at long times when the amount of excess CO_2 is small. If $\tau_{\text{CO2}}^{\text{inst}}(t)$ is increasing over the averaging period T, that increase might unduly weight the integral at long time when the amount of remaining material is small, thereby leading to a lifetime that is longer, perhaps much longer, than that characterizing the bulk of the recovery to the unperturbed state.

270 A measure of the adjustment time that overcomes that concern is the amount-remaining–weighted average adjustment time, defined similarly to the time-average adjustment time but with the weighting factor $x_{\text{CO2}}^{\text{ant}}$,

$$\tau_{\text{CO2}}^{\text{a-avg}}(T) = \frac{\int_{T_c}^{T_c+T} x_{\text{CO2}}^{\text{ant}}(t)\tau_{\text{CO2}}^{\text{inst}}(t)dt}{\int_{T_c}^{T_c+T} x_{\text{CO2}}^{\text{ant}}(t)dt} \, .$$ (2.5)

This amount-weighted adjustment time would be especially pertinent to examination of the integrated effect of an emitted substance, such as integrated radiative effect, pertinent to quantities such as the global warming potential (Shine et al., 1990).

275 A new measure of adjustment time, denoted the equivalent $1/e$ lifetime, that explicitly meets the objective of serving as a measure the time T over which the amount of excess CO_2 present at the time of cessation of emissions has decreased to a given fraction f of its initial value is defined as

$$\tau_E(f) = \frac{t(f)}{-\ln f}$$ (2.6a)

where the expression $\tau_E(f)$ explicitly notes that $\tau_E(f)$ may depend on the fraction remaining, f and generally does so 280 except for exponential decay. The relation between $\tau_E(f)$ and f may be considered a generalization of the relation between the time required for the fraction f of a radioactive substance to decrease to 0.5 of its initial value, that is, the half-life $t_{0.5}$ and the $1/e$ lifetime of that substance $\tau = t_{0.5}/(-\ln 0.5)$. The equivalent $1/e$ lifetime τ_E may alternatively be expressed as a function of time horizon T as

$$\tau_E(t) = \frac{t}{-\ln f(t)}$$ (2.6b)

285 and is thus readily compared to the several other measures of adjustment time as a function of t. The equivalent $1/e$ lifetime, is readily calculated directly from a calculated decay profile as a function of time horizon t. An advantage of τ_E is that determining this quantity does not require calculation of the time derivative of the decay curve, as is required for τ_{inst},

$\tau_{\text{t-avg}}$, or $\tau_{\text{a-avg}}$, commending its use as a measure of the adjustment time, as in **Fig. 1b**. As shown in **Sect. 7.6**, $\tau_{\text{t-avg}}$, $\tau_{\text{a-avg}}$, and τ_E (but not τ_{inst}) are nearly identical and thus τ_E serves as a representative measure of the time constant associated

290 with decrease of a substance over the entire time horizon from cessation to time t.

A widely used measure of the adjustment time is obtained by fitting an exponential decay function to the modeled anthropogenic stock over a specified time range subsequent to cessation of emissions by minimization of chi-squared. Here an important consideration is the baseline of the exponential decay. As the focus of the present study is on the time scale characterizing recovery of CO_2 to its preindustrial value, it would seem that the pertinent baseline is the preindustrial value

295 (*i.e.*, excess CO_2 decaying to zero), even if the modeled CO_2 never actually returns to its preindustrial value. Further considerations are the time period over which to do the fit and the weighting, although these would seem to be secondary. Here the time period is taken as 100 years and all annual points are equally weighted; the resultant lifetime being denoted here τ_{fit}. It should be noted that the fit to an exponential decay function does not require or imply that the data being fit conform to exponential decay; conformance to or departure from exponential decay is readily examined by comparison of

300 the fit to the model output, by examination of linearity in a semilogarithmic plot such as **Fig. 1a**, or by τ_E being constant, **Fig. 1b**.

The several turnover times and adjustment times for excess CO_2 are examined and compared in **Sect. 7.6**. The point here is not that one or the other of these measures is the most suitable, but rather that if these several measures of lifetime of excess CO_2 are suitably defined, they would all be expected to exhibit close agreement. Determination of such suitably defined

305 lifetime of excess CO_2 is a key objective of this study.

3. Budget of CO_2 in the biogeosphere

The analysis of the stocks and fluxes of CO_2 in the biogeosphere that serves as the basis of the present analysis of the CO_2 lifetime is based on the budget of CO_2 developed in detail in **Appendix A** and summarized here. This budget consists of the stocks of CO_2 in the several major compartments of the biogeosphere and the fluxes between these compartments for the

310 preindustrial (PI) state and for the present day (PD, taken as year 2016). The anthropogenic increments in the several stocks and fluxes are obtained by difference, PD minus PI. This budget is based on observations (present and PI values and present annual increment of atmospheric CO_2 mixing ratio, ML and DO stocks of dissolved CO_2, inventories of terrestrial biosphere stock, inventories of annual and cumulative emissions), on independently determined coefficients describing rates of transport between compartments (dry deposition velocity to seawater of insoluble to moderately soluble gases, piston

315 velocity describing the rate of volume exchange of water between the ML and the DO), on well understood physical-chemical properties of CO_2 (Henry's law solubility, acid dissociation equilibria), and on the requirement in the PI steady

state of zero net flux between compartments when summed over all paths. The budget developed here is shown in **Fig. 2** and summarized in **Table 1**. This figure is modified from previous versions given by Sarmiento and Gruber (2002; 2006, p. 393), the Fourth IPCC Assessment Report, AR4, (Denman et al., 2007, Figure 7.3) and the Fifth IPCC Assessment Report, AR5, (Ciais et al., 2013, Figure 6.1), with antecedents going back at least to the Third IPCC Assessment report, AR3, (Prentice et al., 2001, Figure 3.1). Following Sarmiento and Gruber (2002), **Figure 2** presents the PI budget in black, and the anthropogenic perturbation, here for year 2016, in red. The quantities shown in the figure are stocks in each of the several compartments S_i and gross (not net) fluxes F_{ij}, the annual changes in several of the compartments ΔS_i, in blue, and anthropogenic emissions Q_{ff} and Q_{lu}; Q_{lu}, denoted net land-use–change (LUC) emission, represents the net annual carbon flux from the TB into the atmosphere from deforestation, *i.e.*, the flux from deforestation minus the flux from the atmosphere to the TB that is ascribed to afforestation.

Historically the several stock and flux quantities shown in **Fig. 2** have been given to a greater number of digits than the accuracy with which they are known to convey the magnitudes of these quantities with precision sufficient to show their differences. This longstanding practice is maintained here in **Fig. 2** and **Table 1**, even if the implied accuracy with which the quantities are known is overstated. The value for the PI stock of carbon in the TB, S_t^{pi}, is increased here from 2300 Pg and 2500 Pg in AR4 and AR5, respectively, to 2800^{+430}_{-280} Pg, based on a more recent inventory by Carvalhais et al., (2014; uncertainties converted to 1-sigma equivalent), but in actuality, the magnitude, which is dependent on what constitutes the terrestrial biosphere, as governed by a depth horizon, and what carbonaceous species to include, is of little significance in budget considerations other than to serve as a reference against which to compare the magnitudes of anthropogenic changes. Similarly, preindustrial gross primary production GPP, F_{al}^{pi}, and the equal and opposite gross respiration flux F_{la}^{pi}, given here as in other recent versions of this figure as 120 Pg yr^{-1}, are presented mainly to make the point that this large gross flux, which is not known to great accuracy (**Appendix C**), greatly exceeds the net fluxes that result from the anthropogenic perturbation.

Similar considerations apply to the magnitudes given for the fluxes between the atmosphere and the ML ocean, F_{am}^{pi} and F_{am}^{pi}. The values for these quantities given here and in previous assessments, 70 and 70.6 Pg yr^{-1}, respectively, which represent the total global dry deposition flux from the atmosphere to the ocean and the reverse flux from the ocean to the atmosphere, respectively, must be considered uncertain to 30 % (**Sect. 4.1;** Sarmiento and Gruber, 2006). However these magnitudes are not so important as their difference, which represents the net flux. The fact that the two fluxes are nearly equal and much greater than the net flux is indicative of near equilibrium between atmospheric CO_2 and total dissolved CO_2 (i.e., dissolved inorganic carbon DIC), with the magnitudes of the two fluxes serving to manifest this near equilibrium, to provide context for the magnitude of the anthropogenic perturbation, and to establish the time scale for equilibration of the two phases. Here it might also be noted that, small as it is, the net PI flux from the ocean to the atmosphere that compensates

the riverine flux from the TB to the ML, $F_{om}^{pi} = 0.6$ Pg yr^{-1}, assumes some importance in assessments of the CO_2 budget, as, among other reasons, it constitutes the difference between model-based estimates of the anthropogenic flux of CO_2 from the

350   atmosphere to the ocean and measurement-based estimates, which yield the total flux (*i.e.*, the sum of anthropogenic and natural), and that even the uncertainty in this preindustrial flux, perhaps 0.2 Pg yr^{-1}, assumes some significance in such comparisons (**Sect. 7.8**). Because of the continuing increase in atmospheric CO_2 over the Anthropocene there is an additional departure (lag) of S_m relative to its steady state value (as governed only by the riverine flux) due finite rate of mass transport between the two compartments; an expression for this lag developed in **Appendix A** permits calculation of

355   S_m^{ant} given in **Fig. 2**.

A major departure in **Fig. 2** from previous versions of this figure cited above is the subdivision of the TB into two compartments, denoted the *labile* biosphere (LB) and the *obdurate* biosphere (OB). The labile carbon consists of herbaceous and other short-lived ($\lesssim 1$ yr) materials that are produced by photosynthesis, with the fixed carbon rapidly returned to the atmosphere by autotrophic and rapid heterotrophic respiration. The obdurate carbon, which constitutes the great majority of

360   the TB stock, consists of long-lived woody material (trunks, branches, roots, coarse debris), which constitutes the bulk of vegetative biomass (e.g. Pregitzer and Euskirchen, 2004; Fahey et al., 2005), and of soil carbon, which comprises the majority of terrestrial carbon (e.g., Naegler and Levin, 2006; Carvalhais et al., 2014) and which exhibits turnover times of up to several hundred years (Raich and Schlesinger, 1992; Amundson, 2001; Torn et al., 2009). From a budget perspective, in contrast to the total stocks in the TB, and the fluxes between the TB taken as a whole and other compartments, which are

365   rather tightly constrained by observations, apportionment of carbon stocks and fluxes to the LB and the OB is not so constrained. Hence, in the budget presented here, these quantities are given as ranges, for example [200, 700] Pg for the PI stock in the LB, S_l^{pi}. For the total PI stock in the TB S_t^{pi} taken as 2800 Pg, the PI stock in the OB, S_o^{pi}, is likewise characterized by a range, $S_o^{pi} = S_t^{pi} - S_l^{pi} = 2800$ Pg $- [200, 700]$ Pg $= [2600, 2100]$ Pg that is complementary to the range of S_t^{pi}. The total uptake of anthropogenic CO_2 emissions by the TB is rather narrowly constrained (from inventoried emissions

370   and uptake into other compartments) as [227, 261] Pg, the uncertainty being due to uncertainty in the anthropogenic stock in the DO. However the apportionment of this uptake into the LB and the OB is much less constrained, with the amount of uptake of carbon by the LB being given by the range [143, 24] Pg and the increase in the OB stock, being complementary, with range [89, 232] Pg. Taking into account the decrease in OB stock due to LU emissions the net range of anthropogenic stock in the OB is negative to near zero, [-139, 4] Pg. The uncertainties in the TB stocks take into account uncertainty in the

375   DO stock and in the increase in LB stock due to uptake of carbon from the AC, added in quadrature, but dominated by the latter.

The fluxes between compartments are evaluated similarly. The gross flux from the atmosphere to the LB, F_{al}, is taken as gross primary production GPP; a slight additional contribution to gross primary production by increased flux from the AC into the OB, while included in the budget, is neglected here. The extent of increase of GPP over the Anthropocene plays an

380 important role in the present day CO_2 budget, but is highly uncertain, as reflected in recent observational and modeling studies summarized in **Appendix C**. Here, as has been conventional in previous analyses, PI GPP is taken as 120 Pg yr^{-1}; the exact value is of little consequence, with only the increase being of importance in the budget. The increase in GPP is thought to be due to fertilization by excess CO_2 over the Anthropocene and perhaps also to increases in emissions of nutrients, particularly nitrogen compounds. Based on **Fig. C1**, the increase of GPP with increasing CO_2 reported in

385 observational and modeling studies can be closely represented by a power law in CO_2 mixing ratio x_{CO2} or equivalently in atmospheric CO_2 stock S_a,

$$F_{GPP}(t) = F_{GPP}^{pi} \left(\frac{x_{CO2}(t)}{x_{CO2}^{pi}} \right)^b = F_{GPP}^{pi} \left(\frac{S_a(t)}{S_a^{pi}} \right)^b ; \qquad (3.1)$$

such a power-law dependence of GPP on atmospheric CO_2 was suggested at least as early as Rodhe and Björkström, (1979). The exponent b is equal to the fractional increase in GPP per fractional increase in x_{CO2}, commonly used to characterize the

390 CO_2 fertilization effect, $i.e., b = d \ln F_{GPP} / d \ln x_{CO2}$. For b initially allowed exhibit the range [0, 1.3], present day GPP would exhibit the range [120, 196] Pg yr^{-1}. This range is reduced by comparison of model results with observations to [138, 168] Pg yr^{-1} (corresponding to $b = [0.4, 0.9]$) resulting in the range for the anthropogenic enhancement of GPP F_{al}^{ant} given in **Fig. 2** [19, 48] Pg yr^{-1}, $i.e.$, an increase of 16 % to 40 % above preindustrial. The increase in flux from the atmosphere to the LB is largely countered by an increase of comparable magnitude in the gross return flux from the LB back to the

395 atmosphere F_{la}^{ant}. The difference, [0.5, 2.5] Pg yr^{-1}, the net PD anthropogenic flux between the compartments $F_{al,net}^{ant} = F_{al}^{ant} - F_{la}^{ant}$, is equal to the PD rate of increase of the stock of carbon in the LB dS_l^{pd}/dt, which is less, to very much less, than the enhancement in the gross flux between the atmosphere and the LB.

Specification of a value of S_l^{pi} together with the assumption of PI steady state between the LB and the AC permits determination of a steady state PD LB S_l^{pd} resulting from anthropogenic emissions. S_l^{pd} and $S_{l,ant}^{pd}$ depend on both S_l^{pi} and

400 b, for which the initial estimates encompass substantial ranges. Additionally, as with the stock in the ML, there is a slight lag in S_l relative to its steady-state value; an expression for this lag is given in **Appendix A, Eq. A48**, permitting calculation of $S_{l,ant}^{pd}$ for any given value of S_l^{pi}; the resultant range of $S_{l,ant}^{pd}$ is shown in **Fig. 3**. Also shown in that figure is the PD annual rate of increase in $S_{l,ant}^{pd}$, denoted ΔS_i. Here and throughout this study transfer coefficients and other quantities were calculated, either algebraically, as here, or using the model developed in **Sect. 6**, for a grid of points (S_l^{pi}, b), $0 < S_l^{pi} \le 1000$

405 Pg and $0 \le b \le 1.3$, and are displayed as contour diagrams with these variables as coordinates; absence of contours at upper

right of figures denotes regions of (S_l^{pi}, b) for which the modeled total rate of increase in stocks is incompatible with emissions.

Similarly to other quantities the PI flux from the atmosphere to the OB F_{ao}^{pi} and the reverse flux F_{oa}^{pi} are represented by ranges, with the requirement that the net PI flux between these compartments be equal to the riverine flux from the OB to the

410   ML ocean noted above, F_{om}^{pi}, and which is taken as constant (0.6 Pg yr^{-1}) over the Anthropocene. As developed in **Appendix A, Sect. A13** F_{oa}^{pi} can be explicitly related to the two parameters S_l^{pi} and b, together with observations and other constraints (near equilibrium between S_a and S_m; preindustrial steady state between the several compartments). The net anthropogenic flux from the atmosphere to the OB $F_{ao,net}^{ant}$, which, for observationally determined total net anthropogenic flux from the atmosphere to the TB $F_{at,net}^{ant}$, is complementary to the net flux to the LB $F_{al,net}^{ant}$, is a key determinant of the

415   turnover time of excess CO$_2$. Also, initially, subsequent to hypothetical abrupt cessation of emissions, this sink into the OB would be additive to the sink to the deep ocean $F_{md,net}^{ant}$, which in the absence of sinks from the DO is equal to the annual increment in the DO stock, ΔS_d. This total sink rate, indicated in the last row of **Table 1** as $\Delta S_d + \Delta S_o$, depends on stocks in the several compartments at a given time, and not on emissions, and hence this total sink rate would be unchanged immediately following an abrupt cessation of emissions.

420   In the present study the depth of the ML z_m is taken as 100 m; this value was apparently assumed in previous versions of **Fig. 2**, but seems to be explicitly stated only in the predecessor figure shown in AR3 (Prentice et al., 2001). A mean thermocline depth of 75 m used by several prior investigators, importantly, Bolin and Eriksson (1959), appears to derive from the early study by Craig (1957) who gave it as 75 ± 25 meters, or, equivalently, 2 % of the ocean volume. The depth of the deep ocean, z_d, is obtained by difference from the mean depth of the world ocean. The choice of z_m directly influences

425   the magnitudes of the stocks given for the ML, but does not greatly affect the lifetime of excess CO$_2$. The stock given for the ML depends slightly also on the temperature (18°C) and total alkalinity (2349 µmol kg$_{sw}^{-1}$) taken for the ML; changes in these quantities would slightly change the PI stock in the ML but have little effect on anthropogenic perturbations.

The budget developed here and shown in **Fig. 2** also exhibits several substantial quantitative differences from the budgets presented in the IPCC Fourth and Fifth Assessment Reports (Denman et al., 2007; Ciais et al., 2013), **Table 1,** as noted here

430   and detailed in **Appendix A**. The preindustrial value of gross primary production (GPP) given in AR4 (120 Pg yr^{-1}) is retained, but possible enhancement of GPP accompanying the increase in atmospheric CO$_2$ is explicitly recognized; within present observationally based and model estimates this fertilization effect might result in a substantial increase in GPP manifested in **Fig. 2** by the range of anthropogenic increase in F_{al} (and F_{la}, which is only slightly less than F_{al}) up to 48 Pg yr^{-1}. Attention is called also to factor-of-two lower preindustrial fluxes between the ML and the DO, including also the

435   gravitationally induced flux of particulate carbon F_{pc} from the ML to the DO that is subsequently oxidized to DIC and

returned to the ML on long (multicentennial) time scales. The low values adduced here result from a value of the piston velocity v_p describing the rate of exchange of water between the ML and the DO. This piston velocity, which is applicable to any globally distributed tracer, is determined here (**Appendix A, Sect. A6**) from measured rate of heat uptake by the deep ocean over the past 50 years as 5.5 m yr^{-1}. This value of v_p yields a much lower exchange rate between the two

440   compartments than would be consistent with values of kg$_{sw}^{-1}$ and F_{dm}^{pi} (and $F_{md,net}^{pi}$) reported in AR4. (Values for the ML and the DO are not separately reported in Figure 6.1 or Table 6.1 of AR5).

With respect to the anthropogenic perturbation, the magnitudes of integrated net drawdown from the AC into the TB and of integrated net LUC are increased somewhat over the values given by AR5; the cumulative net change in stock in the TB, the difference between the two quantities, -4 to +20 Pg, remains zero within uncertainty. An inherent uncertainty arises in the

445   anthropogenic stocks in the DO and the OB associated with the so-called flattening of atmospheric CO$_2$ in the 1940's and 1950's. The cause of this flattening is not known; it has been ascribed to an increase in DO uptake of CO$_2$ during this period (Trudinger et al., 2002; Bastos et al., 2016; Rubino et al., 2019), but an enhancement of uptake by the OB during this period cannot be ruled out. Hence the budget must allow for either possibility, increasing the uncertainty associated with both S_d^{ant} and S_o^{ant} (and hence also with S_{lo}^{ant}). Also shown explicitly are the cumulative net changes in stocks in the OB and in the

450   total TB not including the decreases in these stocks due to LUC emissions, which are ascribed entirely to the OB. Showing these changes separately highlights the large cumulative net transfer of carbon from the atmosphere into the OB together with the large associated uncertainty range. This large range results mainly from uncertainty in the extent of transfer from the atmosphere to the LB versus the OB; such a large uncertainty does not attach, however, to the net cumulative transfer into the TB taken as a whole, which is constrained by conservation of matter.

455   The net PD anthropogenic flux from the AC into the total TB $F_{a\text{-}lo,net}^{ant} = 4.0 \pm 1.1$ Pg yr^{-1} is determined from observations (**Sect. A13**) as the difference between present emission and uptake of CO$_2$ into the AC, ML, and DO under the assumption that the total amount of CO$_2$ in the system is conserved when emissions are accounted for; the uncertainty is dominated by uncertainty in emissions. This flux is somewhat greater than that given in AR5, 2.6 ± 1.2 Pg yr^{-1}. The greater flux adduced here is in part a consequence of the greater anthropogenic emission in the 2016 time frame than in the earlier time frames of

460   the prior assessments, 11.2 Pg yr^{-1} here versus 8.9 Pg yr^{-1} in AR5. The gross anthropogenic flux F_{ao}^{ant} is essentially equal to the net flux $F_{ao,net}^{ant}$ as the gross flux from the OB to the AC, F_{oa}^{ant}, is virtually zero, mainly because the increase in OB stock due to transport from the AC is greatly diminished because of LUC emissions, which are taken as coming entirely from the OB.

The PD annual increments of the several stocks ΔS_i are determined as follows. The annual increment of the atmospheric

465   stock ΔS_a is determined directly from measurement of the global mean mixing ratio of atmospheric CO$_2$. The annual increment of the ML stock ΔS_m is confidently determined from the equilibrium solubility of DIC together with ΔS_a. The

annual increment of the DO stock, ΔS_d, equal to the net flux $F_{md,net}^{ant}$, is determined from the piston velocity between the ML and the DO, together with the values of the anthropogenic stocks in the two compartments. As the anthropogenic increment in the DO and the transfer coefficient k_{dm} are both small, the resultant uncertainty in F_{dm}^{ant} and in turn in $F_{md,net}^{ant}$ is quite

470   small. The annual increment in the combined LB and OB stocks is confidently obtained by difference between fossil fuel emissions and the annual increments in the AC, ML, and DO; *i.e.*, $\Delta S_{lo} = dS_{lo}^{pd} / dt = Q_{ff} - \Delta S_a - \Delta S_m - \Delta S_d = 4.0 \pm 1.1$ Pg yr^{-1}. The apportionment of ΔS_{lo} to the LB and the OB depends on the net rate of increase of the OB stock due to transfer between compartments (*i.e.*, not including LUC emissions), which is not directly constrained by observation, but ΔS_o is constrained to the range of 1.4 to 3.4 Pg yr^{-1} based on comparison of model results with observations (**Sect. 7**). Because of

475   the long (multi-century) lifetime of carbon in the OB, [250, 600] yr, **Sect. 5.8**, this reservoir is usefully considered a sink of CO_2 on the century time scale. The second such sink is the deep ocean DO, with flushing time 650 yr, **Sect. 5.4**. The sum of the rates of increase in these compartments $\Delta S_o + \Delta S_d = [3.0, 5.0]$ Pg yr^{-1}, last row of **Table 1**, serves as a robust measure of the sink rate of anthropogenic CO_2 in the three remaining tightly coupled compartments, the AC, the ML, and the LB.

In comparison with previous assessments a puzzle arises that despite the large differences in preindustrial fluxes that are

480   seemingly due to different piston velocities, the net anthropogenic flux to the DO obtained here and that given in AR4 are virtually identical, 1.6 Pg yr^{-1}. It might be supposed that the agreement results from the much lower value of S_m^{ant} characteristic of the 1990's, 18 Pg, than that in the budget developed here for 2016, 32 Pg, a factor of 1.8; increasing $F_{md,net}^{ant}$ by that factor would result in $F_{md,net}^{ant} = 2.9$ Pg yr^{-1}. However the value given in AR5 for $F_{am,net}^{ant}$, 2.3 ± 0.7 Pg yr^{-1}, decremented by the annual rate of increase of CO_2 in the ML, $\Delta S_m = 0.5$ Pg yr^{-1} determined here, again yields $F_{md,net}^{ant} = 1.8$

485   Pg yr^{-1}, so the apparent inconsistency in the prior budgets between the low rate of uptake of anthropogenic CO_2 by the DO and the much greater rate of this uptake that would be required for consistency with the preindustrial fluxes is not resolved. The present budget stays with the lower gross and net fluxes between the ML and the DO that are consistent with the piston velocity adduced here and with other estimates of that quantity.

Uncertainties in the several stocks and fluxes presented in **Table 1** are traceable to uncertainties in the underlying

490   observations, or for emissions, in the uncertainties provided with the emissions inventories. However, because the several budget terms are coupled, the uncertainties in the several terms cannot be treated as independent. For example if F_{md}^{ant} is at the high end of its uncertainty range, then $F_{a-lo,net}^{ant}$ would be required to be at the low end of its range, and vice versa; similarly a value of Q_{ant} at the high end of its uncertainty range would require a high value for $F_{a-lo,net}^{ant}$. Hence the several quantities cannot be independently varied over their respective uncertainty ranges; a full assessment of the uncertainties in

495   the several budget terms awaits a more formal examination of these constraints. However for the present purpose of examination of the turnover time of excess CO_2, the quantity contributing the greatest uncertainty to this turnover time is the total sink rate into the reservoir compartments $F_{a-lo,net}^{ant} + \Delta S_d$ evaluated as the difference between annual emissions and the

annual rate of increase in the combined AC and ML compartment, $Q_{ant} - \Delta S_{am}$, which quantities are independently determined, permitting their uncertainty to be estimated as the quadrature sum (**Appendix A, Sect. A14**), yielding fractional

500 uncertainty ±18 %. As the fractional uncertainty in S_{am}^{ant}, the combined anthropogenic stock in the AC and ML is much lower (±2 %), the fractional uncertainty in $Q_{ant} - \Delta S_{am}$ attaches to estimates of the turnover time of excess CO_2 determined in **Sect. 4.7** using the central values of the several quantities that are input into the further analysis.

4. Transfer coefficients

A principal objective of the CO_2 budget analysis presented here is to serve as a framework for a model representing the

505 evolution of the stocks of CO_2 in the several compartments over the Anthropocene and to develop transfer coefficients that, together with the stocks in the leaving compartments S_i permit evaluation of the fluxes between the several compartments F_{ij}. The stocks and fluxes are extensive quantities, *i.e.*, scaling with the amount of material in the system, and are therefore dependent on prior history of emissions. In contrast, the transfer coefficients are intensive quantities that can be considered properties of Earth's geophysical system for a given state of the climate, being controlled by wind speed and temperature

510 (atmosphere-ocean transfer), ocean circulations (exchange between the ML and the DO), the concentration of DIC in the ML, and the productivity of terrestrial vegetation (exchange between the AC and the TB and net uptake of carbon by the TB). Values of the transfer coefficients k_{ij} are related to the stocks in the several compartments S_i and the gross fluxes between the compartments F_{ij} summarized in **Figure 2** and **Table 1** as

$$k_{ij} = \frac{F_{ij}}{S_i},$$ (4.1)

515 where i denotes the leaving compartment and j denotes the receiving compartment. The transfer coefficients k_{ij}, dimension inverse time, specify the fraction of the stock in compartment i that is transferred to compartment j per unit time and are thus central to describing the time evolution of the system. Values adduced here for the several transfer coefficients are summarized in **Table 2**.

For the most part the transfer coefficients, being properties of Earth's geophysical system are constant with time over the

520 Anthropocene. The transfer coefficient from the atmosphere to the ML ocean k_{am} is treated as constant, being governed by wind speed, and the physical (Henry's law) solubility of CO_2, and not dependent on the amount of CO_2 in the AC or in the ML. Similarly, the transfer coefficients between the ML and the DO depend on the rate of exchange of water between the two compartments and not on the concentrations of DIC in either compartment. The transfer coefficients adduced here for CO_2 are applicable also to radiocarbon ($^{14}CO_2$), apart from isotope effects of a few per cent at most (Keeling, 1979),

525 neglected here.

Two important exceptions to the constancy of the transfer coefficients over time are the transfer coefficients of CO_2 and of $^{14}CO_2$ from ML to the atmosphere, which must account for the decrease in solubility of total CO_2 (i.e., the ratio of DIC to atmospheric CO_2 mixing ratio) with higher atmospheric CO_2 (**Sect. 3.1** and **Appendix B**) as atmospheric CO_2 has increased over the Anthropocene. Further exceptions to the constancy of the transfer coefficients are the transfer coefficients from the
530   atmosphere to the LB and the TB, a consequence of the increase in GPP over the Anthropocene not being required to be proportional to the increase in atmospheric CO_2 (**Sect. 4.3**).

4.1. Transfer coefficients between the atmosphere and the ocean mixed layer

The value of the transfer coefficient k_{am} relating the gross uptake flux of CO_2 into the world ocean to the atmospheric stock is shown by multiple means to be about 0.12 yr^{-1}, with uncertainty about 30 %, **Appendix A, Sect. A3**. Although locally
535   and instantaneously the transfer coefficient (or the transfer coefficient describing gross flux of any gas to the surface ocean) varies substantially, depending on situational variables, importantly wind speed (~ second power; e.g., Liss and Merlivat, 1986; Wanninkhof et al., 2013), the global value may be considered an average for climatological wind speed, and indeed the transfer coefficient pertinent to CO_2 is applicable (accounting for differences mainly in Henry's law solubility constant and to lesser extent in aqueous-phase diffusion coefficient) to any uniformly distributed low- to intermediate-solubility gas,
540   and vice versa. As such k_{am} may be considered a constant of Earth's geophysical system, albeit one that is known only with accuracy of about 30 %.

In contrast, as developed in **Appendix B**, the differential transfer coefficient characterizing the rate of relaxation of a perturbation from phase equilibrium between the ML and the AC, k'_{ma}, is specific to CO_2, being related to k_{am} by a differential equilibrium constant for CO_2 solubility, k'_{ma} as

545     $k'_{ma} = K'_{ma} k_{am}$.   (4.2)

K'_{ma}, which is related to the familiar Revelle factor (Revelle and Suess, 1957; Sarmiento and Gruber, 2006, p. 332) is defined as

$$K'_{ma} \equiv \left(\frac{dS_a}{dS_m} \right)_{eq} \qquad\qquad\qquad (4.3)$$

(**Sect. B.1, Fig. B1**), the change in S_a per change in S_m, evaluated at an equilibrium state in the ML-atmosphere system for a
550   particular DIC concentration (or a particular CO_2 mixing ratio). The rate of transfer from the ML to the AC F_{ma} is expressed in terms of the departure of S_m from its equilibrium value as $F_{ma} = k'_{ma} \left(S_m - S_{m,eq} \right) = K'_{ma} k_{am} \left(S_m - S_{m,eq} \right)$. The

differential transfer coefficient k'_{ma} differs substantially from the transfer coefficient, k_{ma}, that would be evaluated from detailed balance consideration as $k_{\mathrm{ma}} = K_{\mathrm{ma}} k_{\mathrm{am}}$, where

$$K_{\mathrm{ma}} = \frac{S_{\mathrm{a}}^{\mathrm{eq}}}{S_{\mathrm{m}}^{\mathrm{eq}}} \tag{4.4}$$

555   is the equilibrium constant characterizing the volatility of DIC (expressed in terms of the stocks). The transfer coefficient k_{ma} is pertinent to the rate of transfer of radiocarbon from the ML to the atmosphere, as this transfer, unlike that of CO_2 itself, does not perturb the acid dissociation equilibria of the CO_2 system. The several quantities k'_{ma} , K'_{ma} , k_{ma} and K_{ma} are not constant but depend on DIC concentration (or mixing ratio of atmospheric CO_2) and hence vary over the Anthropocene (**SI Sect. 3, Fig. S3.2**).

560   Accounting for the CO_2 dissociation equilibria is essential in describing the transfer rates between the AC and the ML because only CO_2 is transferred between the two compartments and because of shifts in the equilibria between H_2CO_3, HCO_3^- , and CO_3^{2-} attendant with that transfer (Sarmiento and Gruber, 2006, p. 330). The differential equilibrium constant K'_{ma} can (and can only) be evaluated numerically from the known equilibrium constants for dissociation of CO_2 in seawater, here using the program CO2SYS (Lewis and Wallace, 1998; Pierrot et al., 2006). As it is referred to the stock in
565   the ML, k'_{ma} is also dependent on (inversely proportional to) z_{m}. As shown in **SI Text Sect. S3**, **Fig. S3.1**, for preindustrial CO_2 mixing ratio 278 ppm and for $z_{\mathrm{m}} = 100$ m, $K'_{\mathrm{ma}} = 5.4$, increasing to about 10 at present; the PD value of K'_{ma} is equal to the ratio of the PD growths in the stocks in the two compartments shown in **Fig. 2**, $K'_{\mathrm{ma}} = \Delta S_{\mathrm{a}} / \Delta S_{\mathrm{m}}$. The uncertainty in k'_{ma} , ± 30 %, derives from uncertainty in k_{am}.

An exception to the transfer coefficients for radiocarbon being taken as the same as for ordinary carbon (within neglect of
570   isotope effects) is the transfer coefficient for radiocarbon from the ML to the atmosphere. The reason for the different transfer coefficient is that for ordinary CO_2, exchange of carbon into or out of the ML results in shift of the equilibrium total solubility (*i.e.*, the ratio of DIC concentration to CO_2 partial pressure), whereas for radiocarbon, the solubility is determined by the solubility of ordinary CO_2. Consequently the detailed-balance requirement for radiocarbon is

$$k_{\mathrm{am}}^* R_{\mathrm{a}}^{\mathrm{eq}} = k_{\mathrm{ma}}^* R_{\mathrm{m}}^{\mathrm{eq}} , \tag{4.5}$$

575   where the asterisk denotes the transfer coefficient for radiocarbon and R_i denotes the radiocarbon stock, from which

$$k_{\mathrm{ma}}^* = \frac{R_{\mathrm{a}}^{\mathrm{eq}}}{R_{\mathrm{m}}^{\mathrm{eq}}} k_{\mathrm{am}}^* = \frac{S_{\mathrm{a}}^{\mathrm{eq}}}{S_{\mathrm{m}}^{\mathrm{eq}}} k_{\mathrm{am}}^* = K_{\mathrm{ma}} k_{\mathrm{am}}^* = K_{\mathrm{ma}} k_{\mathrm{am}} . \tag{4.6}$$

Here the second and third equalities express the equality of the equilibrium constant of dissolution for radiocarbon and ordinary carbon K_{ma} (note that the local equilibrium constant is written here in the sense of the volatility, not solubility), and the final equality explicitly notes that the mass transfer coefficient from the atmosphere to the ML is the same for both species. K_{ma} is about an order of magnitude less than K'_{ma}, the ratio K'_{ma}/K_{ma} being equal to the Revelle factor (**Appendix B**, **Eq B19**; **Appendix F, Fig. F1**; see e.g.. Sarmiento and Gruber, 2006, p. 322). This results in k^*_{ma} being about an order of magnitude less than k'_{ma}, **Table 2**. Again with reference to **Fig. 2**, the PD value of K_{ma}, given by the ratio of the two stocks, is about 0.92.

4.2. Transfer coefficients between the ocean mixed layer and the deep ocean

Transfer between the ML and the DO is characterized by the so-called piston velocity v_p that represents the volume exchange rate between the two compartments divided by the area of the world ocean. This piston velocity is determined independently here from the rate of heat uptake by the world ocean over the past 50 years of increasing global mean temperature as 5.5 ± 1.8 m yr^{-1} (**Appendix A, Sect. A6**). The transfer coefficients between the two compartments are related to the piston velocity as

$$k_{md} = \frac{v_p}{z_m}; \quad k_{dm} = \frac{v_p}{z_d} . \tag{4.7}$$

These transfer coefficients represent the fractional annual rate of transfer between the two compartments of any globally distributed tracer and can be considered properties of Earth's geophysical system The values are $k_{md} = 0.055 \pm 0.018$ yr^{-1} and $k_{dm} = (1.53 \pm 0.5) \times 10^{-3}$ yr^{-1}, where the uncertainties reflect propagated uncertainty in v_p. The values of k_{md} and k_{dm} are dependent also on the values taken for the depths of the respective compartments, the piston velocity, which does not depend on z_i, thus being more fundamental. However this caveat essentially applies only to k_{md}, for which z_m is taken as 100 m, as z_d, equal to the depth of the world ocean 3683 m minus z_m (100 m) is insensitive to the choice of z_m.

4.3. Transfer coefficients between the atmosphere and labile terrestrial biosphere

As indicated in **Fig. 2**, the dominant exchange process between the atmosphere and the terrestrial biosphere is with the labile biosphere, the exchange to the obdurate biosphere being an order of magnitude or more lower. The gross flux of CO_2 from the atmosphere to the LB F_{al} is taken here as gross primary production GPP; this gross flux is countered by a nearly equal flux F_{la} representing autotrophic and short-term heterotrophic respiration. The slight exceedance of present-day F_{al} over F_{la} results in an increase in the stock of the LB, the difference constituting the rate of increase. In the present analysis the GPP flux increases substantially from its preindustrial value, taken as 120 Pg yr^{-1}, as indicated in observationally based analyses

and model estimates examined in **Appendix C**, the increase ascribed to a fertilization effect of increased CO_2. An effective

605   transfer coefficient k_{al} corresponding to the GPP flux from the AC to the TB is defined as the quotient of this gross flux,

F_{GPP} upon the stock in the AC, S_a, all quantities explicitly denoted as a function of time,

$$k_{al}(t) = \frac{F_{GPP}(t)}{S_a(t)} = \frac{F_{GPP}^{pi}}{\left(S_a^{pi}\right)^b}\left(S_a(t)\right)^{b-1},$$ (4.8)

with both GPP and S_a increasing with time over the Anthropocene; the second equality follows from **Eq 3.1**. By this

definition k_{al} is not a constant over time, but would exhibit decrease or increase with time depending on whether the relative

610   increase in GPP is greater or less than that of S_a or equivalently whether $b >$ or < 1 (see **Appendix C**). For the range of the

fertilization exponent b describing the dependence of GPP on x_{CO2} (**eq 3.1**) [0, 1.3] the PD range of k_{al} is [0.14, 0.23] yr^{-1},

virtually independent of the value taken for the preindustrial stock in the labile biosphere S_l^{pi}, **Fig. 4**. As discussed in **Sect.**

7, the ranges of k_{al} and other quantities are substantially further constrained by comparison of model results with

observations. As in **Fig. 3**, the domain in (S_l^{pi}, b) space that in the calculations with the model developed here is consistent

615   with observations is indicated by the light red quadrilateral. Thus k_{al} is further restricted by observations to the range [0.16,

0.19], **Table 2**. In actuality, k_{al} plays little role in the analysis of the carbon system presented here, as the rate of transfer F_{al}

used in the analysis is explicitly calculated as a function of atmospheric CO_2, **Eq 3.1**, rather than as the product of a transfer

coefficient times a stock, and hence the designation of k_{al} as an effective transfer coefficient; k_{al} is presented in **Table 2** in

part to permit comparison with other transfer coefficients. Also, k_{al} is pertinent to examination of the lag time of the LB

620   stock relative to steady state. Finally, k_{al} is explicitly used in the examination of the evolution of radiocarbon.

The transfer coefficient k_{la} describing the flux from the LB to the atmosphere is obtained from the requirement of

preindustrial steady state for the PI stock in the LB,

$$\frac{dS_l^{pi}}{dt} = 0 = F_{GPP}^{pi} - k_{la}S_l^{pi},$$ (4.9)

625   from which k_{la} is given by the quotient of the PI GPP upon the PI stock in the LB,

$$k_{la} = \frac{F_{GPP}^{pi}}{S_l^{pi}},$$ (4.10)

shown in **Fig. 4b**. In contrast to k_{al}, k_{la} is treated as a constant over time, the fraction of the LB stock that is returned

annually to the atmosphere. Also in contrast to k_{al}, k_{la} is independent of b but strongly (inversely) dependent on S_l^{pi}, with

range, as constrained by comparison of model results with observations, 0.19 to 0.8 yr^{-1}, corresponding to turnover time of

630   carbon in the LB of 1.2 to 5.3 yr, increasing with increasing S_l^{pi}.

4.4. Transfer coefficients between the atmosphere and obdurate terrestrial biosphere

Like F_{al}, F_{ao} is taken as a power law in S_a, with the same exponent b,

$$F_{ao} = F_{ao}^{pi} \left(\frac{S_a}{S_a^{pi}} \right)^b \tag{4.11}$$

As a consequence

635 $\quad k_{ao} = \frac{F_{ao}(t)}{S_a(t)})\,, \tag{4.12}$

like k_{al}, is temporally variable (as well as dependent on S_l^{pi} and b). An expression for F_{ao}^{pi} that exhibits the dependence of this quantity on S_l^{pi} and b is developed in **Appendix A, Sect. A12,** and shown in **Fig. A1c**. Like k_{al}, k_{ao} is not directly used in the model calculations, the more directly relevant quantity being F_{ao}. However the magnitude of k_{ao}, **Fig. 4c**, is of interest for scoping, estimation of time constants, and comparison, being at most 5 or 10 % of k_{ao}; as this is such a minor

640 contribution to the flux from the atmosphere to the terrestrial biosphere, it is neglected in identifying preindustrial GPP with the preindustrial flux to the LB. Also shown, in **Fig. 4d**, is the transfer coefficient k_{oa}, evaluated as

$$k_{oa} = \frac{F_{ao}^{pi} - F_{om}^{pi}}{S_o^{pi}}\,. \tag{4.13}$$

Like k_{la}, k_{oa} is temporally constant, but it is dependent on the parameters S_l^{pi} and b, further constrained by comparison of model results with observations to the range 0.0016 to 0.0078 yr^{-1}.

645 ### 4.5. Summary of transfer coefficients

The values of the several transfer coefficients are summarized in **Table 2** and **Fig. 5**. Inspection of **Fig. 5** would seem to imply that representation of the dynamics of CO$_2$ in the four compartments requires eight transfer coefficients: k_{am}, k'_{ma}, k_{md}, k_{dm}, k_{al}, k_{la}, k_{ao}, and k_{oa}. However the number of required independent parameters is readily diminished. First, by **Eq 4.7**, k_{md}, and k_{dm} are each related to the piston velocity v_p as $k_{ij} = v_p/z_i$, thereby reducing the number of required

650 independent parameters by one. Second, the transfer coefficient from the ML to the AC, k'_{ma}, is related by K'_{ma}, the differential equilibrium constant introduced in **Appendix A, Sect. A9** and evaluated in **Appendix B**, to the transfer coefficient from the AC to the ML, k_{am}, as $k'_{ma} = K'_{ma}k_{am}$, (**Eq 4.2**), with further reduction of one independent parameter.

As noted in **Sect. 4.4**, the transfer coefficients k_{al} and k_{ao} are not explicitly used in the present model. However the growth of GPP over the Anthropocene is treated as exhibiting a power law dependence on x_{CO2}, by the fertilization exponent b, **Eq. 3.1**, which, for F_{GPP}^{pi} taken as 120 Pg yr^{-1}, just replaces these parameters by the exponent b, which is treated as an adjustable parameter, with further reduction of one independent parameter. Similarly, the transfer coefficient k_{la}, which is given as the quotient $k_{la} = F_{GPP}^{pi} / S_l^{pi}$, with the preindustrial stock in the LB S_l^{pi}, also treated as an adjustable parameter. The transfer coefficient k_{oa} is evaluated based on the requirement of PI steady state (**Eq 4.12**) and is thus not independent.

Thus in summary the independent parameters of the model are: k_{am}, v_p, S_l^{pi}, and b. Of these, two, v_p and k_{am}, can be considered universal geophysical quantities, v_p being the piston velocity characterizing exchange of matter and heat between the ML and the DO, and k_{am} being a deposition velocity that is the same for all low- to moderate-solubility gases after accounting for Henry's law solubility and a weak dependence on aqueous-phase diffusion coefficient. In contrast S_l^{pi}, and b are specific to the carbon system and not are tightly constrained by observations. Consequently these two parameters must be considered and treated as variable parameters, with the sensitivity to their values examined by running the model initially wide ranges that are narrowed by comparison of model output with observations.

In conclusion of this discussion of transfer coefficients it must be underscored that the transfer coefficients, which are determined based solely on the PI and PD budgets of CO$_2$ and thus derived from observations, are to be considered properties of the biogeophysical system controlling the transfer of CO$_2$ among the several compartments and, as such, to be viewed as temporally constant over the Anthropocene. The exceptions to this are k_{al} and k_{ao}, which are based on temporally changing GPP but, in any event, not used explicitly in the calculations, and k_{ma}, the value of which is controlled by the equilibria involving the changing amount of (total) dissolved CO$_2$, with range indicated by the curly brackets in **Table 2**. Thus the several transfer coefficients must be considered properties of Earth's biogeochemical system, albeit, because of lack of observational constraint, uncertain by the ranges indicated by the square brackets in **Table 2**.

5. Characteristic times in the CO$_2$ system

5.1. Residence time of CO$_2$ molecules in the atmosphere

The turnover time of atmospheric CO$_2$ calculated (**Eq. 2.1**) as the quotient of the atmospheric stock upon the total flux out of the AC would imply an atmospheric residence time of $\sim$ 3 yr for either PI or PD conditions. This short lifetime is the residence time of individual CO$_2$ molecules in the atmosphere would characterize the rate of labeled molecules in the absence of return flux, for example, the time constant characterizing the initial rate of decrease of atmospheric ^{14}CO$_2$ resulting from a short-term emission from nuclear weapons testing prior to any substantial return flux (**Appendix E**).

However this quantity is not relevant to the turnover time of excess CO_2 in the atmosphere, which, because of compensating reverse flows, is much greater than the residence time of individual molecules.

5.2. Turnover time of excess atmospheric CO_2

An initial observationally based estimate of the turnover time of excess atmospheric CO_2 can be obtained as the ratio of the stock to the net leaving flux,

$$\tau_a^{to,obs} = \frac{S_a^{ant}}{Q_{ant} - \Delta S_a} \tag{5.1}$$

where the leaving flux is evaluated as the difference between the anthropogenic emission rate and PD atmospheric growth rate ΔS_a. The resulting turnover time is 44 ± 7 yr, where the uncertainty derives mainly from uncertainty in anthropogenic emission rate. As this turnover time treats uptake into the ML and the LB as sinks, rather than as in rapid exchange with the AC, it is expected to yield an underestimate of the turnover time pertinent to excess CO_2, a concern that is borne out in comparison of the several turnover times and adjustment times in **Sect. 7.6**.

5.3. Equilibration time between the AC and the ML

Knowledge of k_{am} and K'_{ma} permits determination of the time constant τ_{am} for relaxation of a perturbation in the amount of CO_2 in the AC (or in the ML). To good approximation the relaxation time constant coupling these two compartments is

$$\tau_{am} = \left(k_{am} + k'_{ma}\right)^{-1} = \left[k_{am}\left(1 + K'_{ma}\right)\right]^{-1} \tag{5.2}$$

with value $\tau_{am} \approx 1.2$ yr for preindustrial CO_2 and about 0.7 yr at present (**Appendix B**). The uncertainty of ±30 % attached to the value of k_{am} likewise attaches to τ_{am}. Moreover, as K'_{ma} is inversely proportional to the depth taken for the ML, z_m, and as the second term in **Eq 5.2** is the dominant term, τ_{am} is likewise approximately proportional to z_m. Despite the uncertainty and arbitrariness attached to τ_{am}, the value of this time constant leads to the conclusion that a perturbation in atmospheric CO_2, such as from the anthropogenic increment, equilibrates between the atmosphere and the ML on the time scale of about a year. The near equilibrium state of the two compartments is consistent with the nearly equal values of the forward and reverse fluxes, in both the preindustrial and present states, **Fig. 2**. Examination of the relation between S_a and S_m in the output of model calculations confirms the close adherence to equilibrium between these stocks (**Sect. 7.7**).

Because of the greater value of the transfer coefficient from the ML to the atmosphere for radiocarbon k_{ma}^* than for ordinary CO_2 k'_{ma}, the corresponding time constant is likewise greater, decreasing slightly over the Anthropocene, from 5 to 4 years.

5.4. Turnover time of excess CO$_2$ in the atmosphere and the mixed layer together

As pointed out by Rodhe and Björkström (1979), because of rapid equilibration of CO$_2$ between the atmosphere and the ML, it useful to consider these compartments a single compartment. The turnover time of this compartment based on the combined anthropogenic stock, and on the total net anthropogenic leaving flux is

710 $$\tau_{am}^{to,obs} = \frac{S_a^{ant} + S_m^{ant}}{F_{at}^{ant,net} + F_{md}^{ant,net}} \ . \tag{5.3}$$

By conservation of matter, the net flux leaving the combined AC-ML compartment, the sum of the net fluxes into the TB and DO $F_{at,net}^{ant} + F_{md,net}^{ant}$, is equal to the difference between annual anthropogenic emission and the sum of the annual increments in the AC and ML stocks,

$$F_{at,net}^{ant} + F_{md,net}^{ant} = Q_{ant} - \left(\Delta S_a + \Delta S_m \right) \tag{5.4}$$

715 Because of near equilibrium between S_a and S_m, the annual increment in S_m, ΔS_m, is confidently calculated from ΔS_a (**Appendix A, Sect. A9**). Hence the turnover time of excess CO$_2$ in the combined AC-ML compartment can be confidently determined from observations as

$$\tau_{am}^{to,obs} = \frac{S_a^{ant} + S_m^{ant}}{Q_{ant} - \left(\Delta S_a + \Delta S_m \right)}, \tag{5.5}$$

from which $\tau_{am}^{to,obs} = 54 \pm 10$ yr, where the uncertainty (18 %) is dominated by uncertainty in the denominator, which in turn
720 arises from uncertainty in Q_{ant} and year-to-year variation in measured ΔS_a (**SI Text Sect. S5, Fig. S5.1**). Importantly this observationally determined turnover time is immune to uncertainty in v_p or k_{am}; it is likewise immune to uncertainty in the apportionment of the flux into the TB between the LB and the OB. Here it must be recognized that such a turnover time can remain constant only so long as the return flux from either sink compartment is small compared to the forward flux. The turnover time $\tau_{am}^{to,obs}$ is somewhat (32 %) greater than that determined for the AC only, $\tau_a^{to,obs}$, **Sect. 5.2**, because of greater
725 numerator (the combined stocks in the AC+ML versus just the AC) and smaller denominator (subtracting the growth in the two compartments instead of only out of the AC). However, as is he situation with $\tau_a^{to,obs}$, the turnover time $\tau_{am}^{to,obs}$ yields an underestimate of the compared to other measures of the lifetime of excess CO$_2$, because of neglect of the rapid exchange with the LB, **Sect. 7.6**.

5.5. Transfer times between the ocean mixed layer and the deep ocean

730   The inverses of k_{md} and k_{dm} represent flushing times of the ML and DO compartments, 18 and 650 years, respectively, both quantities uncertain to ± 33 % from uncertainty in v_p (in addition to arbitrariness in k_{md} arising from choice of z_m). These flushing times establish that transfer of material, and specifically, here, of DIC, from the ML to the DO takes place on the decadal to centennial time scale, whereas transfer of material from the DO to the ML and ultimate equilibration of these two compartments take place only on the multicentennial to millennial time scale. Thus to good approximation on the

735   century time scale, transfer of DIC from the ML to the DO can be considered an irreversible sink for anthropogenic CO_2. This conclusion has important implications in consideration of the lifetime of excess atmospheric CO_2.

5.6 Turnover time of carbon in the terrestrial biosphere

The turnover time of carbon in the TB (**Eq 2.1**) has been calculated by previous investigators as the quotient of the stock in the TB upon the leaving flux taken as GPP (e.g. Carvalhais et al., 2014; Yan et al., 2017) or NPP (e.g., Friend et al., 2013),

740   the global carbon stock 2807^{+428}_{-278} Pg (Carvalhais et al., 2014; uncertainties converted to central 68 % confidence interval) yielding $23^{+3.5}_{-2}$ yr (Carvalhais et al., 2014). As explicitly stated by Carvalhais et al., this lifetime is a measure of the "mean residence time of a carbon atom in terrestrial ecosystems from its initial fixation by photosynthesis until its respiratory (including autotrophic respiration) or non-respiratory loss." It is argued here that the residence time defined in this way is not the appropriate residence time pertinent to the retention of excess carbon due to anthropogenic emissions by the terrestrial

745   biosphere. Rather, analogous to the turnover time of a CO_2 molecule in the atmosphere, and as noted in **Sect. 3.4**, because of the large and opposing fluxes, this residence time is much shorter than the time scale on which the stock of carbon in the TB would decrease in response to a decrease in atmospheric CO_2, the much more relevant time scale.

5.7 Time for labile biosphere to reach steady state with the atmosphere

Rather than considering the TB as a single compartment much insight is gained from considering the TB as two

750   compartments as in the present budget analysis. With respect to the LB as indicated in **Fig. 2** there is a large two-way flux between the LB and the atmosphere. This situation is analogous to the rapid exchange between the atmosphere and the ML ocean and leads to definition of a time constant for establishing steady state (not equilibrium, as between the AC and the ML) between these compartments,

$$\tau_{al} = \left(k_{al} + k_{la}\right)^{-1},$$ (5.6)

755 which, for present conditions exhibits the range [1,3] yr. Such a short lifetime relative to changes in the carbon system suggests that to good accuracy the LB may be considered to be in steady state with the atmosphere, a conclusion that is borne out in the numerical modeling (**Sect. 7.7**).

5.8 Turnover time of carbon in the obdurate biosphere

In contrast to the LB, but much more like the DO, the OB exhibits a long residence time against return of carbon to the AC.
760 A measure of this lifetime is the quotient of the PI OB stock upon the sum of PI fluxes out of the OB, which at PI steady state is equal to $F_{ao}^{pi} + F_{om}$, yielding a range [125, 525] yr for the turnover time τ_o^{to} (**Appendix A, Eq A43**). Such a lifetime suggests that the OB serves as a sink for carbon on the century time scale but that return from the OB to the AC would be appreciable on the multicentennial time scale.

5.9. Turnover time of excess CO$_2$ in the combined AC-LB-ML compartment

765 If exchanges between the AC and the LB and between the AC and the ML are sufficiently rapid, it is useful to consider these three compartments a single compartment, with anthropogenic stock $S_{alm}^{ant} = S_a^{ant} + S_l^{ant} + S_m^{ant}$; this assumption, examined with the present model in **Sect. 7.7**, is indeed found to be quite accurate, supporting the utility of defining the turnover time of this combined compartment for transfer into the long-lived compartments the DO and the OB as

$$\tau_{alm}^{to,obs} = \frac{S_a^{ant} + S_l^{ant} + S_m^{ant}}{F_{ao}^{ant,net} + F_{md}^{ant,net}} ,$$
(5.7)

770 which may be evaluated as

$$\tau_{alm}^{to,obs} = \frac{S_a^{ant} + S_l^{ant,ss} + S_m^{ant,ss}}{Q_{ant} - (\Delta S_a + \Delta S_m + \Delta S_l)} .$$
(5.8)

For the best estimate of present anthropogenic emissions Q_{ant}^{pd} = 11.2 Pg yr^{-1} what is denoted as a central estimate of this turnover time at present is obtained for values of S_l^{ant} and ΔS_l corresponding to (S_l^{pi}, b) = (400 Pg, 0.6); as seen in **Fig. 3a and b**, this point in the (S_l^{pi}, b) plane falls on contours of $S_{l,ant}^{pd}$ 100 Pg and ΔS_l 1.8 Pg yr^{-1} that pass through the central
775 region of the quadrangle for which the model results are consistent with observations. The remaining quantities on the right hand side of **Eq 5.8** are narrowly constrained by observations and the steady state between the ML and the AC; pertinent quantities are presented in the column in **Table 3** denoted "Central." The resulting central estimate of the turnover time is 103 years. This central estimate can be bounded by two limiting cases, corresponding to low $S_{l,ant}^{pd}$ and ΔS_l, 25 Pg and 0.5 Pg yr^{-1}, respectively, and to high $S_{l,ant}^{pd}$ and ΔS_l, 140 Pg and 2.7 Pg yr^{-1}, respectively, controlled mainly by the allowable
780 range of S_l^{pi}, **Fig. 3**. These bounds yield turnover time 67 and 158 years, respectively; when uncertainty in Q_{ant}^{pd}, 1.1 Pg yr^{-1},

is taken into account the uncertainty range on PD turnover time in the combined AC-LB-ML compartment increases appreciably, to [62, 191] years. This dependence of the turnover time $\tau_{\text{alm}}^{\text{to,obs}}$ on $Q_{\text{ant}}^{\text{pd}}$ highlights the importance of uncertainty in emissions in determination of the lifetime of anthropogenic CO2 and more broadly in the budget of anthropogenic CO2. This measure of the lifetime of excess CO_2 is compared with other measures of this lifetime in **Sect.**
785   **7.6**.

5.10. Observation-based rate of removal of excess CO_2 from the AC and ML over the Anthropocene

Similarly to determination of the PD turnover time as the quotient of the PD stocks and fluxes, this approach can be extended to the entire Anthropocene using measurements over this time of CO_2 atmospheric mixing ratio from glacial ice cores (Etheridge et al., 1996) and from contemporaneous measurements in air together with emissions determined by inventory
790   methods (**SI Text Sect. S4; SI, Data table, sheet 4**). Here, the measured values of $S_{\text{a}}^{\text{ant}}$ and $\triangle S_{\text{a}}$ are augmented by $S_{\text{m}}^{\text{ant}}$ and $\triangle S_{\text{m}}$, respectively, which are small (~10 %) relative to $S_{\text{a}}^{\text{ant}}$ and $\triangle S_{\text{a}}$, with the result that any error in $S_{\text{am}}^{\text{ant}}$ and $\triangle S_{\text{m}}$ from this augmentation would be slight. The resulting plot of $Q_{\text{ant}} - \triangle S_{\text{am}}$ over the Anthropocene, 1750–2016 as a function of $S_{\text{am}}^{\text{ant}}$ is shown in **Fig. 6** for (S_{l}^{pi}, b) consistent with observations, **Sect. 7**. The observation-based removal rate of excess CO_2 from the AC and ML compartments obtained in this way adheres closely to a linear dependence on the amount of excess
795   CO_2 in these compartments throughout the Anthropocene. Further, as shown by the dashed black line forced through the origin and having slope 0.0184 yr^{-1} corresponding to $\tau_{\text{AM}}^{\text{to}}$ = 54.3 yr determined for year 2016 (**Sect. 5.4**), this linear dependence provides a good match to the observations for the entire Anthropocene up to the present time, indicative of the constancy of the governing processes over this period.

800   **6. Model for CO_2 budget over the Anthropocene**

The overview of the CO_2 budget (**Sect. 3**, **Fig. 2**) and the transfer coefficients adduced in **Sect. 4** provide the framework required for modeling the evolution of CO_2 in the several compartments over the Anthropocene and future evolution in response to hypothetical changes in future emissions, including abrupt cessation, which permits determination of the adjustment time. This model, a quite minimalist model, is developed in this section.

805   **6.1. Full model**

As indicated in **Fig. 6**, the model presented here represents the stocks of CO_2 (or carbon) in five compartments, the atmosphere, the mixed-layer ocean, the deep ocean, the labile biosphere, and the obdurate biosphere, and thus requires five equations representing changes in the stocks in those compartments. It should be underscored that a model such as this has

numerous antecedents in the early literature examining the carbon cycle, importantly Craig (1957), Bolin and Eriksson

810 (1959), and Bacastow and Keeling (1973), and more recently Gloor et al. (2010), Raupach (2013), Raupach et al. (2014), and

Graven (2015). Such simple models have largely been supplanted by a suite of CC models with yet many more parameters.

Here the parameters are limited as much as possible to quantities that are constrained by observation.

The rates of change of the stocks of CO_2 (or DIC or terrestrial carbon) in each of the five compartments are represented by a

set of coupled ordinary differential equations (ODEs) with the transfer rates being expressed in terms of the stocks S_i and the

815 transfer coefficients from compartment i to compartment j, k_{ij},

$$\frac{dS_a}{dt} = Q_{ff}(t) + Q_{lu}(t) - k_{am}\left(S_a - S_a^{eq}\right) + k'_{ma}(S_m)\left(S_m - S_m^{eq}\right) - F_{GPP}^{pi}\left(\frac{S_a}{S_a^{pi}}\right)^b + k_{la}S_l - F_{ao}^{pi}\left(\frac{S_a}{S_a^{pi}}\right)^b + k_{oa}S_o \qquad (6.1)$$

$$\frac{dS_m}{dt} = k_{am}\left(S_a - S_a^{eq}\right) - k'_{ma}(S_m)\left(S_m - S_m^{eq}\right) - k_{md}S_m + k_{dm}S_d + F_{om}^{pi} - F_{pc} \qquad (6.2)$$

$$\frac{dS_d}{dt} = k_{md}S_m - k_{dm}S_d + F_{pc} \qquad (6.3)$$

$$\frac{dS_l}{dt} = F_{GPP}^{pi}\left(\frac{S_a}{S_a^{pi}}\right)^b - k_{la}S_l . \qquad (6.4)$$

820 $$\frac{dS_o}{dt} = F_{ao}^{pi}\left(\frac{S_a}{S_a^{pi}}\right)^b - k_{oa}S_o - F_{om}^{pi} - Q_{lu}(t) \qquad (6.5)$$

Equation 6.1 may be seen as an expression of conservation of carbon stock in the entire system, the growth in the AC being

the difference between emissions and net rates of transfer between the AC and the several other compartments. The terms

$Q_{ff}(t)$ and $Q_{lu}(t)$ in denote anthropogenic emissions into the AC of CO_2 from fossil fuel combustion and other industrial

activities and from net emissions into the AC from land use change, respectively (**Appendix A, Sect. A7**); emissions from

825 land use change also diminish the stock in the OB, **Eq 6.5**. Reduction of the stock in the OB by net LUC emissions, and

resultant decrease in F_{oa}, would seem to be essential, although as noted by Friedlingstein et al. (2006) changes in the

physical and biogeochemical properties of vegetation as a consequence of LUC emissions have generally been neglected in

carbon cycle models, at least as of the time of that study.

The several transfer coefficients are as developed in **Sect. 4**. The rates of transfer between the AC and the ML in **Eqs 6.1**

830 **and 6.2** are evaluated in terms of the departure of the actual stock S_i and the stock S_i^{eq} that would be in equilibrium between

the two phases for the time-dependent sum of the two stocks $S_a + S_m$ using the equilibrium volatility constant

$K_{ma} = S_a^{eq} / S_m^{eq}$ (**Sect. 4.1, SI Sect. 3**) and the differential equilibrium constant $K'_{ma} = (dS_a / dS_m)_{eq}$, both obtained here using the program CO$_2$SYS (Lewis and Wallace 1998; see **SI Sect. S2, S3**). The term $F_{GPP}^{pi}(S_a / S_a^{pi})^b$ in **Eqs 6.1 and 6.4** represents GPP, as a power law dependence on S_a with exponent b, treated as an adjustable parameter ranging from 0 to 1.3

835 are taken from observational and modeling studies examined in **Appendix C**; that range is subsequently reduced by comparison of model results with observations, **Sect. 7**. The term $F_{ao}^{pi}(S_a / S_a^{pi})^b$ in **Eqs 6.1 and 6.5** contains the factor F_{ao}^{pi}, the preindustrial flux from the AC to the OB, which is evaluated for specific S_l^{pi} and b using the expression developed in **Appendix A, Sect. A13** and is presented in **Fig. A1**; the term also includes the factor $(S_a / S_a^{pi})^b$ as with the corresponding terms for transfer between the AC and the LB. Included in **Eqs. 6.2 and 6.4** is the preindustrial riverine flux, F_{om}^{pi}, from the

840 OB to the ML and back to the AC and thence to the OB, a net-zero cycle of magnitude 0.6 Pg yr^{-1}, which is responsible for the difference between F_{at}^{pi} and F_{ta}^{pi} and for the slight disequilibrium between the ML and the AC prior to the anthropogenic perturbation (**Sect. 2, Fig. 2; Appendix A, Sect. A2)**. The term F_{pc} in **Eqs 6.2 and 6.3** denotes the gravitational flux of particulate carbon from the ML to the DO, taken as 5.6 Pg yr^{-1}, that gives rise to the preindustrial disequilibrium between these two compartments (**Sect. 2, Fig. 2; Appendix A, Sect. A5**).

845 Because of nonlinearities introduced by the F_{al} and F_{ao} fluxes and the transfer from the ML to the AC, the set of equations must be solved numerically rather than analytically; the nonlinearities are readily dealt with by numerical ODE solvers. The set of equations can be considered a five-compartment closed system, but because of conservation of matter within the five compartments, the dynamics of the system is fully represented by the equations in the stocks of the AC, the ML, the DO, and the LB, with the stock in the OB obtained by difference, and hence it is equivalent to a four-compartment open system. The

850 model exhibits quite low drift, with changes in stocks $\lesssim$ 0.05 Pg over a 1000 year run with zero emissions.

As reported in **Sect. 7** the set of coupled ODEs **(Eq 6.1-6.5)** was solved for historical emissions of CO$_2$ as a function of time over the Anthropocene (1750-2016) with results compared with observations. The initial conditions are the preindustrial conditions taken nominally for year 1750 as specified in **Sect. 3**. The total initial stock in the TB was taken as 2800 Pg; the initial stock in the LB was treated as an adjustable parameter S_l^{pi}, with the initial stock in the OB the complement. The

855 model was also run for hypothetical abrupt cessation of emissions commencing in 2017 to permit determination of adjustment times.

6.2. Model for radiocarbon

A model for radiocarbon is developed in **Appendix E**. This model is essentially the same as that for ordinary carbon, differing principally in representation of exchange of $^{14}CO_2$ between the atmosphere and the ML. As the temporal pattern

860 of anthropogenic emissions of radiocarbon differs greatly from that for ordinary carbon because of the large pulse of

emissions due to atmospheric weapons testing in the 1950's and early 1960's, comparison of model response to observations for radiocarbon, **Sect. 7.3**, affords a stringent test of the model.

6.3. Equilibrium–steady-state (ESS) model

The short time constants (**Sect. 5.3, Sect. 5.7**) for establishing equilibrium between the stocks in the atmosphere and the ML
865 and for establishing steady state between the stocks in the atmosphere and the LB suggest that it should be possible to accurately model the system under the assumption of equilibrium and steady state, respectively. This would reduce the number of compartments that need to be actively represented in the solution of the ODEs, although that is hardly a problem from a numerical perspective. Rather, demonstration of near equilibrium and steady state for the ML and the LB, respectively would lend insight into the dynamics of the global carbon system. As noted in **Sect. 5.9** the assumption that the
870 three compartments are tightly coupled leads to evaluation of the turnover time of excess CO_2 as the ratio of the sum of the anthropogenic stocks in the three compartments upon the flux leaving these three compartments into the DO and the OB, which have much greater time constants. The differential equations leading to the ESS model are developed in **Appendix D**; comparison of the results from application of the model with the results from the full model in **Sect. 7.7** confirms the accuracy of the ESS model thereby further justifying treatment of the three compartments as a single compartment for the
875 purpose of inferring the turnover time and more broadly for interpreting the dynamics of CO_2 in the biogeosphere.

7. Application of the model

7.1. Application of the model over the Anthropocene

The set of equations **Eq 6.1-5** was solved numerically for the time period 1740 to 2739 with the transport coefficients calculated from measured preindustrial and present day stocks and PD rate of annual increase in S_a stock ΔS_a ; anthropogenic
880 CO_2 emissions (both fossil fuel and land-use) were ceased abruptly commencing in 2017 to examine the response of stocks in the several compartments. Because of lack of observational constraint on the two adjustable parameters S_l^{pi} and b, these parameters were initially varied over the range $S_l^{pi} = [1, 100, ..., 1000]$ Pg and $b = [0.01, 0,1, ..., 1.3]$. Calculations were not carried out for values of (S_l^{pi}, b) for which the rate of uptake by the combined LB and OB exceeded the rate of total uptake by the total TB as determined as total emissions minus growth rate in the AC, ML and DO compartments. Calculations were
885 initiated with the preindustrial values of stocks given in **Fig. 2**. Historical anthropogenic emissions from 1750 to 2016 were modified from Le Quéré et al. (2018*a*) by assumption of a linear rate of increase in LUC emissions from 1750 to 1850; the emissions data are shown in **Fig. S4.1** (**SI Text Sect. S4** and are tabulated in **SI, Data table, sheet 3**.

The model developed here readily permits examination of the anthropogenic stocks and fluxes (evaluated as the differences relative to preindustrial) as a function of time for a specified pair of parameters S_l^{pi} and b and for specified emissions. The

890   disposition of emitted CO_2 among the several compartments is shown in **Fig. 7a** over the historical period and following hypothetical abrupt cessation of emissions for S_l^{pi} = 400 Pg and b = 0.6. During the historical period, as expected, the anthropogenic stocks in all the compartments (except for the OB) increase with time, as driven by anthropogenic emissions; the changes in the stocks in the several compartments following abrupt cessation of emissions are examined in **Sect. 7.5**. The anthropogenic stock in the OB is the algebraic sum of uptake due to transfer between the AC to the OB (positive) and LUC

895   emissions (negative). In the present model the stock in the obdurate biosphere decreases throughout the Anthropocene roughly to the present time, although, as shown in **Fig. 7a** and more explicitly from the derivative of the stock shown in **Fig. 7b**, the stock in the OB has reached a minimum and is increasing slightly at present. This is a consequence of increased uptake from the AC to the OB that results from increased stock in the AC; the timing of this minimum depends somewhat on the parameters S_l^{pi} and b. As required by conservation of matter the sum of the anthropogenic stocks in the several

900   compartments plus the integrated LU emissions is equal to the integral of total emissions. Likewise the sum of the stocks in the several compartments is equal to the total FF emissions (including cement manufacture). During the historical period excess CO_2 is present mainly the atmosphere followed by the OB, the DO, and the TB; uptake by the OB (not counting the decrease in OB stock due to LUC emissions), also shown in **Fig. 7a**, is a substantial fraction of the total. Increases in the stocks in the ML and the LB mirror that in the atmosphere, but at lower magnitude. Attention is called to the stock in the AC

905   exceeding integrated FF emissions, Ω_{ff}^{ant}, until about 1968, a situation that was recognized as early as 1989 (Keeling et al., 1989); again the exact crossing point depends slightly on model parameters. This exceedance is due to the relatively large contribution from LU emissions, the annual LU emissions exceeding FF emissions until about 1950, and the integrated LU emissions exceeding integrated FF emissions until about 1985 (**SI Text, Sect. 4**).

Further insight is gained from examination of the fluxes and rates of change in the several stocks shown in **Fig. 7b** and **Fig.**

910   **7c**; fluctuations in the rates of change in S_a and S_O (**Fig. 7b**) are due mainly to year-to-year variation in the emissions employed in the calculation (**SI Text Sect. S4, Fig. S4.1**). The two components of the negative rate of change shown for S_O, net transfer from the AC and the rate of LUC emissions are shown separately in **Fig. 7c**, which has the same vertical scale as **Fig. 7b**. As the rate of transfer from the OB to the AC F_{oa}^{ant} is small, the net rate of transfer $F_{ao}^{ant,net}$ closely matches the gross flux F_{ao}^{ant}, both of which are positive throughout the Anthropocene.

915   **7.2. Comparison with observed CO_2 mixing ratio over the Anthropocene**

Modeled mixing ratios of atmospheric CO_2 over the Anthropocene and subsequent to abrupt cessation of emissions are shown **Fig. 8** for a wide range of parameter values (S_l^{pi}, b), along with observed mixing ratio from Antarctic glacial ice cores and from contemporaneous measurements of CO_2 in air. All model variants reproduce the increase in atmospheric CO_2 observed over the Anthropocene and likewise exhibit substantial decrease in atmospheric CO_2 subsequent to cessation.

920   However within the parameter space examined there are considerable differences in detail. In particular several model variants exhibit the increase in atmospheric CO_2 that is much delayed relative to observations, as shown by the inset centered about year 1925; comparison with observations in this time frame, with the criterion that $x_{CO2}(1925)$ be not less than 300 ppm, permits several model variants to be excluded. The second inset, centered about 2017, similarly compares model results with present-day CO_2 $x_{CO2}(2017)$, a synthesis of multiple contemporaneous measurements as presented by Le

925   Quéré et al., (2018*a,b*), showing that several model variants substantially exceed observations, likewise allowing exclusion of variants for which modeled $x_{CO2}(2017)$ exceeds 410 ppm. All model variants result in substantial recovery of atmospheric CO_2 subsequent to cessation of emissions but on time scales that vary substantially as indicated in the main figure and as examined more systematically examined in **Sect. 7.6**. The dependences of the modeled values of these two observable quantities $x_{CO2}(1925)$ and $x_{CO2}(2017)$, on the parameters (S_l^{pi}, b) shown in **Fig. 9*a*** permit identification of the subset

930   of (S_l^{pi}, b) space that is consistent with the observations as the light blue region between the two bolded contours in the figure. These constraints greatly limit the range of (S_l^{pi}, b) that, within the present model, is consistent with observations.

7.3. Application of the model to radiocarbon and additional observational constraints

Because transfer of radiocarbon in the environment is controlled by the same processes and essentially the same transfer coefficients as ordinary carbon (except for k_{ma}^*; **Sect. 4.2**), the present model must accurately describe the evolution of

935   radiocarbon over the nuclear era and more broadly over the Anthropocene. Radiocarbon provides a further stringent test of the model, and constraint of model parameters, for several reasons. Most importantly in contrast to ordinary carbon, emissions of which increased gradually and more or less monotonically over the Anthropocene, radiocarbon emissions were sharply peaked in the late 1950's and early 1960's, a consequence of atmospheric weapons testing and subsequent nearly complete cessation of such tests immediately following the test ban treaty, **Fig. E1**. This abrupt cessation of emissions serves

940   as a stringent test of the ability of the present model or any model to represent the decrease in atmospheric CO_2 that would follow hypothetical cessation of emissions of ordinary carbon necessary to determine adjustment time of excess atmospheric CO_2. Further, as developed here comparison of modeled and observed radiocarbon provides additional constraints on the model parameters b and S_l^{pi}; details of the model calculations including emissions are reported in **Appendix E**. Model results and observations for atmospheric and oceanic ^{14}C stocks are compared in **Fig. 10** for several pairs of (S_l^{pi}, b).

945   Modeled anthropogenic ^{14}C stocks, **Fig. 10*a***, denote changes relative to 1750; the decrease in the stock in the obdurate biosphere is due to LUC emissions. Atmospheric $^{14}CO_2$ abundance was determined by analysis of dendrochronologically dated tree rings and by direct measurement. Oceanic $^{14}CO_2$ was determined by ocean surveys. Radiocarbon abundances in the several compartments are represented in the model as stock in units of 10^{26} atoms, as is conventional in the oceanic geochemistry literature. In contrast atmospheric abundance of $^{14}CO_2$ is most commonly reported as $\Delta^{14}C$, the difference in

950    $^{14}C/^{12}C$ isotope ratio from that of a standard, corrected for fractionation by reference to the isotope ratio of ^{13}C (Stuiver and Polach, 1977). Reported $\Delta^{14}C$ values of atmospheric CO_2 are converted to stocks according to Levin et al., (2010) as described in **Appendix E**.

Several points in the comparisons with observations should be noted. First the several variants of the present model for different values of parameters S_l^{pi} and b all closely reproduce the observed gradual increase in atmospheric $^{14}CO_2$ over the

955   pre-bomb Anthropocene (1750-1950), **Fig. 10b**. All model variants also closely reproduce the observed rapid increase in $^{14}CO_2$ that is due to emissions from atmospheric weapons testing. However, for model variants corresponding to low values of S_l^{pi}, the modeled increase substantially exceeds the observations, **Fig. 10b**; this is attributed to the inability of the LB to sufficiently draw down the emitted $^{14}CO_2$ with such a low stock in this compartment. These comparisons thus provide a further constraint on (S_l^{pi}, b), shown in **Fig. 9b** by the bold contour at 730×10^{26} atoms.

960   All model variants likewise exhibit a decrease in atmospheric $^{14}CO_2$ subsequent to the maximum, reaching a plateau or minimum around year 2005, as seen also in observations (Graven et al., 2017, Figure 12C) and in modeling (Graven, 2015, Figure S1); the rates of decrease and value of subsequent plateau or minimum at around year 2010 vary with the choice of parameters, although none of the model variants yields an exact match to observations. The observations and several of the model variants show a slow increase subsequent to about year 2005; this increase is attributed mainly to increase in ordinary

965   CO_2 that drives radiocarbon from the ocean to the atmosphere.

The present model results for oceanic radiocarbon (sum of ML and DO) are compared in **Fig. 10c** with observations and with previous model calculations. The comparisons at year 1994 show that variants of the present model with (S_l^{pi}, b) (700, 0.4) and (900, 0.4) result in modeled oceanic radiocarbon that is less than, to well less than, the lower bound to the ocean inventory, 300×10^{26} atoms, thereby excluding such values of S_l^{pi}. These comparisons, shown also in **Fig. 9b** further

970   constrain the range of model variants that are consistent with observations. The present model results also compare well with previous models, **Fig. 10c**. The several comparisons allow identification of the region of (S_l^{pi}, b) space that is consistent with observations, shown by the light red quadrangle in **Fig. 10c** and **d**.

In summary, the application of the present model to radiocarbon, based on well understood equilibria and transfer kinetics, and with transfer coefficients constrained by observations of ordinary carbon, accurately reproduces available measurements

975   of radiocarbon in the several compartments and adds further constraints on the parameters S_l^{pi} and b. This examination of radiocarbon lends further confidence in application of the parent model to ordinary CO_2.

7.4. Dependence of other modeled quantities on adjustable parameters

The several constraints resulting from observational comparisons result in substantial limitation of the allowable range of values of (S_l^{pi}, b) from the initially examined range S_l^{pi} = [0 Pg, 1000 Pg]; b = [0, 1.3]. The resulting allowable range of

980 (S_l^{pi}, b) pairs is shown by the region demarcated by the light red quadrilateral in **Fig. 9d**, the intersection of the regions in (S_l^{pi}, b) space that are consistent with observations within the present modeling framework. Although these constraints considerably limit the values of these parameters, considerable latitude remains in these parameters and in quantities that are dependent on them. These dependences are examined here.

The bounds on the fertilization exponent $0.4 \leq b \leq 0.9$ set bounds on the increase in GPP over the Anthropocene. For GPP

985 related to CO_2 mixing ratio by **Eq 3.1**, for b = 0.9 the PD increase of S_a relative to its PI value in **Fig. 2** would yield an increase in GPP of 40 % *i.e.*, from 120 Pg yr^{-1} to 168 Pg yr^{-1}. Such a value would place PD GPP toward the high end of the range of modeling and observational studies summarized in **Appendix C (Fig. C1)**. In contrast the lower bound on b, about 0.4, would result in an increase in GPP of only 16 % above PI, *i.e.*, from 120 Pg yr^{-1} to 139 Pg yr^{-1}. Within the present model the range in b consistent with observational constraints is thus consistent with an increase in GPP over the

990 Anthropocene ranging from 19 to 55 Pg yr^{-1}, a rather large range that would seem capable of being more tightly constrained by observations.

As noted in **Sect. 4** in conjunction with **Fig. 4**, the transfer coefficients describing fluxes of carbon between the atmosphere and the two terrestrial biosphere compartments exhibit dependence on assumed values of S_l^{pi} and b the ranges of which are substantially limited by the observational constraints on the range of (S_l^{pi}, b). The resulting limitations in range are shown

995 by superposition of the light red quadrilateral in (S_l^{pi}, b) space shown in **Fig. 9d** onto the contour diagrams for the several transfer coefficients; similarly also onto contours for $S_{l,ant}^{pd}$ and dS_l^{pd}/dt , **Fig. 3**.

7.5. Response of stocks and fluxes to hypothetical abrupt cessation of emissions

As noted in **Sect. 7.1**, in addition to the model runs over the Anthropocene using historical emissions, an abrupt cessation experiment was carried out in which anthropogenic emissions were set to zero commencing in 2017, yielding stocks of

1000 carbon in the several compartments as if emissions had ceased subsequent to that year. Results presented in **Fig. 7a** for the example (S_l^{pi}, b) = (400 Pg, 0.6) show peaks in modeled stocks in the AC, LB, and ML at (or within a year or two of) cessation of emissions. Subsequent to cessation the anthropogenic stocks in these compartments all decrease; the time period shown, nearly 200 years following cessation, encompasses that over which atmospheric CO_2 would decrease substantially toward its preindustrial value, the time period of principal interest in this study. For this particular set of parameters the

1005 anthropogenic stock of atmospheric CO_2 decreases to $1/e$ of its value at the time of cessation in 115 years. In contrast the stocks in the DO and the OB continue to increase, thus exhibiting continued removal of carbon from the AC, ML and LB.

The peaks in the stocks in these three compartments are followed by decreases over the next 200 years or so as CO_2 is transferred into the DO and the OB, which are sink compartments on this time scale, the total anthropogenic carbon remaining constant. Over this time period atmospheric CO_2 recovers substantially toward its preindustrial value, establishing

1010 that it is this time period that is pertinent to the lifetime of excess CO_2, as set out in the Introduction.

The rates of change of the several stocks dS_i/dt subsequent to cessation differ qualitatively, **Fig. 7b**. The abrupt decreases and change in sign from positive to negative in the rates of change of S_a, S_l, and S_m shown in **Fig. 7b** show that the stocks in these compartments begin to decrease immediately upon cessation of emissions. The rate of change the stock in the AC $\delta(dS_a/dt)$ exhibits a step-function change of sign, going from positive to negative, as it is no longer driven by emissions,

1015 which, prior to cessation, exceeds loss by transport into other compartments. The magnitude of the decrease in dS_a/dt at the time of cessation, $\delta(dS_a/dt)$, is roughly equal to the present rate of anthropogenic emissions, about 10 Pg yr^{-1} (**Fig. 2**); after cessation the rate of change in S_a consists only of the transport terms. The rates of change of the stocks of the ML and the LB exhibit similar step-function change of sign, as these changes are driven mainly by the annual change in the atmospheric stock, now negative rather than positive. The magnitude of decrease in dS_m/dt, $\delta(dS_m/dt)$, is roughly equal to

1020 $(K'_{ma})^{-1}\,\delta(dS_a/dt)$, **Eq 4.3**; for $(K'_{ma})^{-1}$ about 0.1 at present, **Table 2**, $\delta(dS_m/dt)$ is about 1 Pg yr^{-1}. Similar considerations apply to $\delta(dS_l/dt)$, but with magnitude depending on the parameters S_l^{pi} and b.

In contrast to the AC, ML, and LB, the sink compartments DO and OB continue to exhibit positive rate of increase after cessation of emissions, and the rates of net transfer into the two sink compartments the DO, $F_{md}^{ant,net} = dS_d/dt$, and the OB, $F_{ao}^{ant,net} = dS_o/dt - Q_{LUC}$, (**Fig. 7b**) are initially unchanged, **Fig. 7c**. (The abrupt increase in dS_o/dt at year 2017 is due to

1025 cessation of LUC emissions, after which time dS_o/dt coincides with $F_{ao}^{ant,net}$.) The net fluxes into these compartments are driven by the differences between the stocks in the AC or ML and the respective sink compartments, which do not immediately change at the time of cessation. Over time as the stock in the AC and ML decrease, all derivatives approach zero as the system approaches a new steady state, with the integrated emissions being apportioned to the several compartments as indicated at year 2200 in **Fig. 7a**. Importantly, for values of these parameters consistent with observational

1030 constraints, the excess atmospheric CO_2 due to anthropogenic emissions decreases greatly following cessation of emissions, with the long-term value of x_{CO2} at 300 years after cessation ranging from 297 to 307 ppm (**Fig. 11a**) or 15 to 23 % of the increment in atmospheric stock at the time of cessation, demonstrating the substantial reduction in x_{CO2} following cessation that is a premise of the definition of adjustment time. The long-term evolution of atmospheric CO2 is further examined in **Sect. 7.9**

7.6. Turnover times and adjustment times of excess CO_2

1035

As noted in conjunction with **Eq 2.2** the turnover time of a substance in a reservoir can be evaluated as a function of time as the quotient of the pertinent stock upon the leaving flux. For CO_2 in the biogeosphere identification of pertinent stock or stocks and leaving flux or fluxes is not immediate because of exchanges between reservoirs. If these exchanges are rapid, then it is useful to consider the stocks in the pertinent compartment(s) as a single stock in the numerator, and the sum of the

1040 leaving fluxes from that joint compartment as the denominator. As suggested by comparison of the time constants for establishing equilibrium between the ML and the AC (about a year, **Sect. 5.3**) and for establishing steady state between the LB and the AC (1-3 yr, **Sect. 5.7**) with the present-day observationally determined turnover time of CO_2 in the three compartments taken together (54 – 114 years, **Sect. 5.9**), it seems useful to consider these three compartment as a single stock for purpose of evaluating the turnover time from the model results. This assumption is confirmed by the close

1045 agreement between the ESS model and the full model, **Sect. 7.7**.

The several turnover times and adjustment times defined in **Sect. 2** are compared in **Fig. 12a** using the model results prior and subsequent to cessation of anthropogenic emissions, again for the example of (S_l^{pi}, b) = (400 Pg, 0.6). As noted in **Sect. 2**, turnover times can be evaluated at all times from the budget or from a model, whereas the several adjustment times can be evaluated only in the absence of anthropogenic emissions, requiring a numerical model (or actual cessation of anthropogenic

1050 emissions). Several points should be noted in comparing these lifetimes. For the parameter values of the example, prior to cessation of emissions the instantaneous turnover time for the atmospheric stock τ_a^{to} is about 45 years, that for the combined AC-ML compartment τ_{alm}^{to} is about 54 years, and that for the AC, LB, and ML combined τ_{alm}^{to} is about 112 years. The PD values from the model agree closely with those determined from the PD budget, shown by the filled markers in the figure; such agreement at present is expected because the model parameters are obtained from the observed budget. At the time of

1055 cessation of emissions τ_a^{to} and τ_{alm}^{to} rapidly increase to essentially the same value as τ_{alm}^{to}; in contrast τ_{alm}^{to} remains unchanged. The reason for the increases in τ_a^{to} and τ_{alm}^{to} is that the net leaving fluxes from the AC to the LB and the ML are quickly diminished upon cessation of emissions, **Fig. 7b**, which, with S_a and S_m initially remaining constant, results in the rapid increases in τ_a^{to} and τ_{alm}^{to}. Such a change in turnover time upon the change in emissions is indicative that the turnover time so defined is not an intrinsic property of the system. In contrast, the turnover time τ_{alm}^{to} being unchanged upon

1060 cessation of emissions is indicative that this quantity is intrinsic to the system as opposed to being dependent on the rate of anthropogenic emissions. The reason for the constancy of τ_{alm}^{to} across the cessation is likewise readily understood from the stocks, **Fig. 7a**, and the leaving fluxes, $F_{md}^{ant,net} = dS_d/dt$, **Fig. 7b**, and $F_{ao}^{ant,net}$, **Fig. 7c**, both being continuous across the cessation.

After cessation the turnover times for the AC τ_a^{to} and for the combined AC-ML compartment τ_{am}^{to} rapidly approach that for

1065 the combined AC-ML-LB compartment. This is also readily understood. Because the time constants for establishing

equilibrium and steady state among these compartments are short, the stocks are all proportional to each other and the leaving fluxes are proportional to the individual stocks, **Sect. 7.7**. Hence the ratio of stock to leaving flux is the same for the AC and for the combined AC, ML, and LB compartment. The agreement of the three turnover times subsequent to cessation is further confirmation of the utility of treating the three compartments as a single compartment for the purpose of evaluating

1070 the turnover time at all times. Additionally, the three turnover times coincide also with the instantaneous adjustment times subsequent to cessation. Of course the ambiguity associated with the choice of turnover time does not attach to the definitions of the adjustment times. However the agreement of τ_{alm}^{to} with the adjustment times τ_a^{adj} and τ_{alm}^{adj} in the model calculations, once again demonstrates the necessity of treating the three compartments together in evaluating the turnover time from observational data. The agreement of the lifetimes determined by the several approaches before and after cessation

1075 of emissions confirms that the lifetime of excess CO_2 so determined being due to the workings of the controlling geophysical processes and not an artifact that is due to the temporal profile of anthropogenic emissions.

Subsequent to cessation of emissions, the atmospheric stock of CO_2 decreases as shown in **Fig. 8a** and in **Fig. 12a**, again for the example (S_l^{pi}, b) = (400 Pg, 0.6). As the net leaving fluxes diminish more rapidly than the excess stocks, the instantaneous turnover time and the instantaneous adjustment time, which are temporally local measures of the normalized

1080 removal rate, increase, substantially, **Fig. 12a**, over the time period over which the stocks decrease, from about 110 years at the time of cessation, for this example, to about 225 years in year 2200, by which time anthropogenic atmospheric CO_2 has decreased to about 25 % of its value at the time of cessation. In contrast, the increases are much less in the several adjustment times that are evaluated over a time horizon extending from the time of cessation to a given time of interest: the time-average adjustment time τ_{t-avg} (**Eq 2.4**); the amount-weighted average adjustment time (**Eq 2.5**); and the equivalent

1085 $1/e$ lifetime τ_E, (**Eq 2.6**) shown as a function of time horizon in **Fig. 12a**, all three of which agree closely. For the example examined here, the amount-weighted average adjustment time τ_{a-avg} at year 2200, has increased only to 128 years.

Also shown in **Fig. 12a** is a fit of a decaying exponential function, with zero baseline, to the fraction of excess atmospheric CO_2 at the time of cessation remaining as a function of time subsequent to cessation; the fit was carried out for the initial 100 years subsequent to cessation with annual points equally weighted. The fit closely matches the modeled profile, over the

1090 indicated time period, during which, for this example, CO_2 has decreased to 40 % of its value at the time of cessation. The resultant time constant for this example τ_{CO2Fit} is 105 yr, in close agreement with the other measures of the adjustment time. In sum multiple measures of the lifetime – the turnover time for the combined AC-LB-ML stocks, and the several definitions of the adjustment time – all yield values for the lifetime that agree closely, which, for the example examined, is about 110 yr.

The dependence of τ_{t-avg}, τ_{a-avg}, and τ_E on the fraction of excess CO_2 present at the time of cessation that remains in the

1095 system, **Fig. 12b**, shows the near equality of these several measures of adjustment time until this fraction plateaus out at the

long time value, about 16 %; see also **Sect. 7.9**. Also shown, top axis, is the time since cessation of emissions corresponding to the fractional decrease of excess atmospheric CO_2 on the bottom axis. Throughout the period of time over which CO_2 recovers substantially to its preindustrial value these three measures of adjustment time increase only slowly, until finally abruptly increasing as the plateau is reached.

1100   The same examination of multiple measures of lifetime was carried out for parameter values S_l^{pi} ranging from 0 to 1000 Pg at intervals of 100 Pg, and b, ranging from 0 to 1.3 at intervals of 0.1; the results for the multiple measures of the lifetime are shown in **Fig. 11b-d**. **Fig. 11b** presents the PD turnover time for the combined AC-LB-ML compartment, τ_{alm}^{to} evaluated algebraically as in **Sect. 5.9** for observationally constrained uptake extent and rate in the AC and the ML and for $S_l^{ant,pd}$ and $dS_l^{ant,pd}/dt$ calculated as a function of parameters S_l^{pi} and b. This turnover time compares well with two measures of

1105   adjustment time, the time constant obtained by fit to decay curves of for atmospheric CO_2 over the first 100 years after cessation of emissions τ_{CO2}^{fit} and the equivalent $1/e$ lifetime evaluated at 100 years after cessation $\tau_E(100\ yr)$. The close agreement of these several measures of lifetime throughout the observationally constrained ranges of S_l^{pi} and b provide yet enhanced confidence to the lifetime determined in any of these ways as an accurate measure of the time scale over which, in the absence of anthropogenic emissions, atmospheric CO_2 would recover to its preindustrial value. The range of decay

1110   curves consistent with observationally constrained range of (S_l^{pi}, b), with time constants 70 to 140 years (**Fig. 11c**), is shown also by the central value and the limits of the light red band in **Fig. 1a**. Plotted there on a semilogarithmic scale, these decay curves exhibit slight upward curvature over the 100 year time period examined, consistent with slight increase with time subsequent to cessation of the instantaneous adjustment time (inverse of local slope, apart from a factor of ln 10). The three profiles shown, and more generally all the profiles within the indicated range, exhibit near exponential decay during the time

1115   over which atmospheric CO_2 recovers substantially to its preindustrial value.

7.7. Accuracy of equilibrium–steady-state (ESS) assumption

The accuracy of the assumptions of equilibrium between and atmosphere and the ML and of steady state between the atmosphere and the LB the ESS model (**Sect. 6.3**, **Appendix D**) was examined by running the ESS model for the same conditions as the full model. In brief, as shown in **Fig. 13a-e** for a particular pair of S_l^{pi} and b, these assumptions are quite

1120   accurate. Specifically, the several panels show the anthropogenic stocks (difference between modeled stock and preindustrial value) in the several compartments as evaluated by the exact model (**Eqs 6.1 - 6.5**) and by the ESS model (**Eqs 6.3, 6.5, D10**) for S_d, S_o, and S_a, respectively, together with algebraic expressions (**Eqs D2**, **D5**) for S_m and S_l, respectively. Demonstrating the accuracy this model with a reduced set of differential equations is of little importance in terms of improving the capability of solving the system of ODEs. Rather, its importance is in establishing the utility of considering

l125 the three compartments, the AC, LB, and ML as a single compartment in which the amount of carbon rises or falls together, for the purpose of defining a turnover time pertinent to excess CO_2. The turnover time for the stock in this combined compartment defined under this assumption by **Eq 5.4** and evaluated from observations in **Sect. 5.9** was compared in **Sect. 7.6** with the turnover time evaluated from the model results and with several measures of the adjustment time of excess CO_2 defined in **Sect. 2**. **Figure 13f** compares the anthropogenic stocks in the AC, S_a; ML, S_m; and LB, S_l; each normalized to its

l130 value at the time of cessation of emissions. The close agreement of the three curves demonstrates the proportionality of the several compartments. Hence the several adjustment times pertinent to these reservoirs or combined reservoirs are essentially identical, as shown in **Fig. 12a**.

7.8. Comparison with results from carbon-cycle models and with observations

The results obtained with the present model are compared to those from studies with carbon cycle models of various

l135 complexity and with observations over the past 150 years (**Fig. 14**), and over the past 60 years (**Fig. 15**), for which contemporaneous *in-situ* measurements of atmospheric CO_2 are available. In these figures results from the present model are shown for three values of the parameter pairs (S_l^{pi}, b), specifically (400 Pg, 0.6), (600 Pg, 0.5), and (200 Pg, 0.6), spanning the range of values consistent with observations, **Fig. 9**. As seen in the several panels of **Fig. 14 and Fig. 15**, the modeled quantities are virtually insensitive to the parameters within the indicated range and hardly distinguishable on the scales of the

l140 figures. The present results for atmospheric CO_2 mixing ratio, **Fig. 14a**, exhibit substantially better agreement with measurements than most of the models shown. With respect to the several fluxes, the present model results are broadly consistent, in magnitude and slope, with those obtained with CC models. Perhaps the most striking difference is that the present results exhibit less, to substantially less, interannual fluctuation than individual CC models and, for net flux to the terrestrial biosphere, than the multi-model mean (**Fig. 15b**); these fluctuations result from year-to-year variation in the

l145 meteorological and other processes governing these fluxes on short time scales being represented in the CC models but not in the present model.

In the early years of the run the present model shows significantly greater net atmosphere-to-ocean flux than the CC models (**Fig. 14b**). This is attributed to the CMIP protocol initiating the runs from a prescribed steady state at 1850 and reckoning anthropogenic uptake relative to the flux at that time. The greater flux in the present model results is attributed to the

l150 increase in CO_2 between the start of the present model run, 1750, and 1850 (consistent with measurements, **Fig. 8a**) that gives rise to a net anthropogenic flux into the ocean, with magnitude in 1850, 0.16 Pg yr^{-1}, essentially the same as the difference between the flux calculated with present model and the mean of the CMIP models.

The net anthropogenic flux from the atmosphere to the ocean (ML + DO) determined with the present model is compared also to several measurement-based determinations in **Fig. 15a**. Here it is noted, as pointed out, for example, by Gruber et al.

1155 (2009), that inferring the anthropogenic flux from the net atmosphere-ocean flux (as determined from fluxes calculated as the spatial and temporal integral of the product of the local windspeed-driven transfer coefficient times the local partial pressure difference between atmospheric and dissolved CO_2) requires augmenting the measured net flux by an amount equal to the riverine flux into the ocean that gives rise to a flux from ocean to atmosphere; this riverine flux is assumed to be equal to the preindustrial value (taken as 0.6 Pg yr^{-1}; **Sect. 3; Fig. 2**). For this reason the time series presented by Landschützer et al.

1160 (2015) and by Wang et al. (2016) shown in **Fig. 15a** have been augmented from those given by those investigators by 0.6 Pg yr^{-1}; the time series shown for Rödenbeck et al., (2014) obtained from Le Quéré et al., (2018a) appears to have incorporated that augmentation; the value shown for Takahashi et al. (2009) is that given by those investigators, incorporating their estimate of the riverine flux as 0.4 ± 0.2 Pg yr^{-1}. In contrast, no augmentation is required for the rate of uptake of anthropogenic carbon determined by Graven et al. (2012), which was scaled to the rate of transfer of excess $^{14}CO_2$ (from

1165 nuclear weapons testing in the 1950's and 1960's) from the ML to the DO that was based on measured difference in radiocarbon amounts between the 1988–1995 and 2001–2007 time frames; this uptake, like that of anthropogenic CO_2, is now governed principally by transfer from the ML to the DO. Likewise no such augmentation is required for the flux determined by Gruber et al. (2019), which is based on the rate of increase in the amount of DIC in the world ocean, determined by difference over the time period 1994-2007. In addition to the several determinations shown in **Fig. 15a**,

1170 attention is called also to inference of the oceanic uptake rate by multiple methods summarized by Gruber et al. (2009, Table 1) that is centered about the range 1.5–2.2 Pg yr^{-1} over the 1990's and early 2000's. As seen in **Fig. 15a**, the oceanic uptake rate obtained with the present model is somewhat lower than most observational determinations but within their uncertainty range, except for that of Gruber et al. (2019), which is somewhat greater.

Net uptake by the ocean plus TB in the present model results shows close agreement in magnitude and slope with the

1175 measurement-based determination of this quantity calculated as the difference of emissions and atmospheric growth rate over this period, **Fig. 15c**. The major difference between the temporal profiles of the mixing ratios and transfer rates calculated with CC models versus those obtained with the present model is again the presence of year-to-year fluctuations in the CC model results versus the absence of such fluctuations in the present model results. The agreement between the model and the measurements is consistent with the assumption that k_{at} has not undergone large systematic change over this period.

1180 Comparison (**Fig. 15d**) of the difference between the observed net uptake by the ocean + TB and that calculated by the present model with the difference between observation and the multimodel mean of the ensemble of models presented by Le Quéré et al. (2018a; GCB-17) shows the skill of the present model to be essentially identical to that of the model ensemble.

7.9. Modeled atmospheric CO_2 at longer time scales

Although the emphasis here has been the period of time, roughly 100-200 years, over which atmospheric CO_2 substantially
recovers to its preindustrial value, the longer term behavior of modeled CO_2 was briefly examined for values of the
parameters (S_l^{pi}, b) consistent with observations to 700 years subsequent to cessation of emissions. For the parameter pairs
shown in **Fig. 16**, and more generally for all the parameter pairs, atmospheric CO_2 approaches a constant value at 300 years,
about 16 % to 22 % of the value at the time of cessation, decreasing only very slightly thereafter.

8. Discussion

The budget of CO_2 in the atmosphere and related compartments is of central importance to Earth's biogeochemical
environment as well as of enormous societal importance in view of its role as a driver of climate change and other
environmental issues. A key objective of this study has been determination of the lifetime (turnover time, adjustment time)
of excess CO_2, the amount in excess of preindustrial, as this lifetime is central to understanding the response of CO_2
amount, and resulting changes in climate, to prospective changes in emissions. Knowledge of the lifetime of excess
atmospheric CO_2 is also central to comparisons of integrated radiative forcing of anthropogenic CO_2 and other greenhouse
gases.

This study has examined the processes controlling the amount of atmospheric CO_2 by two approaches: an observationally
based budget for preindustrial and present day conditions and a simple numerical model representing the governing
processes in response to historical anthropogenic emissions. The two approaches are complementary and consistent. Both
approaches examine the atmosphere and the several compartments of the biogeosphere that are closely coupled to the
atmosphere: the ocean, distinguished into the mixed layer ocean and the deep ocean, and the terrestrial biosphere,
distinguished into what are denoted the labile and obdurate biosphere. Stocks in the several compartments and fluxes
between compartments are constrained so far as possible by well characterized geophysical processes, chemical equilibria,
inventories, mass balance, and measurements. The exception to such constraints is the apportionment of the uptake of CO_2
by the TB into the labile and obdurate compartments, which is achieved by use of adjustable parameters. This use of
adjustable parameters is necessary because of the lack of a clear demarcation between these compartments, which are
idealizations of what is clearly a continuum, and by the absence of measurements or theory that would permit such
constraint. As a consequence the apportionment is treated in the numerical model by parameterization of quantities
controlling the rate of uptake of anthropogenic CO_2 by the labile biosphere, specifically the preindustrial carbon stock in the
LB S_l^{pi} and the exponent b expressing the growth of GPP as a power law in CO_2 mixing ratio. Despite the uncertainty
attached to this apportionment it has proved possible to rather narrowly constrain the lifetime of excess atmospheric CO_2.

The present study is hardly the first to represent the dynamics of CO_2 in the biogeosphere in a model with a small number of compartments and parameters, there being antecedents that go back at least to Bolin and Eriksson (1959), Keeling (1973), Oeschger et al., (1975) and Rodhe and Björkström (1979), and that see occasional use up to the present, (e.g., Gloor et al., 2010, Raupach et al., 2014; Graven, 2015). However this study would seem to go substantially beyond those studies by identifying the two biogeophysical parameters that control the lifetime of excess atmospheric CO_2, by observationally constraining their joint range, and by examining their influence on multiple measures of this lifetime.

8.1 Definitions of the lifetime of excess CO_2

The lifetime of excess atmospheric CO_2 was qualitatively defined in **Sect. 2** as *the amount of time it would take, in the absence of anthropogenic emissions, until the CO_2 concentration in the air recovered substantially toward its original concentration*. However, even granting concurrence on this qualitative definition, selecting a specific definition has been problematic, not just for CO_2, for which the situation is complicated by exchange processes between the atmosphere and other compartments, but even for substances for which the removal process from a compartment is irreversible, for which several measures that would coincide in the case of removal with a temporally constant transfer coefficient – the turnover time, the inverse of the fractional removal rate; the *e*-folding time, the mean residence time in the compartment, the mean age of molecules in the compartment – are not necessarily identical even with steady-state emissions, and all the more so with temporally varying emissions and transfer coefficient (Schwartz, 1979; O'Neill et al., 1994, Sierra et al., 2017). Moreover, because of short-term fluctuations in fluxes such as seasonal drawdown by terrestrial vegetation, the turnover time, which remains defined even under non–steady-state conditions (Schwartz, 1979), would have to be evaluated over suitably long periods of time, several years, to average out interannual fluctuations that are manifested in observations (**Fig. 15c**).

Within the qualitative definition above, two classes of lifetimes emerge: adjustment times and turnover times. Ideally, as adjustment times are measures of the time over which the substance in question would decline in the absence of anthropogenic emissions, they would be the desired quantity. However determination of an adjustment time requires a model of future behavior of the system in response to cessation of emissions. For that reason the approach via turnover times seems more attractive as these can be evaluated from observations at any time, not requiring a model of future response. However, especially in the situation of reversible flows between reservoirs, the difficulty arises of identifying the pertinent leaving reservoir and the pertinent exit fluxes. Because of these twin difficulties, determining both the turnover times and the adjustment times would seem to be the most reliable approach, with identification of pertinent specific definitions based on agreement between the two classes of lifetimes. Also as turnover times can be evaluated from model results, the future

turnover times according to specific definitions can be compared with the future adjustment times, with agreement lending further confidence to the definition.

Lifetimes evaluated by the definitions presented here are compared with previously reported values in **Sect. 8.7**

8.2 Budget

1245 Central to determining turnover and adjustment times is the requirement of a budget, for atmospheric CO_2 and for carbon in the closely coupled biogeochemical compartments, here the mixed-layer and deep ocean, and the labile and obdurate biosphere. Following prior work, budgets were developed both for preindustrial conditions and for the anthropogenic perturbation, the latter as the difference between present-day and preindustrial budgets.

The CO_2 budget developed here is based 1) on observations (of stocks in the several compartments and their increase over 1250 the Anthropocene) and inventoried emissions; 2) on an essentially universal exchange velocity, k_{am}, between the atmosphere and the surface ocean that is applicable, accounting for differences in Henry's law solubility, to all low- to moderate-solubility gases, together with well understood chemical equilibria governing the dissolution of CO_2 into seawater; 3) on an essentially universal piston velocity between the mixed-layer ocean and the deep ocean, v_p, that is applicable to all globally distributed tracers, determined here from the rate of heat uptake by the global ocean and consistent with other 1255 measurement- and model-based estimates of this quantity; 4) the requirement of steady state in the preindustrial carbon cycle; and 5) the requirement that the amount of CO_2 in the system be conserved, more specifically that the amount of excess CO_2 in the system at any given time be equal to integrated fossil fuel emissions (also including emissions from cement manufacture). All stocks and fluxes are directly constrained except for the exchange of excess CO_2 between the atmosphere and the terrestrial biosphere and the associated changes in the stocks in the two TB compartments. The sum is 1260 obtained, by conservation of matter, as a difference between total anthropogenic emissions and the sum of atmospheric growth and net flux into the ocean, with the apportionment of the total uptake by the TB between the LB and the OB being parameterized; the stock of the OB is diminished by transfer of LUC emissions the atmosphere.

The budget developed here and summarized in **Fig. 2** differs in several key respects from similar earlier budgets, as summarized in predecessor versions of that figure and that served as the starting point for the budget developed here. 1265 Importantly, the terrestrial biosphere, treated as a single compartment in previous budgets derived from Sarmiento and Gruber (2002), is subdivided here into the labile and obdurate compartments, each with its own stocks and entering and leaving fluxes. The distinction between short- and long-lived components of the TB was drawn early on in the history of compartment models for CO_2 (e.g. Keeling, 1973) but has yet to make its way into assessments of global carbon budgets such as those of the IPCC Assessment Reports (AR5, Ciais et al., 2013) and the Global Carbon Budget (Le Quéré et al., 1270 2018*a*) which report total uptake by the TB as a residual of emissions minus increases in the stocks of the atmosphere and

ocean compartments, often, somewhat misleadingly, referring to total uptake by the TB so evaluated as a "terrestrial sink," or "land sink," a terminology going back at least to Sarmiento and Gruber (2002). To be sure, in the absence of observable constraints, and indeed of physically meaningful boundaries between the two terrestrial subcompartments, the separation into the two compartments is arbitrary, but it seems essential to distinguish the growth of the short- and long-lived components of

1275 the TB. In the analysis presented here it has proved possible to set bounds on the apportionment of the stocks and fluxes for the LB and the OB and thereby to set bounds on the pertinent transfer coefficients.

A second, related difference between the budget presented in **Fig. 2** and its antecedents is the treatment of gross primary production not as a constant but as subject to increase over the Anthropocene, the increase being attributed to fertilization by the increase in atmospheric CO_2. Again, such increase in GPP has long been countenanced but has proved difficult to

1280 quantify. In the present model the increase is parameterized as a power-law dependence in atmospheric CO_2 mixing ratio, with exponent b. It proved possible on the basis of observations, together with the model developed here, to set bounds on b, and in turn on the increase in GPP. However these bounds, although consistent with the range of current estimates of such increase (**Appendix C, Fig. C1),** do not usefully limit that range. The lower bound, $b = 0.4$, corresponding to an increase in GPP over the Anthropocene of 16 %, is seen in some of the observational data sets and model results. The upper bound, $b =$

1285 0.9 would correspond to an increase in GPP of 40 %. Based on these results it would seem that an exponent as great as 1.3, as indicated in the results of Cheng et al. (2017), based on water-use efficiency, is inconsistent with the present model and should perhaps be examined more closely. However, several of the model results, which yield values of b near the upper limit determined here ($b \leq 0.9$), cannot be precluded based on the present analysis.

The budget analysis yields coefficients that describe the rates of transfer of CO_2 between the several compartments, **Sect. 4**.

1290 Because of lack of observational constraint in the apportionment of uptake of carbon by the TB to the LB and the OB, the transfer coefficients coupling the AC with the LB and with the OB are dependent on the parameters S_l^{pi} and b, **Fig. 4**. Specification of the transfer coefficients in turn permits specification of the pertinent time constants of the system, those responsible for establishing near equilibrium or steady state between stocks, those governing the lifetime of carbon in the long-term reservoir compartments the DO and the OB, and those controlling the turnover time of atmospheric CO_2 pertinent

1295 to transfer into the long-term reservoirs. Because of rapid attainment of near equilibrium between the AC and the ML, and of near steady state between the AC and the LB, the stocks in these three compartments are usefully considered a single stock for definition of the turnover time of anthropogenic CO_2. The transfer coefficients determined in this way also serve as input to a simple, transparent numerical model describing the anthropogenic perturbation to the carbon stocks in the several compartments. The numerical model presents a much more differentiated picture of the stocks and fluxes as a function of

1300 historical time that compares well with observations.

8.3 Model

The model developed here and set out in **Sect. 6.1** consists of a set of ordinary near-linear differential equations in the stocks in the five compartments, driven by anthropogenic emissions; an essentially identical model was employed for radiocarbon, **Appendix E**. Because of conservation of total carbon either set of equations may be considered a five compartment closed system or a four-compartment open system. Because of relations among the several transfer coefficients only four independent parameters are required to generate the set of transfer coefficients (**Sect. 4.5**), of which two are of broad geophysical applicability (albeit uncertain), and of which two are pertinent specifically to CO_2, also uncertain, and treated here as adjustable. The transfer coefficients were determined from the budget analysis; the transfer coefficients coupling the LB and OB with other compartments are parametrically dependent on the fertilization exponent b and the preindustrial stock in the LB S_l^{pi}. The equations are slightly nonlinear because the rate of transfer from the AC to the LB (*i.e.*, GPP) is treated as a power law in S_a and because the coefficient k'_{ma} characterizing the rate of transfer from the ML to the AC varies slowly with the stock in the ML. The model was run for a suite of values of both parameters to map out the stocks and fluxes as a function of these parameters, the uncertainties in the transfer coefficients being propagated through the model by multiple runs over the domain of parameter space. The model was run for historical anthropogenic emissions from 1750 to 2016 permitting comparison with observations, which comparisons led to substantial reduction of the parameter range from that initially taken. An experiment was also conducted, again over the range of parameter space, with emissions abruptly ceased commencing in 2017 to examine the subsequent changes of the anthropogenic stocks in the several compartments: decrease in the short-lived compartments – the AC, the ML, and the LB – and continued increase in the long-term sink compartments – the DO and the OB. That abrupt cessation experiment also permits comparison with other studies conducting similar abrupt cessation experiments, **Fig. 1, Fig. 16**. As seen in these figures, the rate of decrease of excess atmospheric CO_2 mixing ratio (equivalently, the stock in the AC) found in the present model study is substantially greater to much greater than given by results of a suite of carbon cycle models.

A key attribute of the present numerical model is that the quantities that govern the evolution of CO_2 – transfer coefficients and equilibrium constants – are physical quantities, properties of Earth's geophysical system, which would be expected to remain constant or to vary only slowly in the future from the values developed in the budget analysis, lending confidence to application of the model to prospective future emissions that might differ substantially from prior emissions. This approach is to be contrasted with an approach such as that of Hellevang and Aagaard (2015), which uses as a parameter the airborne fraction, fraction of annual emitted CO_2 that remains in the atmosphere; this quantity cannot be expected to be a constant for very different emission conditions, the extreme situation being cessation of emissions. The constancy of airborne fraction over much of the Anthropocene is a simple consequence of exponentially increasing emissions in a linear system (Bolin and Eriksson, 1959; Raupach, 2013). However even with parameters that correspond to physical quantities it is possible, as

demonstrated in **Fig. 8**, to accurately represent prior observations, here of atmospheric CO_2 over the Anthropocene, with model variants that diverge substantially subsequent to cessation of emissions. Past performance of a model is no guarantee of future skill. Hence as much information as possible must be brought to bear to constrain the model. Accurate reproduction

1335 of the evolution of atmospheric and oceanic radiocarbon (**Sect. 7.3**), especially for the sharply peaked emissions of radiocarbon from weapons testing, **Fig. 10**, provides an important stringent test of this or any model, as well as providing additional constraints on the values of the parameters S_l^{pi} and b employed in the present model.

8.4 Equilibrium–steady-state assumption

A three-equation version of the model was developed incorporating the assumptions of equilibrium between the stocks in the

1340 AC and the ML and steady state between the stocks in the AC and the LB. This ESS model accurately reproduces the results of the full model. As noted in Sect. 7.7 there is no advantage to be gained by reducing the number of equations to be solved. Moreover the ESS model suffers from lack of transparency and the potential for algebraic or coding errors. Rather the import of the model is to confirm the utility of considering these three compartments as a single compartment for evaluation of the turnover time of excess CO_2. The conclusion of near equilbrium between the AC and the ML, reached as early as Bolin and

1345 Eriksson (1959), is thus extended to incorporate the LB, mandating treating the combined AC-LB-ML stocks as a single stock for the purpose of defining and evaluating the turnover time of the system appropriate to excess CO_2.

The near-equilibrium between the stocks in the AC and the ML implies that the rate of uptake of CO_2 by the ocean is controlled mainly by the rate of exchange of DIC between the ML and the DO and is thus insensitive to the transfer rate between the AC and the ML. Such a conclusion has been recognized for some time (Bolin and Eriksson, 1959; Broecker and

1350 Peng, 1974; Sarmiento et al., 1992). This conclusion is supported as well by the finding of Graven et al. (2012), in large-scale model calculations, of only slight dependence of the inventory of anthropogenic CO_2 in the world ocean on the value of the transfer velocity between the AC and the ML. The departure from equilibrium between the AC and the ML was examined by a somewhat different approach by Broecker et al. (1979) by varying the depth of the ML for fixed transfer coefficients between the two compartments. For ML depth taken as 75 m, the departure was only 3 % and even for ML depth

1355 taken as 380 m, the departure was only 8 %, again lending strong support to treating the two compartments as at equilibrium.

In a subsequent examination of transport of CO_2 between the atmosphere and the ML, Takahashi et al. (2009) found that transfer coefficients calculated using local (4° × 5°), monthly-mean wind speed and other conditions obtained from a meteorological reanalysis ranged widely, by season and location, with monthly- and basin-average values a factor of two either way from the global- and annual-mean that they determined, 0.112 yr^{-1}. That mean value is essentially identical to the

1360 value of k_{am} determined here from the global-mean stocks and fluxes (**Sect. A4**) and presented in **Table 2** and **Fig. 5**, 0.119 ± 0.036 yr^{-1}. Based on examination of measurements of CO_2 in the AC and the ML over three decades, Takahashi et al.

(2009) concluded that because of the differences between processes and time-scales regulating the stocks in the two compartments, it was not possible to reliably determine annual changes for CO_2 in surface water. Those investigators also concluded that because of large seasonal variation and small annual increases, the individual annual rates could not be

1365 compared. Nonetheless Takahashi et al. (2009) were able to conclude that over the three-decade period examined, the relative rates of increase of the atmospheric partial pressure of CO_2 and of the equilibrium partial pressure of CO_2 in surface water were similar and that air-sea CO_2 exchange is dominant in regulating CO_2 in the ML. That analysis certainly supports the conclusion that the rate of transfer is sufficiently rapid to support the assumed near-equilibrium between the anthropogenic stocks in the two compartments. Finally in this context it might be observed that the rapid two-way exchange

1370 of CO_2 between the AC and the ML, and the resultant inevitable large spatial and temporal variation of the magnitude and sign of the local flux, would also make it challenging to determine the global net flux from the atmosphere to the oceans by spatial and temporal integration of local short-term fluxes.

8.5 Flux and transfer coefficient from ML to DO

Because of the near equilibrium between the AC and the ML, transfer from the ML to the DO is the rate controlling step in

1375 net uptake of CO_2 by the DO and thus assumes considerable importance in the dynamics of CO_2 in the biogeosphere. Exchange between the ML and the DO applies also to other uniformly distributed tracers, specifically including heat, as the excess heat in the two compartments arising from increase of global mean temperature over the Anthropocene resides almost entirely in the ML. This reasoning served as the basis for inferring the piston velocity determined here 5.5 ± 1.8 m yr^{-1} (**Appendix A, Sect. A6**), resulting in the gross PD downward carbon flux determined here 1.8 ± 0.6 Pg yr^{-1} (**Appendix A,**

1380 **Sect. A11**). This result is compared here to results from other recent studies.

Using a global inverse model, DeVries et al., 2017 quantified variations in basin-wide and global scale exchange rate between the ML and the DO. While showing a rather more differentiated picture of transport between the ML and the DO than is represented by a single global-mean value of the piston velocity, that study determined global-mean volume exchange rates, expressed as piston velocities, for the 1980's, 1990's and 2000's, as 4.98, 6.29, and 4.28 m yr^{-1}, respectively,

1385 bracketing, and all within the uncertainty range of, the result determined here based on global-mean uptake of heat by the deep ocean over the past 45 years, 5.5 ± 1.8 m yr^{-1} (**Appendix A, Sect. A6**).

Reasoning that because the main reservoir of $^{14}CO_2$ produced in weapons testing, which ceased in the 1960's, has shifted from the atmosphere to the upper ocean, Graven et al. (2012) concluded that the temporal change of this $^{14}CO_2$ is now governed by exchange between the ML and the DO, as also with anthropogenic CO_2, and can hence be used to infer oceanic

1390 uptake of anthropogenic CO_2. On the basis of the distribution of $^{14}CO_2$ between the two compartments those investigators were able to determine the net oceanic uptake of anthropogenic CO_2 between 1990 and 2007 as 2.0 ± 0.3 Pg yr^{-1} (**Sect. 7.8,**

Fig. 15a); To compare this net oceanic uptake to uptake by the DO, the oceanic uptake rate must be diminished by the rate of increase in the ML stock, which is confidently determined as 10 % (**Sect. 5.10**) of the rate of increase of S_a in this time frame, 4 Pg yr^{-1} (**Supporting information Sect. SI5, Fig. S5.1**), *i.e.*, 0.4 Pg yr^{-1}, yielding $F_{md,net}$ for that period 1.6 ± 0.3

1395   Pg yr^{-1}. This net uptake rate is slightly greater than that determined in the present model calculation for year 2000, dS_d/dt, **Fig. 7b**, 1.3 ± 0.4 Pg yr^{-1}, but well within the mutual uncertainty ranges. From the increase in the amount of DIC in the world ocean based on surveys in the mid 1990's and again in the mid 2000's Gruber et al. (2019) determined the rate of increase in the world ocean as 2.6 ± 0.3 Pg yr^{-1}. Again, diminishing this uptake rate by the rate of increase in the ML stock yields $F_{md,net}$ = 2.2 ± 0.3 Pg yr^{-1}. This value is slightly greater than, and outside the mutual uncertainty range from that

1400   determined here, 1.3 ± 0.4 Pg yr^{-1}. Based on these comparisons the transfer coefficient k_{md} determined here, while in the range of present studies, may be somewhat low. A greater transfer coefficient would result in a slightly shorter turnover time and adjustment time for excess CO_2 than that determined here. As well, the residence time of excess carbon in the DO would be somewhat diminished.

8.6. Flux from terrestrial biosphere to atmosphere and lifetime of carbon in the obdurate biosphere

1405   As shown in **Sect. 5.8** the turnover time of the carbon stock in the obdurate terrestrial biosphere that serves as the long-term reservoir for drawdown of excess atmospheric CO_2 must be roughly 300 years (range 125 - 525 yr), as obtained from the observationally determined PI flux from the AC to the OB (**Appendix A, Eq A43**) together with the PI stock in the OB (accounting also for the small preindustrial riverine flux). Such a residence time for obdurate carbon contrasts markedly with the 23 year lifetime of terrestrial carbon determined by Carvalhais et al. (2014) as the quotient of the stock of carbon in the

1410   TB upon the GPP flux. The import of this difference is that excess carbon taken up by the OB (but not the LB) would remain sequestered on the several century time scale following the hypothetical cessation of emissions of anthropogenic CO_2 examined here, as opposed to returning to the atmosphere on a time scale of a few decades. As noted in **Sect. 5.6** the Carvalhais et al. (2014) lifetime, includes carbon that is taken up in photosynthesis but which rapidly leaves the TB, on account of respiration on time scales from subdaily to annual. It is argued here that the bulk of the carbon in the TB exhibits

1415   a much longer lifetime and that it is this longer lifetime that would give rise to a continuing net terrestrial sink of excess atmospheric CO_2 subsequent to cessation of emissions. In support of this argument, as noted in **Sect. 3**, the great majority of the stock of carbon in the TB consists of long-lived components: woody materials and soil carbon. A long lifetime of carbon in the OB is consistent also with the assessment that net drawdown of carbon by the TB is dominated by uptake by and sequestration in established forests (Pan et al., 2011) and the observation that much of the carbon taken up by the TB is taken

1420   up by trees with large diameter (≥ 1 m) trunks (Stephenson et al., 2014).

8.7. Decay rate and lifetime of excess atmospheric CO_2

As noted in **Sect. 2**, numerous definitions have been proposed for the lifetime of a substance in a reservoir generally, and for excess atmospheric CO_2 in particular, for which the situation is complicated by rapid exchange with other compartments. It is useful to distinguish two classes of lifetimes, turnover times and adjustment times, which quantities should agree if suitably defined and evaluated. Because of rapid exchange of carbon between the AC, ML and LB, these compartments must be treated as a single compartment for the purpose of evaluating the turnover time of excess carbon in the biogeosphere, $\tau_{\mathrm{alm}}^{\mathrm{to}}$, defined (**Eq 2.2**) as the ratio of the sum of stocks of excess carbon in these compartments to the sum of net fluxes from these compartments into the DO and TB. Considering just the transfer rate from the atmosphere into all other compartments, or from the AC + ML into all other compartments yields erroneously low turnover times during the period of time when CO_2 is being emitted into the atmosphere, a consequence of the stock in the AC being increased by emissions, resulting in enhancement of the amount of CO_2 being reversibly transferred from the atmosphere into the ML and LB. The several turnover times can be evaluated throughout model runs for any given pair of parameters ($S_{\mathrm{l}}^{\mathrm{pi}}$, b), specifically including the situation in which emissions are abruptly halted. Importantly, the turnover time $\tau_{\mathrm{alm}}^{\mathrm{to}}$ (but not $\tau_{\mathrm{a}}^{\mathrm{to}}$ nor $\tau_{\mathrm{am}}^{\mathrm{to}}$) is essentially constant across that transition, establishing the choice of $\tau_{\mathrm{alm}}^{\mathrm{to}}$ as the appropriate measure of turnover time of excess carbon. Within a few years of cessation of emissions the several turnover times become equal as there is no currently emitted CO_2 that must be transferred into the ML and LB. These turnover times increase substantially following cessation of emissions; however by the time of that increase, the fraction of CO_2 present at the time of cessation has already substantially decreased.

The several adjustment times are measures of the time scale characterizing the rate of decay of excess atmospheric CO_2, or of the sum of carbon in two or more of the AC, ML, and LB compartments, following cessation of emissions. Because determination of adjustment times requires the absence of emissions, a numerical model is required. For consideration of the adjustment time of excess CO_2 an appropriate qualitative definition would be that advanced by Archer et al. (2009) as the time period over which, in the absence of anthropogenic emissions, CO_2 would recover substantially toward its original value. As Archer et al. point out, this lifetime is much greater than the lifetime that individual CO_2 molecules spend in the atmosphere, about 3 years, noting that confusion between these two lifetimes has given rise to a misinterpretation between these two definitions that has "plagued the question of the atmospheric lifetime of CO_2." However, in making this statement it would seem that Archer et al. are setting up a bit of a straw man; no one seriously considers the mean atmospheric lifetime of individual CO_2 molecules to be a measure of the lifetime of excess atmospheric CO_2.

Archer et al. go on to conclude that the lifetime of excess CO_2 is much greater. Using results from suite of carbon cycle models, those investigators found that 20–40 % of excess CO_2 would remain in the atmosphere after equilibration with the ocean, awaiting slower chemical reactions with $CaCO_3$ and igneous rocks. But by then assuming what they characterize as a

"long tail" of 10 % of excess CO_2 that remains in the atmosphere until neutralized by silicate weathering on a timescale of 100,000 years, those investigators concluded the mean lifetime of fossil fuel CO_2 to be 12,000 to 14,000 years or perhaps as great as 45,000 years. The characterization by Archer et al. of the lifetime of excess CO_2 by its mean lifetime, rather than by the time scale of substantial recovery, the measure that they themselves advocated, results in the long tail wagging the dog.

The long tail of excess CO_2 seen in virtually all prior studies is exhibited also by the present model, at least on the millennial time scale examined here, **Fig. 16**. Thus, although abrupt cessation of emissions would greatly reduce atmospheric CO_2, even such abrupt cessation would not restore CO_2 to its preindustrial state but rather to a value above the PI value by 15 to 20 percent of excess CO_2 at the time of cessation. This end state, which is reached rather rapidly (100 - 200 yr), is a floor below which it is not possible to go by emissions reductions alone, an irreducible long-term commitment of prior emissions. Put another way, this floor represents 6 % to 8 % of total anthropogenic emissions prior to cessation. As the excess CO_2 does not go to zero at long time, the climatic effects of the residual CO_2 would likewise persist, but at levels substantially reduced from those at the time of cessation.

The present study has focused on the time scale during which, in the absence of anthropogenic emissions, excess atmospheric CO_2 would substantially decrease. The decrease, quantified by the fraction of excess CO_2 remaining in the atmosphere as a function of time subsequent to cessation $f(t)$, is shown in **Fig. 1** for the present model and for a set of carbon cycle models. As noted in the Introduction some of the spread in the CC model results in **Fig. 1a** is a consequence of a wide spread in CO_2 mixing ratio at the time of cessation x_{CO2}^0, but considerable spread remains even when the range in x_{CO2}^0 is much narrower, as in the ZECMIP intercomparison project (MacDougall et al., 2020), **Fig. 1c**, indicative of differing representation of the processes governing removal of CO_2 from the atmosphere in the different models. More importantly, the decay curves obtained with the present model are lower, to much lower, than those obtained with the CC models. Specializing to $t = 100$ yr, the best estimate, $f(100$ yr) obtained in this study, 41 %, and range consistent with observational constraints on the parameters S_l^{pi} and b, 34 % to 49 %, are less, to much less, than the results of virtually all the other results presented in **Fig 1**.

Multiple measures of adjustment time defined in **Sect. 2** were evaluated and compared in **Sect. 7.6**. The instantaneous adjustment time, τ_{CO2}^{inst}, **Eq 2.3**, the inverse of the time-dependent fractional decay rate of excess CO_2, increases subsequent to cessation, similarly to τ_{alm}^{to}; the agreement of this measure of adjustment time with the several turnover times, **Fig. 12**, confirms the choice of τ_{alm}^{to} as the appropriate measure of turnover time. More relevant to considerations of the lifetime of excess CO_2 over a period of interest subsequent to cessation is the amount-weighted average over this period, $\tau_{a\text{-}avg}$, **Eq 2.5**, which exhibits much less increase over the time period of interest than does the instantaneous lifetime. A difficulty associated with evaluation of $\tau_{a\text{-}avg}$ from model data and even more so from observations is that this evaluation requires taking derivatives to determine the rate of decrease of excess CO_2. This difficulty is avoided with the equivalent $1/e$ lifetime

$\tau_E(t)$, **Eq. 2.6**, evaluation of which requires knowledge only of the fractional amount of excess CO_2 remaining as a function of time t subsequent to cessation $f(t)$, and which, at least in the present model calculations, agrees closely with $\tau_{\text{a-avg}}$.

1485   Within the observationally constrained bounds on (S_1^{pi}, b), the equivalent $1/e$ lifetime $\tau_E(100 \text{ yr})$ of excess CO_2 for time horizon $t = 100$ yr **(Eq 2.6)** obtained from the present model results is rather narrowly constrained, central estimate 112 yr ; range 90 to 150 years, **Figures 1b, 11d, 12**. The several other definitions of lifetime yield essentially the same values (**Figures 11, 12**). As emphasized above, this 100 year time frame characterizes the time during which, in the absence of anthropogenic emissions, atmospheric CO_2 would recover substantially toward its original concentration. The lifetime

1490   obtained here is shorter to much shorter than that for all the CC models represented in **Figures 1 and 17**, importantly, the multimodel mean of Joos et al. (2013a), widely used in assessment studies, for which $\tau_E(100 \text{ yr})$ is 270 yr. Using the same measure of lifetime establishes that the differences are intrinsic to the different models, not merely a consequence of the choice of measure of lifetime.

What is the reason for the difference between the lifetime (adjustment time, equivalent $1/e$ lifetime) of excess CO_2 found

1495   here and the longer lifetimes determined with CC models, and what are the reasons for the differences in lifetimes among the several CC models? It is not due to difference in definition, as all lifetimes are evaluated from the decay curves in the same way. What are the uncertainties in the lifetimes determined by the several CC models, and to what extent do those uncertainties encompass the shorter lifetime found here? Answers to these questions must await examination of the disposition in the CC models of excess carbon among the several compartments and subcompartments, and of the fluxes

1500   between these compartments and subcompartments, before and after cessation. What are the observational constraints on these quantities? What are the transfer coefficients? What is the scientific understanding that is the underpinning of these transfer coefficients? What is the uncertainty in this understanding, and how does that translate into uncertainty in transfer coefficients and ultimately in the fluxes, stocks, and lifetime? In the meantime a suggestion is given by the dependence of lifetime on the parameters S_1^{pi} and b, **Fig. 11**, showing increase in lifetime with increasing values of either of those

1505   parameters, both of which result in greater uptake of CO_2 by the LB versus the OB, the total uptake by the terrestrial biosphere being rather tightly constrained. Uptake of CO_2 by the LB rather than the OB gives rise to less long-term sequestration of anthropogenic CO_2 and in turn to longer lifetime as that carbon is more rapidly returned to the atmosphere.

8.8. Comparison to prior determinations of lifetime based on the CO_2 budget and simple models

Several prior investigators have reported measures of the lifetime of excess CO_2 based on the budget of excess CO_2 in the

1510   atmosphere. Considering the TB to be coupled to the AC and the ML, Rodhe and Björkström (1979) obtained a turnover time of about 100 yr for CO_2 in the combined compartment as governed by transfer into the DO. The time constant obtained by those investigators for relaxation of a perturbation in the system once it had reached a new equilibrium with the DO, 400

yr, is much less relevant to the evolution of the system on the time scale of 100 yr or less. Moore and Braswell (1994) proposed as a measure of the adjustment time of excess CO_2 the time required in the absence of emissions for the difference

1515 between the excess atmospheric CO_2 at some initial time and the infinite-time value of this quantity to decrease by half. Comparing multiple transport models with and without uptake by the terrestrial biosphere, also by several models, these investigators obtained a half life of excess atmospheric CO_2 ranging from 19 to 49 years, depending mainly on how uptake by the terrestrial biosphere was to be considered.

An explicitly defined observationally determined measure of the turnover time of anthropogenic CO_2 was given by O'Neill

1520 et al. (1994) and Gaffin et al. (1995) as the quotient of the atmospheric stock of excess CO_2 upon the total rate of drawdown of CO_2 from the atmosphere, determined by difference of emissions and the annual increase of atmospheric stock, **Eq 5.1**, yielding the value 32.5 ± 10.5 yr (average and standard deviation of annual results, 1959–1989). A similar result, 39–45 yr, based on the same definition but using data for the year 2000, was given by Jacobson (2005). Such short lifetimes are a consequence of not taking into account the tight coupling of the AC, LB, and ML. When that coupling is taken into account,

1525 the resultant turnover time is substantially greater, ranging, for best estimate anthropogenic emissions, from 65 to 158 years depending on S_l^{pi} and b (**Fig. 5c, Table 3**). The approach to determining the lifetime of excess CO_2 as the turnover time and of characterizing the lifetime by a single number, as well as the short lifetimes so determined, have received strenuous criticism by several investigators, **Appendix F**; point by point refutation of these criticisms is presented in that Appendix.

A study of the budget of excess CO_2 with a three-compartment model by Gloor et al. (2010) that matched the fraction of

1530 emitted CO_2 remaining in the atmosphere to observations over the time period 1959–2006, determined what those investigators denoted as a "system time constant" that characterizes the rate of removal of CO_2 from the atmosphere, with value 37.5 yr. In that study removal of atmospheric CO_2 was considered to consist of two components, transfer from the AC to the TB and to the total ocean, with transfer coefficients $k_{\text{ao}} = 0.0144$ yr^{-1} and $k_{\text{ad}} = 0.0123$ yr^{-1}, respectively, referred to the AC, both treated as irreversible and taken as constant over the time period under consideration. This set of assumptions

1535 would correspond to a situation in which there is no uptake of carbon by a labile biosphere nor assumed equilibrium between the AC and the ML. The transfer coefficient from the AC to the OB, which corresponds directly to k_{ao} in the model developed here in the absence of uptake by the LB, agrees closely with the value 0.013 yr^{-1} for (S_l^{pi}, b) = (400 Pg, 0.6), **Fig. 4c**. The equilibrium assumption between the AC and the ML would lead to $k_{\text{ad}} = k_{\text{md}} S_m^{\text{ant,pd}} / S_a^{\text{ant,pd}}$. Using the present results this set of assumptions would lead to $k_{\text{ad}} = 0.0066$ yr^{-1}, well less than the value given by Gloor et al. (2010). The

1540 resultant turnover time referred to the AC $\tau_a^{\text{to}} = (k_{\text{ad}} + k_{\text{ao}})^{-1}$ using values adduced here would be 41 to 69 yr, the difference from the value given by Gloor et al. (2010) attributable almost entirely to the different values of k_{ad}. Much more important, however, is that the turnover time of atmospheric CO_2 calculated in this way is not pertinent to the rate of decay of

atmospheric CO_2 that would follow an abrupt cessation of emissions, as it does not take into account the strong coupling of the AC to the LB and the ML, which greatly increases the adjustment time over this turnover time defined in this way.

1545   Two prior studies that found a rate of decrease of atmospheric CO_2 subsequent to abrupt cessation of emissions comparable to that found here are those of Hare and Meinshausen (2006) and Raupach et al. (2014), both of which, like the present study, used global-scale compartment models with observationally constrained transfer coefficients rather than detailed CC models. These systematic differences between compartment models and CC models suggests that much might be learned by examination of the reasons for these differences.

1550   In a study, quite similar to the present one, Raupach et al. (2014) reported a time-dependent sink coefficient characterizing the rate of loss of atmospheric CO_2 by transfer from the AC into the ML, DO, and TB, combined, evaluated from historical emission estimates and measured atmospheric CO_2 as $\kappa^{obs}_{A \to MTD} = (Q_{ant} - \Delta S_a) / S_a^{ant}$ (their Figure 5, lower left panel); the inverse of this sink coefficient, the turnover time of the stock in the AC to all other compartments, is shown in **Fig. 17**. Following cessation of emissions, this turnover time exhibited an abrupt increase to a value of about = 98 yr, similar to that

1555   exhibited by τ_a and τ_{am} in the present model results for the (S_l^{pi} , b) = (400 Pg, 0.6) model variant, also shown in **Fig. 17**. Raupach et al. attributed the abrupt decrease of sink coefficient in their model results to saturation of what they referred to as "fast modes" in their model resulting from the abrupt change in emissions. However it seems almost certain that the abrupt decrease in sink coefficient (equivalently, abrupt increase in turnover time) is due to the cessation of drawdown of stock from the AC by the LB and the ML as the AC stock is no longer increasing on account of emissions, **Sect. 7.5**. However if

1560   that were the only influence on the turnover time, the turnover time would be expected to level off to a nearly constant value. Contrary to that expectation, after the initial increase, this turnover time continues to increase, to 207 years at year 2112, 100 years after cessation of emissions in that study, versus 135 years in the results of the present model, again for (S_l^{pi} , b) = (400 Pg, 0.6). The decrease in the sink rate that continues through the 100 years following cessation in the Raupach et al. (2014) results and that leads to the large future increase in turnover time shown in **Fig. 17** was attributed by those investigators to

1565   what they characterized as "intrinsic" processes governing the CO_2 system, specifically the dependences of ocean–atmosphere CO_2 fluxes and terrestrial net primary production on CO_2, and the dependence of heterotrophic respiration on temperature. This continued increase in turnover time subsequent to cessation of emissions would thus seem to rest entirely on their models for the governing processes rather than on observations to date.

8.9. Applicability of parameters determined by prior observations to modeling future evolution of CO_2.

1570   An concern that might be raised with the present model is that because the parameters are constrained by observations, the model might be applicable only to climatic conditions sufficiently similar to historical conditions that substantial changes in processes controlling the carbon budget would not be induced by a changing climate. Although such concern might attach to

extending the present model into a future warmer world, from the perspective of the abrupt cessation experiment, this would seem to be of minimal concern, as global temperature, together with climate variables that are driven by temperature, would

1575 follow the change in forcing with little lag (e.g., Held et al., 2010; Boucher et al., 2012), thereby staying in the climatic regime in which the parameters were determined.

8.10. Small number of compartments: Limitation or strength?

A deeper concern that might be raised with the present study is that the conceptual and numerical model developed here is extremely simple. Such simplicity has its strengths and limitations, as examined in the current context by Meinshausen et al.,

1580 (2011). Among the strengths is that the parameters in the differential equations that constitute the model represent physical processes and are derived from observations, and it is thus possible to trace each of these parameters to the underlying observations, the exception here being the parameters S_l^{pi} and b, which are initially varied over a wide range that is then constrained by observations. It is possible as well to examine the consequences of varying those parameters within the limits of the observational constraints. Further, it is possible to readily examine rates of change in the stocks in the several

1585 compartments and the fluxes between compartments. Such transparency, at least in the present model, should facilitate comparison of the changes in stocks and fluxes with the corresponding changes in carbon cycle models such as those that participated in the ZECMIP intercomparison to ascertain the reasons for the differences in those models from the present one.

In view of the simplicity of the present model the question might be raised whether the exchange of CO_2 with the terrestrial

1590 biosphere and the ocean can be accurately represented by two compartments each in the TB and the ocean, as here. With respect to the TB, recent studies with global compartment models have represented the TB by one (Graven, 2015), two (Raupach et al., 2014), or three (Meinshausen et al., 2011) compartments. Raupach et al., showed good agreement between atmospheric CO_2 over the Anthropocene as calculated with their model and as measured. Meinshausen et al. reported that their model (MAGICC6) compared well with large, higher complexity atmosphere-ocean GCMs and carbon cycle models

1595 for idealized emission scenarios. An important study in this respect is that of Naegler and Levin (2009), which assessed the accuracy of modeled amounts of radiocarbon in the atmosphere and world ocean by comparison with observations, focusing on the period before, during, and after the peak in emissions associated with weapons testing. Assessing the accuracy of their model as a function of the number of well-mixed global terrestrial carbon compartments, those investigators noted, as they had expected, that agreement between model and observations increased with increasing number of pools, and parameters.

1600 With only a single terrestrial compartment the model was not capable of realistically simulating the observed inventories of excess ^{14}C, whereas with two well-mixed compartments the simulated stocks agreed rather well with the observations. Those investigators noted that the agreement was somewhat improved for three or four compartments but raised concern that

with increasing number of compartments the parameters became increasingly underdetermined. This limited assessment lends support to the use of two global compartments of terrestrial carbon as in the present model.

1605 With respect to the ocean, reliance is again made on the accuracy of representation of exchange of heat between the upper (ML) ocean and the deep (DO) ocean compartments. For heat, no atmospheric compartment is required because heat is distributed essentially entirely into the ML, the heat capacity of the ML being about 40 times that of the atmosphere, whereas for CO_2, as only 11 % of the excess CO_2 in the two compartments is in the ML (**Fig. 2**), an additional atmospheric compartment is required. However, as the anthropogenic CO_2 is in near equilibrium between these two compartments (**Sect.**

1610 **7.7**), the two compartments essentially comprise a single compartment, strengthening the analogy with heat transfer. The two-compartment model describing the evolution of heat in the climate system, introduced by Schneider and Thompson (1981), has been shown to accurately represent results obtained with complex climate models for a specified set of heat capacities and transfer coefficients (Gregory, 2000; Held et al., 2010; Geoffroy et al., 2013). That accuracy lends strong support to use of a two-compartment ocean model as in the present model. The two-compartment climate model also

1615 provides much insight, for example, identification of a transient climate sensitivity characterizing response to forcing that is achieved much more rapidly than the long-term so-called "equilibrium" response. This would be analogous in the CO_2 system to the response on the multi-decadal to century time scale, governed by the turnover time and adjustment times examined here, versus the response on the millennial scale required for the DO to equilibrate to the ML. Finally it might be noted that a two-compartment emulator is widely employed, for example by AR6, to assess the transient climate response to

1620 specific forcing agents (Forster et al., 2020; Equation 7.SM.2.1; Figures 7.7, 7.8), lending further strong support to the applicability of a two-compartment ocean model to examine the exchange of CO_2 between the atmosphere and the ocean, as in the present model.

In contrast to the modeling approach taken here, the argument might be raised that past, present, and future changes in stocks of carbon in the several compartments of the global biogeosphere can be calculated only by coupled climate–carbon-cycle

1625 models (CCCC models). Arguably only such models would be capable of representing the meteorological and biogeochemical processes that govern exchange of CO_2 between compartments and the responses of these processes to changes in temperature, precipitation, and other variables. However such representation would require detailed understanding that is not yet confidently at hand. For example, as shown in **Appendix C**, estimates of global PI gross primary production range by ± 20 %, and estimates of the growth in global GPP over the industrial period range from 0 to

1630 60 %. Such uncertainty in even these fundamental quantities at the global scale must inevitably raise questions about representing these processes and their changes at seasonal and regional scales needed in CCCC models to determine drawdown of atmospheric CO_2 under past, present, and future climatic conditions.

An example of differences between results with the present model and CC models, is provided by the net annual global flux from the AC to the TB. The CC model results, **Fig. 14c and Fig. 15b**, exhibit large interannual variation that is seen also in observations. It might thus be argued that such models do a better job than models such as the present one, for which the rate of exchange between the AC and the TB is given by the assumed dependence of GPP on x_{CO2} and by transfer coefficients k_{la}, k_{ao} and k_{oa} taken as constant, and which, as a consequence, does not result in such fluctuations. However such improvement is only apparent, as shown by examination of sum of uptake into the ocean and the TB, determined as the difference between annual emission and the annual increase in the stock of atmospheric CO_2, **Fig. 15c**. Although it would appear that the multimodel mean of the sum of fluxes from the AC to the ocean and the TB captures the large interannual variation that is not represented in the present model, this multimodel mean actually exhibits no improvement over the present model in the standard deviation of the residuals of annual fluxes, **Fig. 15d**.

A further key strength of the top-down approach for analysis and interpretation of the global CO_2 budget lies in its utility for practical applications. As the excess CO_2 resulting from a given emission remains in the atmosphere for sufficiently long time that any input becomes uniformly distributed in the global atmosphere, a global picture is the most pertinent to considerations of policy: the excess CO_2 in the global atmosphere is affected equally irrespective of the location of emission. This top-down budget also provides a framework for interpretation of results from detailed CC models, and consistent with this, results from detailed observational and model studies are frequently presented as global average values, the quantities that are determined directly in the top-down approach.

In sum, it should be emphasized that the strength of representing the carbon cycle with a model with just a small number of compartments is the ability to constrain a small number of transfer coefficients by observations together with well established constraints such as chemical equilibria, preindustrial steady state, and conservation of matter, and thereby to lend confidence in the broad accuracy and predictive capability of the model. The more complex the model, the more parameters that are required. Uncertainty in predictive capability does not decrease with increasing number of uncertain parameters; it increases.

8.11. Verification versus falsification

To conclude this discussion it should be noted that a model such as that presented here must be considered a hypothesis, which in principle is never verifiable, only falsifiable. As noted by (Popper, 1962), "It is easy to obtain confirmations, or verifications, for nearly every theory — if we look for confirmations." What is necessary, rather, is to look for accurate representation of situations that differ greatly from those that display the accuracy of the model. As Popper goes on to state, "Confirmations should count only if they are the result of *risky predictions* [italics in the original]." With respect to the present model, such a test of the model developed here might be achieved by society conducting the abrupt cessation

experiment, or at least a substantial reduction in emissions, on the time of a decade or so, which is under active consideration. Because of the rapid response of the model to changes in emissions the results of the experiment would be in
1665 hand on a time scale of a few decades.

9. Conclusions and implications

Because of the importance of CO_2 as the major anthropogenic greenhouse gas, understanding the response of atmospheric CO_2 to prospective future emissions is essential. A key objective of the present study has been determination of the lifetime of excess atmospheric CO_2. This lifetime is highly uncertain in the current literature, with published values ranging from a
1670 few decades to tens of thousands of years. To considerable extent this perceived uncertainty is reduced by agreeing that the appropriate measure of the lifetime is the time scale on which, in the absence of anthropogenic emissions, atmospheric CO_2 would substantially recover to its preindustrial value. However even with such agreement, prior model results shown in **Fig. 1** exhibit wide disparity, and it was that range of disparity that motivated the present study. Clearly the uncertainty in CO_2 lifetime represented by the range of results of current carbon cycle models greatly limits confident formulation of approaches
1675 to limit climate change, specifically, for example, to limit the increase in global temperature to a specific target. Here it is noted that in the model intercomparison of MacDougall et al. (2020), reproduced in AR6 (Lee et al., 2021, Figure 4.39), the range of change in global temperature over the 100-year time period following abrupt cessation of anthropogenic CO_2 emissions is large, -0.9 to + 1.6 K, and uncertain even in sign. The approach taken here, a hybrid budget–modeling approach, tightly constrained by observations and well characterized geophysics, has led to a lifetime of anthropogenic CO_2, quantified
1680 by multiple measures, of 110 ± 30 years, well shorter than given by current carbon cycle models. In the sustained absence of anthropogenic emissions, CO_2 would not fully return to its preindustrial value. However, as the lifetime defined and determined here pertains to the period of time during which CO_2 would return substantially to its preindustrial value, it is this quantity that is the pertinent measure of the lifetime of excess CO_2.

Although the abrupt cessation of emissions examined here can at present be considered only hypothetical, in view of the
1685 heavy reliance on fossil fuel combustion by human society to meet its energy needs, such a complete cessation of emissions is highly relevant as the end state of potential decarbonization of the world's energy economy. Irrespective of practicality, abrupt cessation serves as benchmark by which to consider the response of atmospheric CO_2 to any prospective decrease of emissions. Certainly if the model developed here provides an accurate representation of the response of atmospheric CO_2 to such a cessation, the rapid decrease in CO_2 that would result from abrupt cessation of emissions would be dramatic: a 50 %
1690 decrease in excess CO_2 in as short a time as 50 to 100 years, much shorter than the 550 years that would be required based on the multimodel mean of Joos et al. (2013*a*), widely used as a benchmark in current analyses, and likewise much shorter than the results from the several models that participated in the intercomparison of MacDougall et al. (2020). Such a

decrease in atmospheric CO_2 would be accompanied by a decrease in radiative forcing, 0.9 W m^{-2} and by a corresponding decrease in global temperature. The decrease in atmospheric CO_2 would be mirrored also by a decrease in dissolved

1695   inorganic carbon in the surface ocean, with resultant increase in pH of 0.07.

Finally I return to the importance of the adjustment time of excess atmospheric CO_2 to climate system response to prospective reductions in anthropogenic CO_2 emissions. Of the two time constants governing response of global mean surface temperature (GMST) to change in CO_2 emissions, namely the time constant of response of atmospheric CO_2 amount to change in emissions τ_{CO2}, and the time constant of response of GMST to change in forcing τ_{GMST}, the latter is much

1700   shorter, five to 10 years. Hence it is τ_{CO2} that governs the time scale of the overall response of the climate system to changes in emissions. If τ_{CO2} is as great as 300 years or so, as indicated for the multimodel mean in the comparison study of Joos et al. (2013) shown in **Fig. 1a**, then decrease in GMST in response to reduction in anthropogenic CO_2 emissions would take place only on this multicentennial time scale. In contrast, the present results indicate that the effects of controls on emissions might be realized much more quickly and that concerted action to control anthropogenic emissions of CO_2 could yield,

1705   dramatic, tangible results on a time scale as short as a human lifespan.

Appendix A: Budget of CO_2 in the biogeosphere

The objective of the examination of the budget of CO_2 presented here is to obtain an accurate and quantitatively self-consistent picture of the stocks, fluxes, and annual growth of CO_2 in and between the several compartments in the biogeosphere governing the amount of CO_2 in the atmosphere. Specifically, these compartments are the atmosphere

1710   (atmospheric compartment, AC), the world ocean, subdivided into two compartments, the mixed-layer ocean (ML), the deep ocean (DO), and the terrestrial biosphere (TB), also subdivided into two compartments, a labile biosphere (LB) and an obdurate biosphere (OB). The AC and the two ocean compartments are each considered well mixed and to exhibit (in the AC) uniform mixing ratio of CO_2 or (in the ocean compartments) concentration of total dissolved inorganic carbon, DIC, the sum of carbonic acid H_2CO_3 and bicarbonate HCO_3^- and carbonate CO_3^{2-} ions, predominantly bicarbonate. This analysis

1715   first examines the preindustrial budget, on which the anthropogenic perturbation is imposed, and then examines the anthropogenic perturbation.

The framework for this analysis is **Fig. 2**, which identifies the several compartments and presents the results from this analysis in terms of the stocks in these compartments, the fluxes between the compartments, and the annual increases in several of the stocks. The intent is to develop values of the several quantities that derive from measurements or well

1720   established relations between the several quantities, importantly the equilibrium total solubility of CO_2, the amount of DIC in equilibrium with atmospheric CO_2. Some differences in several of these quantities have been exhibited among the several

prior versions of the figure, resulting from definitional changes, improvements in measurement and understanding, and updating. The present examination has resulted in further substantial changes in several of the quantities, as detailed below.

A1. Preindustrial stocks

1725 The preindustrial stock of atmospheric CO_2 is accurately known from glacial ice cores (Neftel et al., 1985; Etheridge et al., 1996). The stock of atmospheric CO_2 S_a, is related to the dry-air mixing ratio of CO_2 x_{CO2} as

$$S_a = \Gamma_{CO2} x_{CO2},\qquad\qquad(A1)$$

where $\Gamma_{CO_2} \approx 2.120$ Pg C ppm^{-1} (**SI Text Sect. S2**) can be considered a constant of Earth's geophysical system. The PI CO_2 mixing ratio 278 ppm, uncertain to perhaps 2 ppm, corresponds to stock 589.4 ± 4 Pg. The stock of carbon in fossil fuel

1730 reserves, determined by inventory, is subject to large uncertainty for reasons of definition or by changes in inventory method, but for consideration of the budget of atmospheric and oceanic CO_2 such uncertainty is of secondary importance. Stocks of CO_2 dissolved in the two ocean compartments are related to average concentrations by the depth of the ML, $z_m =$ 100 m, consistent with previous versions of this figure, and of the DO, $z_d = 3583$ m, for total mean depth of the global ocean 3683 m, and area of the global ocean $A_o = 3.62 \times 10^{14}$ m^2 (Eakins and Sharman, 2012), together with the density of

1735 seawater ($\rho_{saw} = 1025$ kg m^{-3}). Throughout this study the equilibrium concentration of DIC corresponding to a given CO_2 dry-air mixing ratio x_{CO2} has been calculated with the program CO2SYS (Lewis and Wallace, 1998), with temperature taken as 18 ˚C and total alkalinity 2349 μmol kg$_{sw}^{-1}$, the latter selected to yield mixed-layer stock 900 Pg in near equilibrium with the preindustrial CO_2 mixing ratio as given in earlier versions of the figure; these values of alkalinity and temperature are used throughout the present study. The dependence of equilibrium DIC concentration on x_{CO2} is shown in **SI Text Sect. S3,**

1740 **Fig. S3.1**, which also shows the corresponding stocks in the two compartments. Conversions relating stocks and concentrations are also given in **SI Text Sect. S2**.

The total stock in the preindustrial TB is treated as consisting of two components the PI LB and its complement the PI OB. Here the value of the total stock in the PI TB S_t^{pi} is taken as 2800 Pg based on a survey of present-day carbon stocks by Carvalhais et al. (2014), which yielded 2807_{-278}^{-428} Pg (uncertainty range adjusted to 68 % likelihood) together with the net

1745 change in S_t between preindustrial time and present day (difference between net deforestation and net uptake of anthropogenic CO_2) being small. The stock in the PI LB S_l^{pi}, which assumes some importance in the present analysis as it exerts a major influence on the amount and rate of anthropogenic CO_2 taken up by the LB, is considered uncertain and is limited by comparison of present model results and observations to the range [200, 700] Pg, **Sect. 7**.

A2. Preindustrial steady state

1750   A requirement of the preindustrial state is that the stocks in all compartments are constant with time (steady state), and therefore that the fluxes between all compartments be equal when summed over all paths. In this regard attention is called first to the large and essentially cancelling fluxes between the AC and the ML, **Sect. A4**, and between the AC and the LB. The gross fluxes between the AC and the LB are set to estimates of PI gross primary production, **Sect. A3**. The gross fluxes from the AC to the OB and from the OB to the AC, the ranges of which are constrained by comparisons of observations with

1755   results from calculations with the model developed here, are much smaller. Attention is called to the slightly greater flux from the AC to the OB than the return flux, a difference of 0.6 Pg yr^{-1}, that is compensated by a riverine flux from the OB to the ML. This riverine flux into the ML results in the value for concentration of DIC in the ML [DIC]$_m$, shown as 2020.2 µmol kg$_{sw}^{-1}$, slightly exceeding the concentration in equilibrium with the atmospheric mixing ratio 278 ppm (2018.4 µmol kg$_{sw}^{-1}$; S_m = 899.2 Pg) and in turn to the flux from the ML to the AC F_{ma}^{pi} slightly exceeding that from the AC to the ML

1760 F_{am}^{pi} (70.6 vs 70 Pg yr^{-1}). Although this difference in flux is slight relative to the flux itself, and to the accuracy with which the flux is known, the difference is substantial in the context of the anthropogenic increment in net flux between the AC and the ML and must be accounted for in the budget (Sarmiento and Sundquist, 1992; Takahashi et al., 2009). The corresponding augmented stock in the ML S_m^{pi} = 900 Pg consistent with recent versions of **Fig. 2**. This situation results in a steady state for the three compartments.

1765   **A3. Preindustrial flux between the atmosphere and the terrestrial biosphere**

   The flux from AC to LB F_{al}^{pi} given in **Fig. 2** is meant to represent annual gross primary production, GPP, that is, the entire amount of CO$_2$ taken up by photosynthesis including the amount that is rapidly released by vegetative respiration. Here as the global annual preindustrial fluxes F_{al}^{pi} and F_{la}^{pi} are taken as compensating, their exact magnitudes are unimportant for consideration of budgets. In fact, an early version of the figure given (Sarmiento and Gruber, 2002) gave the flux from the

1770   atmosphere to terrestrial vegetation as the estimated net primary production, NPP, 60 Pg yr^{-1} rather than the 120 Pg yr^{-1} that corresponds to GPP given in later versions of the figure. GPP has conventionally been estimated as twice NPP (e.g., Beer et al., 2010), hence the value of 120 Pg yr^{-1}. However neither the 60 Pg yr^{-1} estimate for NPP nor the factor of 2 is known with great accuracy (e.g., Piao et al., 2010). The value 120 Pg yr^{-1} given for GPP in recent versions of **Fig. 2** is taken here as PI gross flux from the atmosphere to the LB, F_{al}^{pi}.

1775   An important addition to **Fig. 2** relative to previous versions of this figure is inclusion of fluxes denoting the preindustrial drawdown of carbon from the atmosphere to the obdurate biosphere OB and the return of this carbon from the OB to the atmosphere either directly or, to much lesser extent, through the ocean mixed layer. As developed in **Appendix A13 and Section 3**, the range of F_{ao}^{pi}, [4.6, 20.6] Pg yr^{-1}, is constrained by comparisons of results from the model developed here with

observations. The return flux F_{oa}^{pi} [4.0, 20.0] Pg yr^{-1} is less than F_{al}^{pi} by the riverine flux from the OB to the ML $F_{om}^{pi} = 0.6$ Pg yr^{-1}.

A4. Preindustrial flux between the atmosphere and the mixed-layer ocean

A principal objective of this analysis of the CO$_2$ budget is to develop transfer coefficients characterizing the fluxes between compartments F_{ij} in terms of the stocks of the source compartments, S_i as

$$F_{ij} = k_{ij}S_i \ . \tag{A2}$$

where the transfer coefficient pertinent to the global annual mean is generally a constant but is not a constant for transfer between the ML and the AC (**Appendix B**). By **Eq A2** the ratio of the flux of CO$_2$ from the atmosphere to the ocean to the atmospheric stock defines the transfer coefficient k_{am},

$$k_{am} \equiv F_{am}^{pi} / S_a^{pi} \ . \tag{A3}$$

The preindustrial atmospheric stock and atmosphere-to-ocean flux shown in **Fig. 2**, which are taken from earlier versions of this figure, result in the value $k_{am} = 0.119$ yr^{-1}. This transfer coefficient corresponds to a global and annual mean transfer velocity v_{am} (often denoted deposition velocity), the ratio of global mean flux density $\varphi_{am} = F_{am}/A_o$ to mean gas-phase CO$_2$ volumetric concentration at the surface C_{as},

$$v_{am} = \frac{\varphi_{am}}{C_{as}}, \tag{A4}$$

the subscript s denoting surface concentration. As shown in **SI Text Sect. S2**, v_{am}, which is related to k_{am} by A_o and the volume of the global atmosphere (reckoned at the global and annual mean temperature and pressure at the ocean surface) V_a,

$$v_{am} = \frac{k_{am}V_a}{A_o}, \tag{A5}$$

is approximately 16 cm h^{-1}. As the mass transport is controlled by aqueous-phase diffusion of dissolved CO$_2$ in the laminar layer of seawater immediately adjacent to the atmosphere, v_{am} does not depend on the concentration or extent of ionic dissociation of dissolved CO$_2$ (e.g., Liss and Slater, 1974; Schwartz, 1992; Sarmiento and Gruber, 2006, pp. 82-89). This deposition velocity falls squarely within the range of estimates of global-mean aqueous-phase transfer velocities for CO$_2$, as summarized, e.g., by Sarmiento and Gruber (2006; p. 85), 11 to 20 cm h^{-1}. (Indeed, the value for F_{am}^{pi} of 70 Pg yr^{-1} given in **Fig. 2** and in multiple earlier versions of this figure almost certainly derives from estimates of the global and annual mean aqueous-phase transfer velocity together with specified S_a). These estimates result from averages of local and instantaneous

transfer velocity, a quantity that depends strongly on wind speed (roughly as the second power) and to lesser extent on other

1805 situational variables (e.g., Liss and Merlivat, 1986; Takahashi et al., 2009; Wanninkhof et al., 2013). The transfer coefficient k_{am} denoting the global and annual mean gross transfer rate of CO_2 from the atmosphere to the surface ocean divided by the amount of CO_2 in the global atmosphere is independent of the amount of CO_2 in the atmosphere and of the amount or concentration of dissolved CO_2 in the ocean. Indeed, after accounting for Henry's law solubility, this transfer coefficient is applicable to any low- to moderate-solubility gas, the uptake of which is controlled by aqueous-phase mass transport, with

1810 slight dependence on the diffusivity of the dissolved gas in seawater. The value for k_{am} is given here, as also for other quantities, to far greater precision than is justified by the accuracy with which it is known, the uncertainty in k_{am}, the value of which is based on modeling studies and perhaps with greater confidence on the rate of uptake of natural and weapons-produced radioactive tracers, being about ±30 %. (Sarmiento and Gruber, 2006, p. 85). Again, however, because of cancellation in the up and down fluxes, **Fig. 2**, the actual values of the gross fluxes assume secondary importance in

1815 consideration of the CO_2 budget.

The transfer coefficient between the atmosphere and the ML referred to gas-phase CO_2 is related to the transport coefficient between the two compartments referred to aqueous-phase CO_2, v_{am}, by the dimensionless volumetric Henry's law solubility coefficient H (Sander et al., 2021) amount per volume in solution divided by amount per volume in the gas phase, as

$$v_{ma} = \frac{v_{am}}{H} \qquad\qquad (A6)$$

1820 (e.g., Liss and Slater, 1974; Schwartz, 1992). For CO_2, because H is near unity (0.83 at 291 K; Weiss, 1974; Lewis and Wallace, 1998), v_{ma} is roughly equal to v_{am}. The resulting global- and annual mean value of v_{ma} is 19 cm h^{-1}, again with uncertainty ± 30 %.

As developed in **Appendix B**, the flux from the ML to the AC does not exhibit constant proportionality to the amount of total dissolved inorganic carbon (DIC) in the ML as it is proportional, rather, to the amount of dissolved H_2CO_3, which is

1825 the species that exchanges with atmospheric CO_2. This situation is readily dealt with using well established equilibrium relations between concentrations of DIC and H_2CO_3 but has the consequence that the transfer coefficient k_{ma} is dependent on the concentration of DIC and is thus not a constant in the same sense as k_{am}.

A5. Gravitational flux of particulate carbon

In the preindustrial situation, in order for steady state to be maintained, the total flux from the ML to the DO must equal the

1830 reverse flux from the DO to the ML. Here, in addition to the contributions to these fluxes from exchange of water containing DIC between the two compartments, with fluxes F_{md}^{pi} and F_{dm}^{pi}, transfer occurs also by gravitational settling of biogenic

particulate carbon from the ML to the DO, with flux denoted F_{pc}, the so-called biological pump (Volk and Hoffert, 1985; Sarmiento and Gruber, 2006, p. 332). The particulate carbon transferred to the DO is subsequently oxidized to inorganic carbon and returned to the mixed layer as part of F_{dm}^{pi}, thereby requiring, in steady state, that

1835
$$F_{md}^{pi} + F_{pc} = F_{dm}^{pi}.$$
(A7)

The global-mean flux densities of dissolved CO_2 transferred between the two compartments can be related to the concentrations (C_i, mass/volume) in the two compartments,

$$C_i = \frac{S_i}{A_o z_i}$$
(A8)

and to the rate of volume of seawater exchange between the two compartments, v_p as

1840
$$F_{md}^{pi} = A_o v_p C_m{}^{pi}; \quad F_{dm}^{pi} = A_o v_p C_d{}^{pi}.$$
(A9)

As v_p has the dimension of velocity, it is often denoted a "piston velocity", the volume of water (per area and time) that would be displaced by a piston moving at that velocity; this global piston velocity characterizes the rate of transfer of any globally distributed tracer between the ML and the DO. Here the piston velocity is determined from the rate of transfer of heat energy from the ML to the DO in recent decades (**Appendix A Sect. A6**). From **Eqs A5-A9** the concentrations in the

1845 two compartments are related by

$$C_d{}^{pi} = C_m{}^{pi} + \frac{F_{pc}}{A_o v_p}$$
(A10)

From (A10) it may be seen that the sinking of particulate carbon results in the concentration of DIC in the deep ocean being greater than that in the mixed layer. **Eq (A10)** may be inverted to yield a value of the flux of particulate matter from the mixed layer to the deep ocean that is consistent with a specified difference between the concentrations in the deep and

1850 mixed-layer ocean.

$$F_{pc} = A_o v_p \left(C_d{}^{pi} - C_m{}^{pi} \right)$$
(A11)

Here the preindustrial DIC concentration in the mixed-layer is taken as 2020 μmol kg_{sw}^{-1}, equivalent to 0.02487 kg m^{-3} and that in the deep ocean 2250 $\pm$ 25 μmol kg_{sw}^{-1} (Key et al., 2004; McKinley et al., 2017), equivalent to 0.02770 kg m^{-3}. The requirement of preindustrial steady state together with the piston velocity determined in **Appendix A, Sect. A6**, 5.5 $\pm$ 1.8 m

1855 yr^{-1} constrains the gravitational flux of particulate carbon from the ML to the DO F_{pc} to 5.6 $\pm$ 1.8 Pg yr^{-1}, where the

uncertainty is dominated by uncertainty in v_p. This value is considerably less than, the value given in prior versions of **Fig. 2**, 11 Pg yr^{-1}, a value that derives from an inverse model calculation by Schlitzer et al. (2000). However prior and subsequent estimates of this quantity, based on measurements with sediment traps and on determination of ocean productivity from satellite measurements together with yield of particulate matter, or by model calculations vary over a

1860   substantial range: Keeling (1979) 3.5 Pg yr^{-1}; Martin (1987) 5; Karl et al. (1996), 5; Six and Maier-Reimer (1996), 11; Falkowski et al. (1998), 16; Laws et al. (2000), 11; Del Giorgio and Duarte (2002), 27.5; Henson et al. (2011), 5. In this context the value that is consistent with the difference between DIC in the ML and the deep ocean under preindustrial conditions, together with the piston velocity determined from heat uptake by the world ocean, $F_{pc} = 5.6 \pm 1.8$ m yr^{-1}, seems not unreasonable. (In contrast, values of F_{pc} of 11 or 16 Pg yr^{-1} would require unreasonably high piston velocity, 11 and 17

1865   m yr^{-1}, respectively.) The stock of DIC in the DO compartment consistent with the DIC concentration in the DO, 35917 Pg, corresponding to [DIC] = (2250 $\pm$ 25 μmol kg$_{sw}^{-1}$), is slightly less than that given in earlier versions of the figure, 37100 Pg, which appears to have been evaluated for an assumed total ocean stock of 38000 Pg decremented by the 900 Pg in the mixed layer. Again, although these stocks provide important context for the budget of anthropogenic CO_2, the actual values are of minor importance.

1870   **A6. Piston velocity between mixed layer and deep ocean**

The piston velocity quantifying the rate of transfer of water, and by extension of any tracer, between the ML and the DO is of great importance and interest in many geophysical applications. An early determination of this quantity, 3 to 3.5 m yr^{-1}, was obtained from the difference in the ratio of $^{14}CO_2$ to $^{12}CO_2$ in the upper ocean versus that in the DO, using the half-life of $^{14}CO_2$ as a clock (Broecker and Peng, 1982, pp. 236-243; also Sarmiento and Gruber, 2006, p. 12) .

1875   An alternative approach to determine v_p, taken here, comes from recognition that the piston velocity governing exchange of CO_2 between the ML and the DO would likely find a good analogy in the flux of heat energy from the ML to the DO that has been induced by the increase in global mean surface temperature over the Anthropocene era, especially given the similar time history of these perturbations. The global heat flux into the world ocean has received much attention in measurements. Typically the heat flux density has been quantified by a global heat transfer coefficient κ_H as

1880 $$F_{H,md} = \kappa_H \Delta T \tag{A12}$$

where ΔT, the driving force for the heat transfer, denotes the increase in global mean surface temperature over the Anthropocene era. Here the value is taken as given by the IPCC 2013 assessment (Hartmann et al., 2013, Box 2.2) for year 2010, 0.78 [$\pm$ 0.07] K; the square brackets denote the 5-95 % uncertainty range as commonly given by the IPCC assessments. The rate of increase in ocean heat content is determined from the increase in global heat content, dominated by

1885   the increase in ocean heat content, that is obtained as the integral of heat content over the global ocean. This increase in heat content is divided by the time between the successive measurements. Based on such measurements the 2013 IPCC Assessment report provided best estimates and associated uncertainties of the amount of global heat increase (Rhein et al., 2013, Box 3.1). The increase of global heat content from 1971 to 2010, 274 [196–351] $\times 10^{21}$ J, yields the heating rate of the planet 0.43 [0.31–0.55] W m^{-2}; the increase from 1993-2010, 163 [127–201] $\times 10^{21}$ J, yields a somewhat greater rate of

1890   increase, 0.60 [0.47–0.74] W m^{-2}. Following Rhein et al. (2013), ascribing 93 % of the increase in heat content to the global ocean and taking into account the ocean area fraction of the planet 0.708 yields ocean heating rates 0.56 [0.40 - 0.72] and 0.78 [0.61–0.97] W m^{-2}. (Rhein et al. (2013) give the latter quantity, evidently erroneously, as 0.71 W m^{-2}). Averaging these and retaining the uncertainty limits yields a total heating rate of the global ocean $dH_{\text{tot}}/dt = 0.672$ [± 0.28] W m^{-2}.

In order to determine the transfer velocity it is necessary to recognize that the total heating rate consists of two components,

1895   the heating of the mixed layer and the flux density that corresponds to transfer of heat to the deep ocean,

$$\frac{dH_{\text{tot}}}{dt} = \frac{dH_{\text{m}}}{dt} + F_{H,\text{md}} , \tag{A13}$$

where the second term on the right is the quantity of interest here. The first term, the mixed-layer heating rate, is evaluated as the rate of increase of global temperature times the heat capacity of the upper ocean, evaluated as z_{m} times the volumetric heat capacity of seawater, c_{vol},

1900
$$\frac{dH_{\text{m}}}{dt} = \frac{dT_{\text{m}}}{dt} c_{\text{vol}} z_{\text{m}} . \tag{A14}$$

For $dT_{\text{m}}/dt = 0.0106$ [0.080–0.132] K yr^{-1}, $c_{\text{vol}} = 3.99 \times 10^6$ J m^{-3} K^{-1}, and z_{m} again taken as 100 m, $dH_{\text{m}}/dt = 0.134$ [± 0.02] W m^{-2}; this must be subtracted from dH_{tot}/dt to yield the deep ocean heating rate of the global ocean, $dH_{\text{d}}/dt = 0.538$ [± 0.28] W m^{-2}. By **Eq (A12)** the heat transfer coefficient of the world ocean, $\kappa_H = 0.689$ [± 0.36] W m^{-2} K^{-1}. In turn the piston velocity, which is related to the heat transfer coefficient as

1905 $v_{\text{p},H} = \kappa_H / c_{\text{vol}} ,$ (A15)

is 5.46 [± 2.9] m yr^{-1}. For consistency with the one-sigma estimates of uncertainty used here for the CO$_2$ budget, the 5-95 % uncertainty range is reduced by a factor of 1.64 (representing the ratio of widths for a gaussian distribution) to yield $v_{\text{p},H} = 5.5 \pm 1.8$ m yr^{-1} (relative uncertainty 33 %, 1 sigma). The piston velocity between the mixed layer ocean and the deep ocean determined in this way from measurements of the heating rate of the global ocean, which is consistent with that determined

1910   by the ^{14}CO$_2$ method, provides an independent, observationally based measure of this quantity that can be used with confidence in determining components of global CO$_2$ budget.

Knowledge of the piston velocity v_p permits determination of the net flux density of exchange of any tracer between the ML and DO compartments as

$$\varphi_{net,md} = v_p \left([Tr]_m - [Tr]_d\right) \tag{A16}$$

1915 where [Tr] denotes the volumetric concentration of the tracer. The two terms represent the flux density from the ML to the deep ocean, φ_{md}, and that from the deep ocean to the ML, φ_{dm}, respectively. Noting that the flux is related to the flux density by the area of the world ocean A_o, and that the concentrations in the two compartments are related to the respective stocks by the volumes of the respective compartments (for the atmosphere reckoned at the temperature and pressure of the surface; **SI Text Sect. S2**) leads to an expression for the net flux in terms of the respective stocks

1920 $$F_{net,md} = k_{md}S_m - k_{dm}S_d \tag{A17}$$

where the transfer coefficients k_{md} and k_{dm} characterize the gross flux from the ML to the DO and from the DO to the ML, respectively. These transfer coefficients are related to the piston velocity as

$$k_{md} = \frac{v_p}{z_m}; \quad k_{dm} = \frac{v_p}{z_d}. \tag{A18}$$

The values are $k_{md} = 0.055 \pm 0.018$ yr^{-1} and $k_{dm} = (1.53 \pm 0.5) \times 10^{-3}$ yr^{-1}, where the uncertainties reflect propagated
1925 uncertainty in v_p.

Recently, as discussed in the main text, **Sect. 7.8, Sect. 8.5**, the ocean uptake rate of CO_2 has been determined from the globally integrated increase in DIC between two time periods, 1994 and 2007 (Gruber et al., 2019), permitting determination of the piston velocity. analogously to the approach taken here from increase in ocean heat content. The mean rate of increase in DIC over this time period determined by Gruber et al. was 2.6 ± 0.3 Pg yr^{-1}; after subtraction of 0.48 Pg yr^{-1} for increase
1930 in the ML, this yields 2.1 Pg yr^{-1} for the DO. For anthropogenic stock in the ML 26.0 Pg for year 2000, the piston velocity, uncorrected for return flux, is 8.2 m yr^{-1}, which after correction for the return flux yields $v_p = 8.0 \pm 1.1$ m yr^{-1}, substantially greater than the value determined from uptake of heat, 5.5 ± 1.8 m yr^{-1}, although just outside the mutual uncertainty range.

A7. Anthropogenic emissions

The anthropogenic perturbations to the CO_2 stocks and fluxes shown in red in **Fig. 2** have been and continue to be driven by
1935 emissions from fossil fuel combustion and other industrial activities (primarily calcination of limestone in cement production) Q_{ff}, and by land-use changes (the net of deforestation and afforestation), Q_{lu}. Emissions are calculated by inventory methods as summarized recently by Le Quéré et al. (2018*a*), who provide tabulated annual emissions from both

categories as well as estimates of associated uncertainties (Data Sources; Supporting Information **SI Text Sect. S4**). For the uncertainty associated with Q_{ff}, Le Quéré et al. (2018a) recommend ± 5 %, 1-sigma, independent of time. Present Q_{ff} is

1940 estimated as 9.9 ± 0.5 Pg yr^{-1} (Boden et al. 2017) and Q_{lu} as 1.4 ± 0.7 Pg yr^{-1}, the average of two bookkeeping methods (Houghton and Nassikas, 2017; Hansis et al., 2017), with the uncertainty reflecting a best value judgment. These present emissions given here and in **Fig. 2** denote the averages of the last three years (2014–2016) of the Le Quéré et al. (2018a) tabulation, yielding present annual anthropogenic emission and associated uncertainty 11.2 ± 0.9 Pg yr^{-1}. Although emission from land-use change Q_{lu} is now only 12 % of the total anthropogenic emission, its uncertainty actually exceeds that of Q_{ff};

1945 this greater uncertainty arises from large uncertainty in both the amount of land-use change and the net emission associated with specific types of land-use change. As developed in **Sect. 5.9** and **Table 3** and below **(Sect. A10, Sect. A11)** uncertainty in present anthropogenic CO_2 emission contributes substantially to uncertainty in the inference of the rate of removal of anthropogenic CO_2 from the atmosphere and hence to the turnover time and other measures of the lifetime of excess CO_2.

The cumulative emission from fossil fuel combustion and cement production Ω_{ff} from 1750 to 2016 is calculated as the

1950 integral of annual emission over this period to yield 422 ± 21 Pg. The fractional uncertainty associated with Q_{lu} is estimated as ± 50 % for the annual emission, and hence the absolute uncertainty in integrated emission in Ω_{lu}, 114 Pg, is 5 times that for Ω_{ff}. The total cumulative anthropogenic emission, 1750–2016, Ω_{ant} = 649 Pg, with uncertainty ± 116 Pg or about 18 %. This uncertainty in cumulative emission does not greatly affect the present analysis.

A8. Anthropogenic enhancement of atmospheric stock

1955 The increase in the mixing ratio of atmospheric CO_2 over the Anthropocene has been accurately determined by contemporaneous measurement commencing in 1959 (Keeling et al., 1976; 2001 as updated; Ballantyne et al., 2012, as updated by Dlugokencky and Tans, 2018), and for earlier time from glacial ice cores (Neftel et al., 1985; Etheridge et al., 1996), with CO_2 considered for this purpose well mixed in the atmosphere. The present (2016) mixing ratio is 405 ppm, corresponding to 858.6 Pg; the anthropogenic increase in the stock of CO_2 in the AC, S_a^{ant} = 269.2 Pg, is uncertain to

1960 perhaps 2 ppm, corresponding to 4 Pg, or about 1.6 % of the increment.

Of the cumulative total anthropogenic emission about 41 ± 7 % remains as excess CO_2 in the atmosphere, the balance having been taken up by the ocean and the terrestrial biosphere, shown in **Fig. 2** as 131 and 191 Pg, respectively. Net uptake by the marine biosphere is thought to be small (Sarmiento and Gruber, 2006, p. 424), most fixed CO_2 being rapidly returned to the atmosphere and any anthropogenic perturbation still smaller. Although the sum of the oceanic and terrestrial biosphere

1965 sinks is rather well constrained (to the uncertainty of the aggregate emission, the uncertainty in the incremental amount in the atmosphere being small), the apportionment between the oceanic and terrestrial sinks should be considered much more uncertain, **Appendix A, Sect. A13**.

The annual increment for S_a, $\triangle S_a$, is evaluated as the difference in S_a in successive years as determined, since 1959, by contemporaneous measurements of CO_2 mixing ratio in air. The present annual increment, estimated by regression fit, **SI Text Sect. S5, Fig. S5.1**, is 5.2 ± 0.4 Pg yr^{-1}, the uncertainty arising from fluctuations in the rates of removal processes and/or annual emission. This annual increment represents about half of current emissions (46 ± 5 %), where the uncertainty takes into account uncertainties in $\triangle S_a$ and Q_{tot}. The annual uptake of current emissions by dissolution into the ocean and by the terrestrial biosphere, obtained by difference, is 6.1 ± 1.0 Pg yr^{-1}, where the uncertainty is dominated by uncertainty in annual emission. Much insight is to be gained from examination of the distribution of this rate of uptake into the ML, DO and TB compartments.

A9. Anthropogenic enhancement of DIC in the mixed-layer ocean

The starting point for determination of the stock of anthropogenic DIC in the ML S_m^{ant} is the value for DIC concentration in equilibrium with the atmospheric partial pressure of CO_2. The DIC concentration in equilibrium with any given x_{CO2} can (and can only) be evaluated numerically from the well established equilibrium constants for CO_2 solubility and dissociation (dependent on total alkalinity and salinity and temperature) together with the partial pressure of atmospheric CO_2. This equilibrium relation is shown in **SI Text Sect. S3, Fig. S3.1**. At the present (2016) CO_2 mixing ratio, x_{CO2} = 405 ppm, the equilibrium anthropogenic stock of DIC in the ML would be equal to the stock in equilibrium with this x_{CO2}, 933.7 Pg; this value must be augmented slightly, to 934.2 Pg, to yield an additional flux of 0.6 Pg yr^{-1}, as in the preindustrial situation, and this, minus the similarly augmented preindustrial stock, 900.0 Pg, yields $S_{m,aug}^{ant}$ = 34.2 Pg, where "aug" denotes the augmentation to account for the preindustrial imbalance. This value for $S_{m,aug}^{ant}$ slightly exceeds (5 %) the actual value S_m^{ant} for two reasons: a lag in S_m relative to its (augmented) equilibrium value with respect to S_a by not keeping up with the rate of increase of S_a, and a decrease in S_m due to net removal of CO_2 from the ML to the DO. That is

$$\delta S_m^{ant} \equiv S_{m,aug}^{ant} - S_m^{ant} = \delta_{lag} S_m + \delta_{sink} S_m , \qquad (A20)$$

or alternatively

$$S_m^{ant} = S_{m,aug}^{ant} \left(1 - \frac{\delta S_m}{S_{m,aug}^{ant}} \right) \qquad (A21)$$

The magnitudes of these difference terms are evaluated here.

For a given rate of increase in $S_{m,eq}$ that is driven by the rate of increase in S_a the magnitude of the lag in S_m relative to its equilibrium value is, to good approximation, equal to the time constant describing the relaxation of a perturbation between the two phases τ_{am} times the rate of increase of $S_{m,eq}$, *i.e.*,

1995
$$\delta_{\text{lag}} S_{\text{m}}^{\text{ant}} = \tau_{\text{am}} \frac{dS_{\text{m,aug}}}{dt} \approx \tau_{\text{am}} \frac{dS_{\text{m,eq}}}{dt}.$$
(A22)

For present (2016) CO_2 mixing ratio, 405 ppm, τ_{am} is about 0.74 yr, for assumed $z_{\text{m}} = 100$ m (**Appendix B**). The annual rate of increase in $S_{\text{m,eq}}$, $dS_{\text{m,eq}}/dt$, is given by

$$\frac{dS_{\text{m,eq}}}{dt} = \left(\frac{dS_{\text{m}}}{dS_{\text{a}}}\right)_{\text{eq}} \frac{dS_{\text{a}}}{dt} = K_{\text{ma}}'^{-1} \frac{dS_{\text{a}}}{dt}$$
(A23)

where

2000
$$K_{\text{ma}}' \equiv \left(\frac{dS_{\text{a}}}{dS_{\text{m}}}\right)_{\text{eq}}$$
(A24)

is a quantity that plays an important role in characterizing the rate of transfer of CO_2 between the ML and the AC accounting for the dissociation equilibria of dissolved CO_2. K_{ma}' may be thought of as a differential equilibrium constant, the derivative of S_{a} with respect to S_{m} under equilibrium conditions, that relates the transfer coefficients between the two compartments as

2005 $k_{\text{ma}} = K_{\text{ma}}' k_{\text{am}}$.
(A25)

K_{ma}' is a function of DIC concentration (or equivalently of the CO_2 partial pressure in equilibrium with DIC concentration), which must be determined numerically from the known dependence of equilibrium [DIC] on x_{CO2}, but which is readily determined (**Appendix B**, **Fig. B1**). For present atmospheric CO_2 mixing ratio $K_{\text{ma}}' \approx 10$. With the rate of increase of S_{a}, $dS_{\text{a}}/dt = 5.2$ Pg yr^{-1} obtained from observations (**Appendix A, Sect. A8; SI Text S5**), $dS_{\text{m,eq}}/dt = 0.52$ Pg yr^{-1}, from which

2010 the resultant departure from phase equilibrium is $\delta_{\text{lag}} S_{\text{m}} = 0.40$ Pg or about 1.2 % of $S_{\text{m}}^{\text{ant}}$.

The second contribution to the difference between $S_{\text{m}}^{\text{ant}}$ and $S_{\text{m,aug}}^{\text{ant}}$ arises because of the sink of DIC from the ML to the DO. To good approximation this difference is given (**SI Text Sect. S3**) as the fraction of sink to the DO upon the total gross rate of DIC leaving the ML compartment,

$$\delta_{\text{sink}} S_{\text{m}} = S_{\text{m,aug}}^{\text{ant}} \frac{k_{\text{md}}}{k_{\text{am}} K_{\text{ma}}' + k_{\text{md}}} \approx S_{\text{m,aug}}^{\text{ant}} \frac{k_{\text{md}}}{k_{\text{am}} K_{\text{ma}}'} .$$
(A26)

2015 The approximation results from k_{md}, the coefficient describing transfer of DIC from the ML to the DO being much less than $k_{\text{ma}} = k_{\text{am}} K_{\text{ma}}'$, the transfer coefficient of DIC from the ML to the atmosphere at the current DIC concentration, with K_{ma}' being determined numerically (**Appendix B**). For $k_{\text{md}} = 0.055$ yr^{-1} (**Eq. A18**) and $K_{\text{ma}}' \approx 10$ for $x_{\text{CO2}} = 405$ ppm, the

decrease in S_m due to the sink to the DO $\delta_{\text{sink}} S_m = 1.51$ Pg or 4.4 %, for a total departure from equilibrium of 1.91 Pg or 5.6 % of S_m^{ant}, resulting in $S_m^{\text{ant}} = 32.2$ Pg. The associated uncertainty, derives from uncertainty in S_a^{ant}, and which is essentially completely correlated with that uncertainty, is small, about 0.6 Pg.

The annual change in the ML stock is evaluated as

$$\triangle S_m = \frac{dS_m^{\text{ant}}}{dt} = \frac{d}{dt}\left[S_{m,\text{eq}}^{\text{ant}} \left(1 - \frac{\delta S_m}{S_{m,\text{eq}}^{\text{ant}}} \right) \right] \approx \frac{dS_{m,\text{eq}}^{\text{ant}}}{dt} \left(1 - \frac{\delta S_m}{S_{m,\text{eq}}^{\text{ant}}} \right) \tag{A27}$$

where the approximation rests on the fractional departure of S_m^{ant} from $S_{m,\text{eq}}^{\text{ant}}$ not changing appreciably over a year. Thus $\triangle S_m$ is evaluated as 0.55 Pg yr^{-1} or about 10 % of annual growth of the atmospheric stock S_a, $\triangle S_a$, roughly in the same proportion as the ratio of the anthropogenic stocks in the two compartments, 32.2/269, but a bit lower because of the continuing decrease in incremental solubility of CO_2 with increasing x_{CO2} and [DIC]. The uncertainty in $\triangle S_m$, dominated by year-to-year fluctuation in $\triangle S_a$, is about 0.06 Pg yr^{-1}, correlated with uncertainty in $\triangle S_a$.

A10. Anthropogenic enhancement of CO$_2$ in atmosphere and mixed-layer ocean together

In view of the small difference between $S_{m,\text{eq}}^{\text{ant}}$ and S_m^{ant}, anthropogenic DIC in the ML can be considered to fairly good approximation as in equilibrium with the stock of anthropogenic CO_2 in the AC. It is thus useful to consider the AC and the ML as a single compartment, denoted S_{am}, in analysis of the fate of anthropogenic CO_2, lending great heuristic value to interpretation of the CO_2 budget and pertinent time scales, while introducing slight error. This equilibrium assumption is a consequence of the time constant for equilibration of CO_2 between the atmosphere and the ML being short relative to other time constants governing evolution of the system (**Main text, Sect. 5.3, Sect. 7.7**). The annual increase in S_{am}, $\triangle S_{am} \equiv \triangle S_a + \triangle S_m = 5.7$ Pg yr^{-1}. As the anthropogenic stocks in these two compartments are tightly coupled, the uncertainties must be viewed as additive rather than independent. Thus the uncertainty in S_{am} is 6 Pg, and the uncertainty in $\triangle S_{am}$ is 0.5 Pg yr^{-1}. More substantively, the near equilibrium between excess CO_2 in the two compartments suggests the utility of considering these two compartments as a single compartment, with stock $S_{am}^{\text{ant}} = (269 + 32)$ Pg = 301 Pg, in consideration of time scales characterizing evolution of anthropogenic CO_2.

A11. Net flux of anthropogenic CO$_2$ into the deep ocean

Knowledge of S_m^{ant} permits evaluation of the flux from ML to the DO. In the absence of any return flux from the DO to the ML this flux is given (**Eq A17**) as $F_{md}^{\text{ant}} = k_{md} S_m^{\text{ant}}$, proportional to S_m^{ant}, as the exchange between ocean compartments operates on total DIC. The resulting flux is 1.8 ± 0.6 Pg yr^{-1}, where the uncertainty is dominated by uncertainty in k_{md} and

in turn v_p; it might be observed that unlike S_m^{ant} or k_{md}, F_{md}^{ant} is immune to the choice of z_m, as this quantity cancels out

2045   between S_m^{ant} and k_{md}. This gross flux must be diminished by the return flux to yield the net flux

$$\triangle S_d = F_{md,net}^{ant} = k_{md}S_m^{ant} - k_{dm}S_m^{ant} = k_{md}S_m^{ant}\left(1 - \frac{S_d^{ant}}{S_m^{ant}}\frac{z_m}{z_d}\right). \tag{A28}$$

The major contribution to uncertainty in $\triangle S_d$ is uncertainty in k_{md}, 33 %. The second term on the RHS, representing the return flux of anthropogenic DIC from the DO to the ML is small compared to unity, the factor $z_m/z_d = 1/40$ offset by the ratio of the anthropogenic stocks, S_d^{ant}/S_m^{ant}. For this purpose the anthropogenic increase in the stock in the DO is taken as =

2050   124 Pg, yielding $S_d^{ant}/S_m^{ant} = 131/32.2$, or about 4, for a net return flux of about 10 %. The resulting return flux, 0.2 Pg yr^{-1}, is small relative to other terms in the budget of anthropogenic CO_2. As this term is small, even a fairly large uncertainty in S_d^{ant} say, 50 %, yields an uncertainty in the return flux, 0.1 Pg yr^{-1} that does not contribute substantially to the uncertainty in the overall budget. In turn, $\triangle S_d = 1.6 \pm 0.6$ Pg yr^{-1}, the uncertainty dominated by uncertainty in v_p.

The value 124 Pg for S_d^{ant} comes from numerical integration using the present model, incremented by an additional 20 Pg

2055   that would account for the so-called "flattening" of the atmospheric CO_2 mixing ratio record in the 1940's inferred from glacial ice cores (Trudinger et al., 2002) that is attributed largely if not entirely to an unexplained increase in ocean uptake of 2–3 Pg yr^{-1} for a 6 to 8 year period. This flattening is evident in comparison of modeling results (which do not take the flattening into account) and observations as presented in **Fig. 8** of the main text. The resulting value of $\triangle S_d$ given in **Fig. 2** is 1.5 Pg yr^{-1} with uncertainty ± 0.5 Pg yr^{-1}. The uncertainty in S_d^{ant} is likewise dominated by uncertainty in v_p, ± 33 % or 34

2060   Pg, with an additional, structural uncertainty arising from the increment associated with the observed flattening of atmospheric CO_2 mixing ratio in the 1940's, taken as ± 10 Pg, small compared to that from v_p, for a total uncertainty of ± 36 Pg.

Comparison of the annual increments in the ML and DO compartments shows that the increment in the DO compartment is dominant, by a factor of 3 or so. The flux of dissolved CO_2 from the ML to the DO assumes a much greater importance to

2065   the budget of excess CO_2 than the flux between the AC and the ML, not just because of its magnitude but because this flux is to first order an irreversible sink of CO_2 until the incremental return flux from the deep ocean to the upper ocean becomes appreciable relative to the incremental downward flux.

As the residence time in the DO is long (~ 650 yr, **Main text, Sect. 5.4**) relative to the century time scale that is the primary focus of the present analysis, the DO can be considered to be a sink for anthropogenic CO_2 on this time scale. The net return

2070   flux from the DO to the ML reflected **in Eq (A28)** is a consequence of the integrated uptake of CO_2 from the ML to the DO over the Anthropocene and is a measure of the extent to which the DO can be considered an irreversible sink for

anthropogenic CO_2. The return flux from the DO to the ML would be expected to increase in the future as the DO equilibrates with the Ml and would need to be accounted for in any long-term projections.

A12. Total oceanic uptake of anthropogenic CO_2

2075 The sums of the anthropogenic stocks in ML and DO compartments $S_{md}^{ant} = S_m^{ant} + S_d^{ant}$ and of the annual increments to these stocks $\triangle S_{md} = \triangle S_m + \triangle S_d$, representing the total oceanic uptake of anthropogenic CO_2 are of value in consideration of the disposition of anthropogenic CO_2, especially as the latter quantity is reported by many investigators. From the values given for these quantities in **Sect. A9 and Sect. A11,** $S_{md}^{ant} = 156 \pm 36$ Pg and $\triangle S_{md} = 2.2 \pm 0.6$ Pg yr^{-1}. As discussed in **Sect. A9,** S_m^{ant} and $\triangle S_m$ are fairly tightly constrained by equilibrium with the stock and annual increment of CO_2 in the AC. Hence 2080 both uncertainties are dominated by uncertainty in v_p.

A13. Stock of anthropogenic CO_2 in the terrestrial biosphere and associated fluxes

In contrast to uptake of anthropogenic CO_2 by the two ocean compartments, for which observation-based fluxes have been evaluated using independently determined transfer coefficients and solubilities, there is no direct approach to determination of the additional amount of CO_2 taken up by the terrestrial biosphere (TB = LB + OB) over the Anthropocene S_{lo}^{ant} or of its 2085 annual increment, $\triangle S_{lo}^{ant}$. However, under assumption that the TB is the only remaining reservoir for anthropogenic CO_2, then by conservation of the amount of carbon, S_{lo}^{ant} is determined as the difference between the total anthropogenic CO_2 introduced into the atmosphere Ω_{tot} and the anthropogenic increment in the AC, ML, and DO stocks,

$$S_{lo}^{ant} = \Omega_{ant} - S_a^{ant} - S_m^{ant} - S_d^{ant} - \Omega_{lu} = \Omega_{ff} - S_a^{ant} - S_m^{ant} - S_d^{ant} , \tag{A29}$$

where the latter equality includes emissions only from fossil fuel combustion and other industrial activities, not LUC 2090 emissions, as LUC emissions deplete the stock of the TB. For total anthropogenic emission $\Omega_{ff} = 422 \pm 21$ Pg (**Appendix A, Sect. A7**) and the values of the several stocks developed above S_{lo}^{ant} thus far over the Anthropocene is coincidentally near zero, 8 ± 12 Pg. (A similar conclusion, but with substantially greater uncertainty, was reached by Arora et al., 2011).

Similarly the annual change in the TB stock is given by

$$\triangle S_{lo} = Q_{ant} - \triangle S_{am} - \triangle S_d - Q_{lu} = Q_{ff} - \triangle S_{am} - \triangle S_d , \tag{A30}$$

2095 where the $\triangle S_a$ and $\triangle S_m$ terms are combined because of their tight coupling. This annual change is to be distinguished from the net transfer flux from the AC to the TB,

$$F_{a\text{-lo,net}}^{ant} \equiv F_{at}^{ant} - F_{ta}^{ant} = \triangle S_{lo} + Q_{lu} = Q_{ff} - \triangle S_{am} - \triangle S_d + Q_{lu} = Q_{ant} - \triangle S_{am} - \triangle S_d \tag{A31}$$

Attention is called to the difference between the last equalities of **Eqs A30** and **A31**; the expression for $\triangle S_{lo}$ contains just fossil fuel emissions Q_{ff}, whereas the expression for $F_{at,net}^{ant}$ contains total anthropogenic emissions Q_{ant}. The latter equality of **Eq A31** permits observational determination of $F_{a\text{-}lo,net}^{ant}$ as 4.0 ± 1.1 Pg yr^{-1}.

A key quantity in the interpretation of the fluxes between the atmosphere and the obdurate biosphere and hence in governing the lifetime of excess atmospheric CO_2 is the preindustrial (PI) flux from the atmosphere to the obdurate biosphere OB, F_{ao}^{pi}. As developed here this quantity cannot be uniquely determined from observations as it depends on assumed value of the stock of the PI labile biosphere S_l^{pi} and on the exponent b characterizing the dependence of gross primary production GPP on atmospheric stock. However based on observations the range of F_{ao}^{pi} can be considerably constrained, and this in turn places constraints on S_l^{pi} and b. These constraints, within the present model, are developed here.

As noted in the **main text** the dominant flux from the atmosphere to the terrestrial biosphere is to the labile biosphere LB and is taken as GPP, the magnitude of which is given by a power law dependence on atmospheric stock (**Eq 3.1**).

$$F_{al} = F_{GPP}^{pi} \left(\frac{S_a}{S_a^{pi}} \right)^b , \tag{A32}$$

The flux from the atmosphere to the OB is given by the same power-law dependence:

$$F_{ao} = F_{ao}^{pi} \left(\frac{S_a}{S_a^{pi}} \right)^b \tag{A33}$$

The only removal pathway from the LB is the return flux to the atmosphere, from which

$$\frac{dS_l}{dt} = F_{al} - F_{al} \tag{A34}$$

The reverse flux is taken as proportional to the stock in the LB S_l, with temporally constant transfer coefficient k_{la}, from which

$$\frac{dS_l}{dt} = F_{GPP}^{pi} \left(\frac{S_a}{S_a^{pi}} \right)^b - k_{la} S_l \tag{A35}$$

At PI steady state $\dfrac{dS_l^{pi}}{dt} = 0$ \hfill (A36)

from which $k_{la} = \dfrac{F_{GPP}^{pi}}{S_l^{pi}}$. (A37)

PI GPP F_{GPP}^{pi} is taken as 120 Pg yr^{-1}; hence k_{la} depends inversely on assumed S_l^{pi}, which is initially allowed to vary over a
2120   considerable range, 1 to 1000 Pg, which range is subsequently greatly constrained by observations.

Focusing now on the fluxes between the AC and the OB the rate of increase of stock in the OB due to transfer of materials
between compartments, *i.e.*, not including the rate of decrease in S_O due to LU emissions, denoted $\triangle S_o^{tr}$ is

$$\triangle S_o^{tr} = F_{ao} - F_{oa} - F_{om}^{pi}$$ (A38)

where F_{om}^{pi} denotes the PI flux from the OB to the ML ocean, which is taken as temporally constant and in any event is quite
2125   small, 0.6 Pg yr^{-1}. With F_{oa} taken as proportional to S_O with transfer coefficient k_{oa}, like k_{la}, taken as temporally constant,

$$\triangle S_o^{tr} = F_{ao}^{pi}\left(\dfrac{S_a}{S_a^{pi}}\right)^b - k_{oa}S_o - F_{om}^{pi}$$ (A39)

At PI steady state $\triangle S_o^{pi} = 0 = F_{ao}^{pi} - k_{oa}S_o^{pi} - F_{om}^{pi}$ (A40)

from which $k_{oa} = \dfrac{F_{ao}^{pi} - F_{om}^{pi}}{S_o^{pi}}$ (A41)

Specializing to present day values **Eq A39** becomes

2130 $$\triangle S_o^{tr,pd} = F_{ao}^{pi}\left(\dfrac{S_a^{pd}}{S_a^{pi}}\right)^b - \dfrac{F_{ao}^{pi} - F_{om}^{pi}}{S_o^{pi}}S_o^{pd} - F_{om}^{pi}$$ (A42)

which yields for F_{ao}^{pi}

$$F_{ao}^{pi} = \dfrac{\triangle S_o^{tr,pd} - F_{om}^{pi}\left(\dfrac{S_o^{pd} - S_o^{pi}}{S_o^{pi}}\right)}{\left(\dfrac{S_a^{pd}}{S_a^{pi}}\right)^b - \dfrac{S_o^{pd}}{S_o^{pi}}}$$ (A43)

Evaluation of F_{ao}^{pi} thus requires knowledge of the present day rate of increase of S_O due to transfer, $\triangle S_o^{tr,pd}$, and PI and PD
S_O, S_o^{pi} and S_o^{pd}, all of which depend on observations and depends as well as on assumptions on S_l^{pi} and b, yielding a range
2135   of values for F_{ao}^{pi}. This range of F_{ao}^{pi} is determined as follows.

First, the present day (PD) total net rate of transfer of carbon into the TB $\triangle S_{\text{lo}}^{\text{tr,pd}}$ is confidently evaluated as the difference between emissions (of fossil plus cement CO_2) and the sum of annual increments in the several other compartments, **Eq A30**, the uncertainty dominated by uncertainty in emissions, yielding $\triangle S_{\text{o}}^{\text{tr,pd}} = 4.0 \pm 1.0$ Pg yr^{-1}. The net rate of transfer into the OB stock $\triangle S_{\text{o}}^{\text{tr,pd}}$ is determined by subtraction of the net rate of transfer between the atmosphere the LB,

2140 $$\triangle S_{\text{o}}^{\text{tr,pd}} = \triangle S_{\text{lo}}^{\text{tr,pd}} - \triangle S_{\text{l}}^{\text{pd}};$$ (A44)

no qualifier denoting transfer is required for $\triangle S_{\text{l}}^{\text{pd}}$ as there are no flux components for that compartment other than transfer to and from the atmosphere.

The net rate of transfer into the LB stock is equal to the annual increment in this stock, which is obtained under assumption of near steady state between the stocks in the AC and the LB together with assumptions on the two parameters S_{l}^{pi} and b as

2145 the time derivative of F_{GPP} as given by **Eq 3.1**,

$$\triangle S_{\text{l}}^{\text{pd}} = \frac{dS_{\text{l}}^{\text{pd,ss}}}{dt} = b \frac{S_{\text{l}}^{\text{pi}}}{\left(S_{\text{a}}^{\text{pi}}\right)^{b}} \left(S_{\text{a}}^{\text{pd}}\right)^{b-1} \frac{dS_{\text{a}}^{\text{pd}}}{dt}.$$ (A45)

The resulting PD annual increment in S_{O} due to transfer from other compartments $\triangle S_{\text{o}}^{\text{tr,pd}}$ is shown by the contour lines in **Fig. A1b** for the entire range of S_{l}^{pi} and b examined (consistent with positive $\triangle S_{\text{o}}^{\text{pd}}$); that range is greatly reduced, to the domain indicated by the light red quadrilateral, by further comparisons with observations, as discussed in the **Main Text,**

2150 **Sect. 7.2**, yielding a range for $\triangle S_{\text{o}}^{\text{tr,pd}}$ of 1.3 to 3.6 Pg yr^{-1}, where the range does not include the uncertainty on $\triangle S_{\text{lo}}^{\text{tr,pd}}$. This range covers a substantial fraction of the total annual uptake by the TB; as developed **Sect. 7.2**, even with observational constraints on $\triangle S_{\text{lo}}^{\text{tr,pd}}$, the dynamics of excess CO_2 subsequent to hypothetical cessation of emissions varies substantially depending on the value of this quantity.

A value for the total PI stock in the TB $S_{\text{t}}^{\text{pi}} = S_{\text{o}}^{\text{pi}} + S_{\text{l}}^{\text{pi}} = 2800$ Pg is assumed, based on inventory by Carvalhais et al. (2014);

2155 the PI stock in the OB is thus dependent on S_{l}^{pi} as $S_{\text{o}}^{\text{pi}} = S_{\text{t}}^{\text{pi}} - S_{\text{l}}^{\text{pi}}$; as S_{l}^{pi} is small relative to S_{t}^{pi}, S_{o}^{pi} depends only weakly on assumed S_{t}^{pi}.

The present-day stock in the OB S_{o}^{pd}, like $\triangle S_{\text{lo}}^{\text{tr,pd}}$, is evaluated, based on conservation of matter, as the difference between emissions (here integrated emissions over the Anthropocene) and the increments (here total increments) in the several other compartments over the Anthropocene, diminished also by land-use-change emissions of carbon (taken as entirely from the

2160 OB):

$$S_{\text{o}}^{\text{Ant,pd}} = \Omega_{\text{ant}}^{\text{pd}} - (S_{\text{a}}^{\text{Ant,pd}} + S_{\text{m}}^{\text{Ant,pd}} + S_{\text{d}}^{\text{Ant,pd}} + S_{\text{l}}^{\text{Ant,pd}}) - \Omega_{\text{luc}}^{\text{pd}}$$ (A46)

where Ω denotes integrated emissions. Noting that integrated total emissions is the sum of integrated fossil fuel and land-use change emissions, $\Omega_{ant}^{pd} = \Omega_{ff}^{pd} + \Omega_{luc}^{pd}$ yields

$$S_o^{Ant,pd} = \Omega_{ff}^{pd} - (S_a^{Ant,pd} + S_m^{Ant,pd} + S_d^{Ant,pd} + S_l^{Ant,pd}) \tag{A47}$$

2165   Here Ω_{ff}^{pd} is from inventory. $S_a^{Ant,pd}$ from direct observation is 269.2 Pg. $S_m^{Ant,pd}$ from **Appendix A9** is 32.2 Pg. $S_d^{Ant,pd}$ is taken as 116 Pg, based on integration of net exchange rate of stocks in the ML and DO over the Anthropocene. Finally $S_l^{Ant,pd}$ is evaluated similarly to $S_m^{Ant,pd}$ based on the slight lag of LB stock relative to steady state between the AC and the LB, yielding

$$S_l^{Ant,pd} = S_l^{Ant,pd,ss} - \frac{dS_l^{Ant,pd,ss}}{dt}\tau_{al}, \tag{A48}$$

2170   where $S_l^{Ant,pd,ss}$ denotes the PD steady state stock in the LB,

$$S_l^{Ant,pd,ss} = S_l^{pi}\left(\frac{S_a^{pd}}{S_a^{pi}}\right)^b - S_l^{pi}, \text{ and} \tag{A49}$$

$$\tau_{al} = \frac{\dfrac{S_a^{pd}}{F_{GPP}^{pi}}}{\left(\dfrac{S_a^{pd}}{S_a^{pi}}\right)^b + \dfrac{S_a^{pd}}{S_l^{pi}}}, \tag{A50}$$

both of which quantities are evaluated in terms of observables and the two parameters S_l^{pi} and b. The resulting values of $S_o^{Ant,pd}$, **Fig. A1a**, exhibit a considerable range, even within the observational constraints indicated by the light red

2175   quadrilateral.

The resulting range of values of F_{ao}^{pi}, obtained based on observational constraints and assumptions on S_l^{pi} and b and shown in **Fig. A1c**, is about 5 to 20 Pg yr^{-1} or about 4 to 17 % of F_{al}^{pi}. Knowledge of F_{ao}^{pi} permits evaluation, **Eq A39**, of the time dependent flux from the atmosphere into the OB F_{ao}. Although this flux is technically part of GPP, as it is small compared to that quantity, identifying F_{al} as F_{GPP} leads to no significant error in interpretation.

2180   Knowledge of F_{ao}^{pi} permits evaluation of the transfer coefficient k_{oa} by **Eq A41**, shown in **Fig. 4d** of the main text. For the observationally constrained range of (S_l^{pi}, b) this transfer coefficient ranges from 0.0015 to 0.004 yr-1; the corresponding range for lifetime of carbon in the OB, taken as the inverse of k_{oa}, is 125 to 700 yr, comparable to, to well longer, than the time scale of substantial decrease of excess atmospheric CO_2 subsequent to abrupt cessation of emissions and thus consistent

2185   with the OB being essentially an irreversible sink for excess CO_2 on this time scale. Based on the transfer coefficient k_{oa} and the small net anthropogenic change in S_O, **Fig. A1*b***, the PD anthropogenic flux from the OB to the AC is likewise quite small [-0.1, -0.3] Pg yr^{-1}, shown in **Fig. 2** of the main text.

Appendix B. Rate of transfer of CO_2 between the atmosphere and the ocean mixed layer

B1. Kinetics of transfer of CO_2 between gas and aqueous phases

The only CO_2 species in the atmosphere is gaseous CO_2. In solution, however, dissolved CO_2 (commonly denoted as the

2190   hydrate, carbonic acid, H_2CO_3) dissociates to an equilibrium mixture of H_2CO_3, bicarbonate ion HCO_3^-, and carbonate ion CO_3^{2-}, the totality of the three species being denoted dissolved inorganic carbon DIC. The equilibria are well characterized, and the kinetics of these dissociation-association reactions are sufficiently rapid that equilibrium can be assumed on the time scales of interest here. Because the only species that exchanges between solution and the gas phase is CO_2, the rate of this exchange is proportional to the concentration of H_2CO_3, not to that of DIC. This has an effect on the kinetics of the

2195   equilibration between gaseous CO_2 and DIC and on how the rates of exchange between the two phases are related to the stocks of CO_2 and DIC, the quantities of principal interest here. This phenomenon is well recognized (e.g., Sarmiento and Gruber, 2006, pp. 330-331) but is nonetheless worth revisiting to develop relations between flux densities (expressed in terms of concentrations) and fluxes (expressed in terms of stocks in the two compartments).

The gross flux density from the atmosphere to the ML is proportional (by the transfer coefficient γ_{am}) to the volumetric

2200   concentration (denoted by square brackets) of gaseous CO_2,

$$\phi_{am} = \gamma_{am}[CO_2(g)].$$ (B1)

As noted in the text the coefficient γ_{am} for this phase transfer process is not a constant (at a given temperature and pressure) as would be the case for a rate coefficient of a chemical reaction, but depends on situational variables, importantly the wind speed that induces convective mixing in the vicinity of the interface. For moderate- to low-solubility gases such as CO_2 the

2205   rate-limiting step is mass transport on the water side of the interface. The gross flux density from the ML to the atmosphere is similarly proportional to the concentration of aqueous H_2CO_3,

$$\phi_{ma} = \gamma_{ma}[H_2CO_3(aq)]$$ (B2)

The concentrations have dimension amount per volume; the flux densities ϕ have dimension amount per area and time; and the transfer coefficients γ have dimension amount per area and time per (amount per volume) or length per time (and are thus

2210   frequently denoted a transfer "velocity"). The net flux density is the difference between the gross flux densities

$$\phi_{\text{am,net}} = \gamma_{\text{am}}[CO_2(g)] - \gamma_{\text{ma}}[H_2CO_3(aq)]. \tag{B3}$$

At equilibrium the net flux $\phi_{\text{am,net}} = 0$, from which it is seen that the two transfer coefficients are related by H, the equilibrium constant for dissolution of CO_2, commonly denoted the (dimensionless, volumetric) Henry's law solubility constant, which is a function of temperature but is only weakly dependent on solution composition and very weakly on atmospheric pressure and CO_2 partial pressure.

$$H = \frac{\gamma_{\text{am}}}{\gamma_{\text{ma}}} = \left(\frac{[H_2CO_3(aq)]}{[CO_2(g)]} \right)_{\text{eq}} \tag{B4}$$

As an equilibrium constant, H is not dependent on wind speed, in contrast to the individual transfer coefficients γ_{am} and γ_{ma}.

Equation **B4** permits examination of the kinetics of relaxation of a perturbation from a system initially at equilibrium in order to determine the time constant of this relaxation. For a closed system initially at equilibrium that is perturbed by addition of an incremental small amount of CO_2,

$$\phi_{\text{am,net}} = \gamma_{\text{am}} \left([CO_2(g)]_0 + \delta[CO_2(g)] \right) - \gamma_{\text{ma}} \left([H_2CO_3(aq)]_0 + \delta[H_2CO_3(aq)] \right) \tag{B5}$$

where the subscript 0 denotes the initial equilibrium state, and where δ denotes the departure from equilibrium, from which

$$\phi_{\text{am,net}} = \gamma_{\text{am}} \delta[CO_2(g)] - \gamma_{\text{ma}} \delta[H_2CO_3(aq)]. \tag{B6}$$

By **Eq (B4)**

$$\phi_{\text{am,net}} = \gamma_{\text{am}} \left(\delta[CO_2(g)] - \frac{1}{H} \delta[H_2CO_3(aq)] \right). \tag{B7}$$

It is desired to express the reverse flux density in terms of [DIC] rather than [H$_2$CO$_3$]. Following Sarmiento and Gruber (2006, p. 330), application of the chain rule

$$\delta[H_2CO_3] = \frac{d[H_2CO_3]}{d[DIC]} \delta[DIC]. \tag{B8}$$

together with the definition

$$\beta \equiv \frac{d[H_2CO_3]}{d[DIC]} \tag{B9}$$

yields the expression

$$\phi_{\text{am,net}} = \gamma_{\text{am}}\left(\delta[CO_2(g)] - \frac{\beta}{H}\delta[\text{DIC}]\right) \tag{B10}$$

The quantity β is an equilibrium property of the CO_2–DIC system that can (and can only) be evaluated numerically from
2235 knowledge of the equilibrium constants for dissociation of H_2CO_3. β has the dimension of an equilibrium constant, the ratio of the concentrations of reagent and product, but it is a differential quantity, the ratio of the changes in concentrations resulting from a slight perturbation, rather than the ratio of the concentrations themselves, and consequently it is denoted here a differential equilibrium constant. Importantly β is dependent on ocean alkalinity and to lesser extent, through the equilibrium constants, on salinity and temperature. For the purpose of the present analysis the alkalinity of seawater is taken
2240 as 2349 µmol kg_{sw}^{-1} (consistent with the values of S_m and S_a given for preindustrial conditions in the several prior versions of **Fig. 2**) with salinity 35, and temperature 18˚C. The dependence of β on CO_2 mixing ratio over the range of interest for the Anthropocene is shown in **Fig. B1** for these conditions.

B2. Application to transfer of CO_2 between the atmosphere and the world ocean

For consideration of rates of transfer of CO_2 in the atmosphere–ML system it is desired to relate rates of change of stocks in
2245 the several compartments, expressed in terms of flux F rather than flux density φ, to stocks S rather than concentrations C. The flux between the AC and the ML and the stocks in the two compartments are related to the flux density and the two concentrations as

$$\phi = \frac{F}{A_o}; \quad S_m = A_o z_m[\text{DIC}]; \quad S_a = V_{\text{atm}}(T_{\text{sfc}}, p_{\text{sfc}})[CO_2(g)] \tag{B11}$$

where A_o is the area of the world ocean, z_m is the depth of the ML, and $V_{\text{atm}} = N_{\text{air}}RT_{\text{sfc}}/p_{\text{sfc}}$, with N_{air} the amount (moles)
2250 of air in the global atmosphere. Substitution into **Eq B10** yields the global net flux of CO_2 from the atmosphere to the mixed layer for small departure from phase equilibrium as

$$F_{\text{am,net}} = \frac{\gamma_{\text{am}}A_o}{V_{\text{atm}}}\left(\delta S_a - \frac{V_{\text{atm}}}{A_o z_m}\frac{\beta}{H}\delta S_m\right). \tag{B12}$$

Comparison with **Eq A3** of **Appendix A** that defines the transfer coefficient relating the gross flux of CO_2 from the atmosphere into the world ocean to the atmospheric stock,

2255 $$k_{\text{am}} \equiv F_{\text{am}}/S_a, \tag{A3}$$

permits the identification $k_{\text{am}} = \frac{\gamma_{\text{am}}A_o}{V_{\text{atm}}}$ $\tag{B13}$

so that $F_{\text{am,net}} = k_{\text{am}}\left(\delta S_a - K'_{\text{ma}}\delta S_m\right),$ (B14)

where $K'_{\text{ma}} = \dfrac{V_{\text{atm}}}{A_o z_m H}\beta = \left(\dfrac{dS_a}{dS_m}\right)_{\text{eq}}$ (B15)

More generally, as k_{am} does not depend on DIC concentration, **Eq B14** applies to any state of the system (not just small departures from equilibrium), with K'_{ma} viewed as a function of DIC concentration in the ML, or equivalently of S_m,

$F_{\text{am,net}} = k_{\text{am}}\left(S_a - K'_{\text{ma}}(S_m)S_m\right),$ (B16)

where the dependence of K'_{ma} on S_m is explicitly indicated. Like β, K'_{ma} may be thought of as a differential equilibrium constant but pertinent not to x_{CO2} and [DIC], but to the two stocks. However unlike k_{am}, which can be considered a geophysical constant, independent of the CO_2 partial pressure or of the DIC concentration, K'_{ma} exhibits a dependence on DIC concentration (or equivalently on the x_{CO2} in equilibrium with DIC concentration); as well, K'_{ma} depends on the arbitrary choice of the depth taken for the mixed layer z_m. As K'_{ma} is proportional to β by geophysical constants (as well as inversely proportional to z_m) it can be shown on the same graph as β, by a proportional axis, **Fig. B1**, with numerical value of increasing from 5 to 10 over the Anthropocene; for $z_m = 100$ m, as employed throughout this analysis, the proportionality factor in **Eqs B12 and B15** $V_{\text{atm}}/(A_o z_m H) = 139.26$. K'_{ma} can equivalently be interpreted as the ratio of the reverse transfer coefficient (from the ML to the AC) to the forward transfer coefficient (from the AC to the ML) k'_{ma},

$K'_{\text{ma}} = \dfrac{k'_{\text{ma}}}{k_{\text{am}}}.$ (B17)

where k'_{ma} represents the transfer coefficient characterizing the flux from the ML to the AC expressed in terms of the departure of S_m from its equilibrium value as

$F_{\text{ma}} = k'_{\text{ma}}\left(S_m - S_{m,\text{eq}}\right) = K'_{\text{ma}}k_{\text{am}}\left(S_m - S_{m,\text{eq}}\right).$ (B18)

The transfer coefficient k'_{ma} so defined is used in solution of the differential equations for evolution of the stocks of CO_2 in response to the anthropogenic perturbation as it automatically takes into account the redistribution of the DIC species associated with transfer of CO_2 from the ML to the AC.

The differential equilibrium constant K'_{ma} is closely related to a quantity known as the buffer factor or Revelle factor (Sarmiento and Gruber, 2006, p.332)

$\mathfrak{R} \equiv \left(\dfrac{d\ln p_{\text{CO2}}}{d\ln[\text{DIC}]}\right)_{\text{eq}}$ (B19)

that is commonly employed to relate the change in CO_2 partial pressure to the change in DIC taking into account the equilibria of the DIC species.

$$K'_{ma} = \left(\frac{dS_a}{dS_m}\right)_{eq} = \left(\frac{S_a}{S_m}\right)_{eq}\left(\frac{d\ln S_a}{d\ln S_m}\right)_{eq} = \left(\frac{S_a}{S_m}\right)_{eq}\left(\frac{d\ln p_{CO2}}{d\ln[DIC]}\right)_{eq} = \Re\left(\frac{S_a}{S_m}\right)_{eq}. \tag{B20}$$

Expressing F_{ma} by **Eq B18** thus automatically satisfies this Revelle relation, as examined in **Appendix F, Fig. F1**.

Appendix C. Dependence of gross primary production on CO_2 mixing ratio, and fertilization exponent b

As input to the observational and modeling based analysis of the CO_2 budget it was necessary to specify the increase in global gross primary production (GPP) over the Anthropocene. An increase in the rate of accretion of CO_2 by the TB over the past several decades is indicated in numerous studies (e.g., Keeling et al., 2011; Los, 2013; Keenan et al., 2016; Schimel et al., 2015; Zhang et al., 2016; Zhu et al., 2016; Cheng et al., 2017), but the enhancement of CO_2 uptake is not unequivocally attributed to increased CO_2 (e.g., Kondo et al., 2018, Zhu et al., 2018). Increased drawdown of CO_2 by terrestrial vegetation is found also in numerous studies with vegetation models or as the residual between emissions and atmospheric growth after accounting for ocean uptake of CO_2, the latter likewise determined by modeling, summarized by Keenan et al. (2016).

A survey of recent observational and modeling studies is summarized in **Fig. C1** with estimates of GPP plotted against mixing ratio of atmospheric CO_2 on a double logarithmic plot. The slopes of the lines fit through the data points correspond to the exponent b in **Eq 3.1** of the main text relating GPP to CO_2 mixing ratio or, equivalently to atmospheric stock S_a,

$$F_{GPP}(t) = F_{GPP}^{pi}\left(\frac{x_{CO2}(t)}{x_{CO2}^{pi}}\right)^b = F_{GPP}^{pi}\left(\frac{S_a(t)}{S_a^{pi}}\right)^b; \tag{3.1}$$

The estimates of PD GPP span a range of more than a factor of 2, with satellite based determinations generally lower than model-based estimates. More important from the present perspective is the rate of change of GPP. The several satellite based observations tend to exhibit little increase with time, whereas the model-based estimates uniformly exhibit increase with time, as does the estimate of Cheng et al. (2017) that is based on observations of water use and water use efficiency. The range of exponents 0 to 1.3 formed the basis for the parameterization of b in the model calculations reported in the main text. As noted in **Sect. 7.2, Sect. 7.3** of the main text the observational constraints on the PI stock in the labile biosphere S_l^{pi} and on PD CO_2 mixing ratio set bounds on b, $0.4 \leq b \leq 0.9$. For PI F_{GPP} taken as 120 Pg yr^{-1}, the resultant range of PD F_{GPP},

2305   is 139 Pg yr^{-1} $\leq F_{\text{GPP}}^{\text{pd}} \leq$ 163 Pg yr^{-1}, or an increase of 16 to 40 %. These ranges for b and F_{GPP} are much narrower than observational and model based estimates in **Fig. C1**.

Appendix D. Equilibrium–steady-state (ESS) model.

As noted in **Sect. 6.3**, the stocks in the AC and the ML are expected to be in near equilibrium on account of rapid exchange between these compartments. Likewise the stocks in the AC and the LB are expected to be in near steady state on account of

2310   rapid exchange between those compartments. Here the assumptions of equilibrium and steady state are applied to express the stocks in the ML and the LB in terms of the AC stock in a set of ODEs in a smaller number of quantities. The intent is not to use this model, denoted the equilibrium–steady-state (ESS) model, in lieu of the full model but rather to compare the results from the ESS model with those from the full model and thereby gain insight into the dynamics of the full model and more broadly of the evolution of anthropogenic carbon in the biogeosphere.

2315   From **Eq 6.1**, and expressing the stocks in terms of the anthropogenic changes (*i.e.*, differences from values in year 1750),

$$\frac{dS_a^{\text{ant}}}{dt} = Q_{\text{ff}}(t) + Q_{\text{lu}}(t) - \frac{dS_m^{\text{ant}}}{dt} - \frac{dS_l^{\text{ant}}}{dt} - \frac{dS_d^{\text{ant}}}{dt} - \frac{dS_{o,t}^{\text{ant}}}{dt} , \tag{D1}$$

where the several derivatives on the RHS denote the changes in the several stocks (conservation of carbon stock); the additional subscript t in the last term denotes that this term represents only the transport component of that change in stock.

Under assumption of equilibrium between the ML and the atmosphere (cf., **Eq 4.4**),

$$S_m^{\text{eq,ant}} = K_{\text{am}}\left(S_a^{\text{eq,ant}} + S_a^{\text{pi}}\right) - S_m^{\text{pi}} , \tag{D2}$$

where $K_{\text{am}} = K_{\text{ma}}^{-1}$ is the equilibrium constant characterizing the solubility of CO_2 as DIC (again expressed in terms of the stocks) and where it is noted that K_{am} is itself a function of the total stock of CO_2 (in either compartment). The time derivative $dS_m^{\text{eq,ant}}/dt$ required for **Eq 6.1** is calculated (cf., **Eq 4.3**) as

$$\frac{dS_m^{\text{ant}}}{dt} = \frac{dS_m^{\text{eq}}}{dS_a^{\text{ant}}}\frac{dS_a^{\text{ant}}}{dt} = K'_{\text{am}}\frac{dS_a^{\text{ant}}}{dt} . \tag{D3}$$

2325   A similar approach is taken to evaluate $dS_l^{\text{ss,ant}}/dt$. Under assumption of steady state in the LB, *i.e.*, $dS_l/dt \approx 0$, **Eq. 6.4** yields for the SS LB stock

$$S_{\mathrm{l}}^{\mathrm{ss}} = \frac{F_{\mathrm{GPP}}^{\mathrm{pi}}}{k_{\mathrm{la}}}\left(\frac{S_{\mathrm{a}}}{S_{\mathrm{a}}^{\mathrm{pi}}}\right)^b = \frac{F_{\mathrm{GPP}}^{\mathrm{pi}}}{k_{\mathrm{la}}}\left(\frac{S_{\mathrm{a}}^{\mathrm{ant}}+S_{\mathrm{a}}^{\mathrm{pi}}}{S_{\mathrm{a}}^{\mathrm{pi}}}\right)^b, \tag{D4}$$

which, together with **Eq 4.10** yields

$$S_{\mathrm{l}}^{\mathrm{ss}} = S_{\mathrm{l}}^{\mathrm{pi}}\left(\frac{S_{\mathrm{a}}^{\mathrm{ant}}+S_{\mathrm{a}}^{\mathrm{pi}}}{S_{\mathrm{a}}^{\mathrm{pi}}}\right)^b. \tag{D5}$$

2330 Noting that

$$\frac{dS_{\mathrm{l}}^{\mathrm{ss}}}{dt} = \frac{dS_{\mathrm{l}}^{\mathrm{ss}}}{S_{\mathrm{a}}^{\mathrm{ant}}}\frac{S_{\mathrm{a}}^{\mathrm{ant}}}{dt} = \frac{S_{\mathrm{l}}^{\mathrm{pi}}}{S_{\mathrm{a}}^{\mathrm{pi}}}b\left(\frac{S_{\mathrm{a}}^{\mathrm{ant}}+S_{\mathrm{a}}^{\mathrm{pi}}}{S_{\mathrm{a}}^{\mathrm{pi}}}\right)^{b-1}\frac{S_{\mathrm{a}}^{\mathrm{ant}}}{dt}, \tag{D6}$$

then within the steady state approximation, the rate of change in $S_{\mathrm{l}}^{\mathrm{ant}}$ is related to the rate of change in $S_{\mathrm{a}}^{\mathrm{ant}}$ as

$$\frac{dS_{\mathrm{l}}^{\mathrm{ant}}}{dt} = \frac{dS_{\mathrm{l}}^{\mathrm{ss}}}{dt} = b\frac{S_{\mathrm{l}}^{\mathrm{pi}}}{S_{\mathrm{a}}^{\mathrm{pi}}}\left(\frac{S_{\mathrm{a}}^{\mathrm{ant}}+S_{\mathrm{a}}^{\mathrm{pi}}}{S_{\mathrm{a}}^{\mathrm{pi}}}\right)^{b-1}\frac{dS_{\mathrm{a}}^{\mathrm{ant}}}{dt}. \tag{D7}$$

Substitution into (**Eq D1**) yields

$$\frac{dS_{\mathrm{a}}^{\mathrm{ant}}}{dt} + K'_{\mathrm{am}}\frac{dS_{\mathrm{a}}^{\mathrm{ant}}}{dt} + \frac{S_{\mathrm{l}}^{\mathrm{pi}}}{S_{\mathrm{a}}^{\mathrm{pi}}}b\left(\frac{S_{\mathrm{a}}^{\mathrm{ant}}+S_{\mathrm{a}}^{\mathrm{pi}}}{S_{\mathrm{a}}^{\mathrm{pi}}}\right)^{b-1}\frac{dS_{\mathrm{a}}^{\mathrm{ant}}}{dt} = Q_{\mathrm{ff}}(t)+Q_{\mathrm{lu}}(t)$$
2335
$$-\left[k_{\mathrm{md}}\left[K_{\mathrm{am}}\left(S_{\mathrm{a}}^{\mathrm{ant}}+S_{\mathrm{a}}^{\mathrm{pi}}\right)-S_{\mathrm{m}}^{\mathrm{pi}}\right]-k_{\mathrm{dm}}S_{\mathrm{d}}^{\mathrm{ant}}\right]-\left(k_{\mathrm{ao}}S_{\mathrm{a}}^{\mathrm{ant}}-k_{\mathrm{oa}}S_{\mathrm{o}}^{\mathrm{ant}}\right) \tag{D8}$$

from which

$$\frac{dS_{\mathrm{a}}^{\mathrm{ant}}}{dt} + K'_{\mathrm{am}}\frac{dS_{\mathrm{a}}^{\mathrm{ant}}}{dt} + \frac{S_{\mathrm{l}}^{\mathrm{pi}}}{S_{\mathrm{a}}^{\mathrm{pi}}}b\left(\frac{S_{\mathrm{a}}^{\mathrm{ant}}+S_{\mathrm{a}}^{\mathrm{pi}}}{S_{\mathrm{a}}^{\mathrm{pi}}}\right)^{b-1}\frac{dS_{\mathrm{a}}^{\mathrm{ant}}}{dt} = Q_{\mathrm{ff}}(t)+Q_{\mathrm{lu}}(t)$$
$$-\left[k_{\mathrm{md}}\left[K_{\mathrm{am}}\left(S_{\mathrm{a}}^{\mathrm{ant}}+S_{\mathrm{a}}^{\mathrm{pi}}\right)-S_{\mathrm{m}}^{\mathrm{pi}}\right]-k_{\mathrm{dm}}S_{\mathrm{d}}^{\mathrm{ant}}\right]-\left(k_{\mathrm{ao}}S_{\mathrm{a}}^{\mathrm{ant}}-k_{\mathrm{oa}}S_{\mathrm{o}}^{\mathrm{ant}}\right) \tag{D9}$$

yielding

$$\frac{dS_{\mathrm{a}}^{\mathrm{ant}}}{dt} = \frac{Q_{\mathrm{ff}}(t)+Q_{\mathrm{lu}}(t)-\left[k_{\mathrm{md}}\left[K_{\mathrm{am}}\left(S_{\mathrm{a}}^{\mathrm{ant}}+S_{\mathrm{a}}^{\mathrm{pi}}\right)-S_{\mathrm{m}}^{\mathrm{pi}}\right]-k_{\mathrm{dm}}S_{\mathrm{d}}^{\mathrm{ant}}\right]-\left(k_{\mathrm{ao}}S_{\mathrm{a}}^{\mathrm{ant}}-k_{\mathrm{oa}}S_{\mathrm{o}}^{\mathrm{ant}}\right)}{1+K'_{\mathrm{am}}+\frac{S_{\mathrm{l}}^{\mathrm{pi}}}{S_{\mathrm{a}}^{\mathrm{pi}}}b\left(\frac{S_{\mathrm{a}}^{\mathrm{ant}}+S_{\mathrm{a}}^{\mathrm{pi}}}{S_{\mathrm{a}}^{\mathrm{pi}}}\right)^{b-1}}. \tag{D10}$$

2340 **Equation D10** together with **Eqs 6.3 and 6.5** for the evolution of the stocks in the DO and the OB constitute the set of three ODEs that comprise the evolution of the system under the ESS approximations, with S_l^{ant} and S_l^{ant} being evaluated algebraically, (**Eqs D2 and D5**). Comparison of results from this reduced set of ODEs with that of the full set of equations (**Eqs 6.1 - 6.5**) in **Sect. 7.7** demonstrates the high accuracy of the EQ and SS approximations. That result lends further support to treatment of the AC, ML and LB as a single compartment for the purpose of evaluation of turnover time and

2345 adjustment times.

In contrast, as shown in **Appendix E**, application of the ESS approximations to radiocarbon yields a poor representation for the evolution of radiocarbon stocks, a consequence of the greater time constants associated with radiocarbon and the rapid changes in emissions.

Appendix E. Application to anthropogenic radiocarbon.

2350 Evolution of the distribution of ^{14}C among the five compartments is represented in a numerical model virtually identical to that employed for ordinary carbon as described in **Sect. 6**. Of principal interest is anthropogenic radiocarbon (^{14}C) that results from atmospheric testing of (mainly) thermonuclear weapons in the 1950's and early 1960's. so-called "bomb radiocarbon," and to lesser extent from nuclear industry. In addition there is a slight amount of natural ^{14}C present in the carbon system produced by spallation of atmospheric nitrogen by cosmic rays. Radiocarbon is subject to the same physical,

2355 chemical, and biochemical processes as ordinary carbon; fractionation, based on mass ratio of the isotopes is at most 2 or 3 % (Keeling, 1979) and is neglected here. Importantly, from the perspective of testing carbon models, radiocarbon exhibits very different emission history from that of anthropogenic CO_2. Thus modeling radiocarbon and comparison with observations provides an independent assessment of the model for CO_2 developed in this study. That model is readily applied to anthropogenic radiocarbon with only minor changes as described here.

2360 The ODEs governing the evolution of the stocks of radiocarbon R_i in the several compartments, which are analogous to those for ordinary carbon in **Eqs 6.1-6.5**, are as follows:

$$\frac{dR_a}{dt} = Q_R(t) + Q_{Rlu}(t) - k_{am}R_a + k_{ma}^*(t)R_m - k_{al}R_a + k_{la}R_t - k_{ao}R_a + k_{oa}R_t - \lambda_{14C}R_a \tag{E1}$$

$$\frac{dR_m}{dt} = k_{am}R_a - k_{ma}^*(t)R_m - k_{md}R_m + k_{dm}R_d - G_{pc} - \lambda_{14C}R_m \tag{E2}$$

$$\frac{dR_d}{dt} = k_{md}R_m - k_{dm}R_d + G_{pc} - \lambda_{14C}R_d \tag{E3}$$

2365
$$\frac{dR_l}{dt} = k_{al}R_a - k_{la}R_l - \lambda_{14C}R_l.$$
(E4)

$$\frac{dR_o}{dt} = k_{ao}R_a - k_{oa}R_o - Q_{Rlu}(t) - \lambda_{14C}R_o - G_{om}^{pi}$$
(E5)

Here G_{pc} denotes radiocarbon flux in particulate carbon gravitationally settling from the ML to the DO analogous to the F_{pc} term in **Eq 6.2**; G_{om}^{pi} denotes the preindustrial riverine flux from the OB to the ML (cf., **Eq 6.2**), evaluated as the product F_{om}^{pi} and the specific activity of preindustrial carbon $\alpha_s = R_a^{pi} / S_a^{pi}$ is 0.613×10^{26} atoms ^{14}C per Pg C; λ_{14C} denotes the

2370 radioactive decay coefficient of ^{14}C, 1.2096×10^{-4} yr^{-1}. Except as noted, the transfer coefficients are taken as those for ordinary carbon. Here it is explicitly noted that the equations are framed in stocks, and not in departure of isotope ratio from a standard ($^{14}\Delta$C) as is customary. Although not so familiar as equations in $^{14}\Delta$C, the equations are perhaps more straightforward than those in $^{14}\Delta$C, and the solutions benefit from independence from the stock of ordinary carbon, and this approach is seeing some use e.g., Broecker et al., 1995, Caldeira et al. (1998); Levin and Hesshaimer (2000); Naegler and

2375 Levin (2006); Roth and Joos (2013), and Graven (2015).

As noted in **Sect. 4.1**, a key difference between the models for ordinary carbon and radiocarbon is that the transfer coefficient k_{ma}^{*} describing transfer of radiocarbon from the ML to the AC is based on detailed balance consideration for the entire stocks in the two compartments and is about an order of magnitude less than k_{ma}', which is based on the differential equilibrium constant coupling S_a and S_m. The transfer coefficient k_{ma}' is time dependent because of the time dependence of

2380 the equilibrium ratio of the stocks in the AC and the ML

$$k_{ma}^{*}(t) = K_{ma}(t)k_{am}$$
(E6)

is readily evaluated from knowledge of the time dependence of K_{ma}, which is determined from the solutions to the ODEs for ordinary carbon, which are obtained prior to solving the ODEs for radiocarbon.

In contrast to the situation for ordinary carbon, wherein GPP was parameterized in terms of carbon stock, for radiocarbon a

2385 transfer coefficient k_{al} is required, evaluated as

$$k_{al} = \frac{F_{GPP}(t)}{S_a(t)} = \frac{1}{S_a(t)} F_{GPP}^{pi} \left(\frac{S_a(t)}{S_a^{pi}} \right)^b$$
(E7)

where time-dependent GPP is from the parameterization **Eq 3.1** together with modeled $S_a(t)$.

In order to initialize the stocks and to compare modeled radiocarbon stocks with measurements customarily reported as $^{14}\Delta C$, it is necessary convert from $^{14}\Delta C$ to radiocarbon stock in the pertinent compartment. A formula for such conversion is presented by Levin et al. (2010) as

$$\frac{\Delta^{14}C}{1000} = \frac{\lambda N_A}{A_{ABS} M_C} \frac{N_{14C}}{N_C} \left[1 - \frac{2\left(25 + \delta^{13}C\right)}{1000} \right] - 1 . \tag{E8}$$

Here $\Delta^{14}C$ is the generally reported (Stuiver and Polach, 1977) decay- and fractionation-corrected departure of the stock of atmospheric $^{14}CO_2$ in per mil (‰) relative to an internationally agreed upon standard; λ denotes the radioactive decay constant for ^{14}C, 3.8332×10^{-12} s^{-1}; N_A denotes the Avogadro constant; M_C is the atomic weight of carbon, 12.011 g mol^{-1}; A_{ABS} denotes the absolute specific activity (*i.e.*, activity per carbon mass) of the internationally agreed upon radiocarbon standard, 0.2261 Bq gC^{-1}; and N_C and N_{14C} denote the amounts of total carbon and ^{14}C, respectively, in a sample or reservoir of interest, in the same units (here numbers of atoms). The quantity in brackets accounts for the fractionation of ^{14}C against ^{12}C being twice that of ^{13}C; $\delta^{13}C$ denotes the departure of ^{13}C fraction in the sample relative to the standard for this isotope, in ‰. As $\delta^{13}C$ of atmospheric CO_2 has varied little over time (Levin et al., 2010), the generally employed constant value of -7‰ is used here. Upon substitution Eq (1) becomes

$$\frac{\Delta^{14}C}{1000} = \frac{1}{v} \frac{N_{14C}}{S_a} - 1 . \tag{E9}$$

$$\text{where } v = 10^{15} \frac{A_{ABS}}{\lambda} \left[1 - \frac{2\left(25 + \delta^{13}C\right)}{1000} \right]^{-1} = 6.13 \times 10^{25} \text{ atoms Pg}^{-1} \tag{E10}$$

Equation E8 may be inverted to yield the number of ^{14}C atoms in the global atmosphere N_{14C} corresponding to a given value of $\Delta^{14}CO_2$ for $^{14}CO_2$ taken as well mixed in the atmosphere

$$N_{14C} = v \left(1 + \frac{\Delta^{14}C}{1000} \right) S_a . \tag{E11}$$

For $\Delta^{14}C$ taken as 1.2‰, as measured in dendrochronologically dated tree rings Stuiver et al. (1998), R_a^{pi} was obtained as 361.279×10^{26} atoms. Stocks of ^{14}C in the other compartments were evaluated under assumption of steady state, as follows.

$$\frac{dR_m^{pi}}{dt} = 0 = k_{am} R_a^{pi} - k_{ma}^* R_m^{pi} - k_{md} R_m^{pi} + k_{dm} R_d^{pi} - \lambda_{14C} R_m^{pi} - G_{pc} + G_{om}^{pi} \tag{E12}$$

2410 $$\frac{dR_d^{pi}}{dt} = 0 = k_{md}R_m^{pi} - k_{dm}R_d^{pi} - \lambda R_d^{pi} + G_{pc} .$$ (E13)

Solving **Eq D13** yields R_d^{pi} in terms of R_m^{pi},

$$R_d^{pi} = \frac{k_{md}R_m^{pi} + G_{pc}}{k_{dm} + \lambda_{14C}}$$ (E14)

With substitution

$$R_m^{pi} = \frac{k_{am}R_a^{pi} + k_{dm}\dfrac{G_{pc}}{k_{dm} + \lambda_{14C}} - G_{pc} + G_{om}^{pi}}{k_{ma}^* + k_{md} - k_{dm}\dfrac{k_{md}}{k_{dm} + \lambda_{14C}} + \lambda_{14C}}$$ (E15)

2415 Similarly $$\frac{dR_l^{pi}}{dt} = 0 = \alpha_s F_{GPP}^{pi} - k_{la}R_l^{pi} + \lambda R_l^{pi}$$ (E16)

from which $$R_l^{pi} = \frac{\alpha_s F_{GPPpi}}{k_{la} + \lambda}$$ (E17)

Likewise $$\frac{dR_o^{pi}}{dt} = 0 = k_{ao}R_a - G_{om} - k_{oa}R_o^{pi} + \lambda R_o^{pi}$$ (E18)

from which $$R_o^{pi} = \frac{k_{ao}R_a^{pi} - G_{om}}{k_{oa} + \lambda}$$ (E19)

As the transfer coefficients k_{la}, k_{ao}, and k_{oa} depend parametrically on S_l^{pi} and b, the initial radiocarbon stocks also depend

2420 on those parameters.

Sources of ^{14}C to the atmosphere and related compartments that are needed as input to the model are natural production, production from atmospheric testing of nuclear weapons (Naegler and Levin, 2006, 2009a,b; data provided by T. Naegler, January, 2020), and nuclear industry (Zazzeri et al., 2018); as ^{14}C from nuclear weapons testing is deposited in the stratosphere, these emissions were convolved with 1.0 year exponential decay to account for lag in transfer of $^{14}CO_2$ from

2425 the stratosphere to the troposphere (Naegler and Levin, 2009). Natural production was evaluated under assumption of PI steady state $P_{14C}^{nat} = \lambda_{14C}R_{tot}^{pi} = 2.577 \times 10^{26}$ atoms yr-1, where R_{tot}^{pi} is the sum of ^{14}C stocks in the five compartments, close to the value given by Roth and Joos (2013), with the difference well within fluctuations over the past several centuries given by those investigators. Additionally ^{14}C is transferred from the TB to the atmosphere in conjunction with LUC

emissions of carbon from the OB to the AC; here the amount of transfer is taken as proportional to the stock of ^{14}C in the

2430   OB as evaluated in the model, and hence exhibits weak dependence on parameters S_l^{pi} and b. Emissions are shown in **Fig. E1** and are tabulated in **SI Data table, sheet 3**. The logarithmic plot compares the several source terms over the Anthropocene to compare continuing low-magnitude emissions with those from nuclear weapons tests in the 1950's and early 1960's; the linear plot shows the near delta-function source of ^{14}C from weapons testing abruptly curtailed by the test-ban treaty.

2435   Results from application of the model to radiocarbon, are compared in **Sect. 7.4** with observations of time series of atmospheric $^{14}CO_2$ as inferred from tree-ring analysis and contemporaneous measurements and with inventories of dissolved inorganic radiocarbon in the world ocean. The modeled stocks show broad conformance, over the pre-bomb era and during and after the time period of much greater emissions associated with weapons testing, for a wide set of parameters S_l^{pi} and b. These comparisons serve also to further limit the range of those parameters consistent with observations. Key

2440   results from the radiocarbon modeling, **Fig. 10**, are a slight increase in atmospheric $^{14}CO_2$ stock R_a over the pre-bomb period to 1950. This is attributed primarily to transfer of $^{14}CO_2$ from the OB to the AC in conjunction with LUC emissions and to outgassing of $^{14}CO_2$ from the ocean to the atmosphere in conjunction with acidification of ocean water resulting from uptake of ordinary CO_2 (Bolin and Eriksson, 1959). Modeled R_a increases abruptly, following emissions from weapons testing, and then rapidly decreases subsequent to cessation of these emissions, reaching a minimum at about year

2445   2000, the magnitude and year dependent on parameters S_l^{pi} and b, **Fig. 10b**; such a minimum is found also in observations. Modeled ocean uptake of bomb radiocarbon likewise matches observations but appreciably underestimates the observations at values of b, **Fig. 9b** and **Fig. 10c**, further narrowing the range of allowable values of these parameters.

Subsequent to the emissions pulse, peaking in the early 1960's, atmospheric $^{14}CO_2$ decreases rapidly with time, **Fig. 10**. This rapid decrease is shown also in the normalized excess stock, calculated as the fractional increment relative to the

2450   baseline prior to emissions from weapons testing, taken as the value in 1950, **Fig. E2a**; also shown, for comparison, is normalized excess of ordinary carbon as function of time subsequent to hypothetical cessation of emissions in 2017. Excess $^{14}CO_2$ decreases much more rapidly than does ordinary CO_2, as reflected also in comparison of the equivalent $1/e$ lifetimes τ_E, which, for $^{14}CO_2$, is initially as short as about 12 years, much shorter than any of the time constants associated with excess ordinary CO_2 and approaching the lifetime of individual CO_2 molecules in the atmosphere. The reason for the

2455   increase in lifetime is that for radiocarbon there is initially very little return flux from the ML and the OB so that those compartments serve as sinks for $^{14}CO_2$ (Broecker and Peng, 1982, p. 533). Subsequently, however, as those compartments approach steady state with the AC the net rate of uptake by those compartments greatly decreases resulting in increase in the apparent lifetime of atmospheric $^{14}CO_2$; as the atmospheric stock of $^{14}CO_2$ is leveling off with time and actually starting to increase slightly, not much significance should be attached to the value of τ_E toward the end of the time record shown.

2460   The accuracy of the equilibrium–steady-state (ESS) approximation was examined also for radiocarbon, **Fig. E3**. For the ML,
assumption of equilibrium between the AC and the ML leads to overestimation of the radiocarbon stock because the net sink
to the DO due to radioactive decay in the DO is appreciable relative to the rate of establishing equilibrium between the AC
and the ML. That overestimation is eliminated in the steady-state approximation. However the steady-state approximation,
and also the equilibrium approximation, exhibit much faster response to the sharply peaked emissions from weapons testing
2465   than the exact calculation, a consequence of both the rapidly changing atmospheric stock and the transfer coefficients
establishing the steady state. A similar situation is found for the LB, for which the increase is likewise damped compared to
the steady-state approximation in the weapons testing era.

Appendix F. Prior arguments against determination of the lifetime of excess CO$_2$ by top-down observations, and rebuttals

2470   The approach to determine the lifetime of excess CO$_2$ based on the current budget of CO$_2$ has drawn strenuous criticism.
Those arguments are recapitulated here and rebuttals presented to forestall their being raised once again in criticism of the
present study.

1. Tans (1997) argues that all that CO$_2$ emitted from fossil fuel combustion does is "slosh back and forth" between rapidly
exchanging reservoirs, never leaving the system, and that hence, in contrast to greenhouse gases that are destroyed by
2475   chemical reaction, that the lifetime concept cannot be applied to CO$_2$. While, by conservation of matter, carbon is indeed
never removed from the system, the present model demonstrates that excess CO$_2$ would be effectively removed from the
atmosphere (or equivalently from the combined AC-LB-ML compartment) to great extent (58 % to 77 % in 100 years)
following an abrupt cessation of emissions and thus that the lifetime concept is entirely appropriate to excess atmospheric
CO$_2$ on this time scale.

2480   2. Archer et al. (2009) concede that "If fossil fuel CO$_2$ in the atmosphere was expected to diminish according to linear
kinetics, then it would be possible to calculate the lifetime simply using the present-day excess CO$_2$ concentration in the
atmosphere (~100 ppm or 200 Pg C) and the natural uptake rate, currently ~2 Pg C yr^{-1} ... each into the oceans and into the
land biosphere." However Archer et al. reject such a treatment, stating that "For the nonlinear CO$_2$ uptake kinetics, as
predicted by CC models, however, this apparent lifetime would increase with time after the CO$_2$ is released." Although
2485   Archer et al. do not explicitly specify the time scale to which they refer, it would seem that these investigators are
countenancing an increase in the lifetime that would occur on the time scale over which atmospheric CO$_2$ would decrease
substantially towards its preindustrial value in the absence of emissions, the time scale over which CO$_2$ "recovers
substantially toward its original concentration" that they advocate as the time scale of interest as quoted in **Sect. 2 of the
main text**. Although an increase in adjustment time of about 50 % in the initial 100 years subsequent to cessation of

2490 emissions is indeed exhibited in the results of the present model, as shown in **Fig. 12a**, this increase hardly affects the decrease of excess CO_2 over this time period, during which time this excess would decrease by about 70 %. Alternatively, an increase in the lifetime might result from changes in the rates and/or mechanisms of processes that govern the removal of CO_2 from the atmosphere on this time scale, due, perhaps, to decrease in CO_2 fertilization of terrestrial vegetation, increase in turnover of soil and litter carbon, and/or changes ocean circulations, as suggested by Joos et al. (2013a,b). Although such

2495 changes cannot be precluded in the future, no such change is evident thus far over the Anthropocene, **Fig. 6**.

3. Similarly to Archer et al. (2009), Joos et al. (2013b) assert "CO_2 does not undergo a first order decay," observing that "Anthropogenic carbon is redistributed among the major carbon reservoirs in the Earth System." It must be stressed that the approximate first-order decay of excess CO_2 exhibited in the abrupt cessation runs with the present model is not built into the model, but is a consequence of the magnitudes of the transfer coefficients that result in the dependence of the net flux

2500 into the two sink compartments, the DO and the TB, being indistinguishable from proportionality to the excess CO_2 in the combined AC and ML compartment for the entire Anthropocene thus far (**Fig. 6**). The nearly exponential decay subsequent to cessation of emissions continues until the return flux from the DO to the ML becomes appreciable to the flux from the ML to the DO, which occurs only when excess CO_2 has become substantially reduced from its value at the time of cessation of emissions.

2505 4. Archer et al. (2009) would seem to be focusing unduly on long-time scale processes, rather than on the time scale the time scale of substantial recovery that they advocate in that paper. Specifically Archer et al. (2009) cite an earlier study (Archer et al., 1997) as having found that "The mean lifetime of the elevated CO_2 concentration of the atmosphere resulting from fossil fuel combustion has been calculated to be tens of thousands of years (Archer et al. 1997), not at all similar to the 50- to 100-year lifetime calculated using the linear approximation based on fluxes immediately following a release of CO_2 to the

2510 atmosphere." The mean lifetime of excess CO_2 is inordinately influenced by a long tail of low magnitude in the model results examined by Archer et al. (1997, 2009). By using the mean lifetime of excess CO_2 as a measure of the adjustment time, Archer et al, (2009) would seem to be veering greatly from the time scale of substantial recovery.

5. Archer et al. (2009) seem to minimize or neglect the role of the terrestrial biosphere in drawdown of excess atmospheric CO_2. They state "[T]he leftover CO_2 in the atmosphere after ocean invasion interacts with the land biosphere and is taken up

2515 by pH-neutralization reactions with calcium carbonate ($CaCO_3$) and the CaO component of igneous rocks (Table 1)." The only processes identified in their Table 1 are buffering by seawater, neutralization by $CaCO_3$, and weathering of silicate, of which they state that "The timescales for these processes range from thousands to hundreds of thousands of years," again well beyond the time scale of substantial recovery.

6. Joos et al. (2013*b*) state that an exponential-decay model takes no cognizance of the multiple mechanisms of uptake and
2520 release of CO_2 by the land through photosynthesis and the related conversion of CO_2 to organic carbon, calling attention to carbon release through oxidation (autotrophic, heterotrophic, fire) of organic material back to CO_2 and carbon sink processes in the land biosphere include forest regrowth and woody encroachment, fertilization of plant growth by increased availability of fixed nitrogen and higher CO_2 concentrations. Although net uptake of CO_2 by the TB is undoubtedly a consequence of these and other processes, nonetheless, the total uptake rate (to the TB and the ocean) has exhibited essentially linear
2525 dependence on excess CO_2, as inferred from observations over the Anthropocene thus far and as accurately represented in the present model (**Fig. 6**). The approximately exponential decay of excess CO_2 subsequent to cessation of emissions shown in **Figures 1 and 12*a*** is not imposed on the model but is a consequence of the decay being governed by transfer coefficients, derived from physical and chemical mechanisms that are temporally constant or nearly so over the changes in CO_2 thus far over the Anthropocene.

2530 7. A further concern raised by Joos et al. (2013*b*) is the assertion, in reference to an equation describing the decrease of excess CO_2 by a single exponential, that "It is no surprise that [a] single equation works to represent the atmospheric CO_2 increase over the industrial period. This increase is driven by approximately exponentially increasing emissions. It is basic calculus that many systems with a wide range of intrinsic time scales respond to an exponential forcing exponentially and with a single 'apparent' time scale." Joos et al. continue that such "models are purely diagnostic, applicable to approximately
2535 exponential forcing only, and do not represent the functioning of the global carbon cycle." Similar concerns have been raised previously by O'Neill et al. (1994) and by Raupach (2013), the argument being that in an exponentially forced linear system the eigenstates, and linear combinations of them, would all scale with the exponentially increasing emissions, resulting in constant ratios of stocks and fluxes.

The argument that the short lifetime of excess CO_2 is due to exponentially increasing forcing during the time that the
2540 turnover time is determined may readily be refuted. First, as shown in **Fig. 12*a*** of the main text, upon cessation of emissions the turnover time evaluated by **Eq 5.7** as $\tau_{\mathrm{alm}}^{\mathrm{to}} = (S_{\mathrm{a}}^{\mathrm{ant}} + S_{\mathrm{l}}^{\mathrm{ant}} + S_{\mathrm{m}}^{\mathrm{ant}})/(F_{\mathrm{ao}}^{\mathrm{ant,net}} + F_{\mathrm{md}}^{\mathrm{ant,net}})$ varies continuously and smoothly across the point in time at which emissions are abruptly halted and is thus clearly independent of emissions. The attribution of the observationally determined turnover time to constant ratios of eigenstates resulting from continued exponential growth of emissions is likewise refuted by this continuity.

2545 The possibility that the lifetime of excess CO_2 found in the present model might be a consequence of exponential growth rate of emissions is further explicitly examined by a model run (**SI Text Sect. S6**) for which emissions were approximated as a linear function of time, commencing in 1925 (**Fig. S6*a***), in lieu of the approximately exponentially increasing historical emissions. The turnover time in that experiment is essentially the same as for the actual historical emissions, **Fig. S6*c***;

likewise, the time constant of an exponential fit to the atmospheric CO_2 profile subsequent to abrupt cessation of emission,

2550 is 113 yr, **Fig. S6b**, essentially the same as that for the historical emissions for the same (S_l^{pi} , b), 105 yr.

Finally, the skill of the model developed here, appropriately extended, in representing the temporal profiles of radiocarbon from an essentially pulse emission due to atmospheric testing of nuclear weapons (**Appendix D**) provides yet further evidence that this skill is not simply a consequence of exponential growth of emissions.

These several lines of reasoning would seem to allay any concern that the turnover time determined either directly from the

2555 budget or from the model calculation is a consequence of the approximately exponential growth of historical emissions.

8. Joos et al. (2013b) state that a single lifetime model characterizing the decay of excess CO_2 does not take cognizance of the reaction of dissolved CO_2 to form bicarbonate ions, as would be reflected by the fact that "the Revelle factor (or buffer factor) which is defined by the relative change in p_{CO2} divided by the relative change in dissolved inorganic carbon (Delta-$p_{CO2}/p_{CO2,0}$)/(Delta-DIC/DIC,0) is about 10." This concern is readily examined with the present results. The Revelle factor,

2560 although not directly built into the present model, is readily examined in the output of the present model, **Fig. F1**, which shows that the Revelle relation is indeed satisfied, not just during the period of growth of emissions, but also, apart from a brief transient resulting from the numerics, subsequent to abrupt cessation of emissions commencing in 2017, during which time excess CO_2 decreases nearly exponentially. The slight systematic departure from the value of the Revelle factor obtained from the model results from that evaluated for equilibrium conditions is attributed to slight disequilibrium between

2565 the AC and the ML during the model runs. These results from the present model should serve to allay this concern of Joos et al. (2013b).

Acknowledgment. Supported by the U.S. Department of Energy under Contract No. DE-SC0012704. The author declares no conflict of interest. I thank Ernie Lewis, Henning Rodhe, and Anders Björkström for valuable discussion. I thank Martin Heimann for constructive criticism and challenging questions. Portions of this work were presented at the American

2570 Geophysical Union Fall Meeting, December 2018 (Stephen Schneider Lecture).

Data Tables. One Excel file consisting of 6 sheets. Pertinent figures are identified.

Sheet 1. Contents of data file, by sheet.

Sheet 2. Concentrations of dissolved inorganic constituents in equilibrium with CO_2.

Sheet 3. Emissions by year.

2575 **Sheet 4**. Observed CO_2, Radiocarbon.

Sheet 5. Transfer coefficients, lifetimes, by S_l^{pi} and b.

Sheet 6. Modeled stocks, fluxes, lifetimes by year, for specified S_l^{pi} and b.

Data Sources. Data from the following publicly available data sets were employed in this study.

Global Carbon Budget 2017 Global_Carbon_Budget_2017v1.3, last updated March 2018. Downloaded 2018-0803 from https://doi.org/10.18160/GCP-2017 .

Merged Historical Atmospheric–Ice-Core Yearly CO_2 record. Downloaded 2015-0301 from http://scrippsCO$_2$.ucsd.edu/data/Fmerged_ice_core/merged_ice_core_yearly.csv .

High-precision radiocarbon age calibration for terrestrial and marine samples. https://www.cambridge.org/core/journals/radiocarbon/article/highprecision-radiocarbon-age-calibration-for-terrestrial-and-marine-samples/1660E9D7A43772ACBB56614C1DD09D46 .

Compiled records of carbon isotopes in atmospheric CO_2 for historical simulations in CMIP6, Supplement of *Geosci. Model Dev.*, 10, 4405–4417, 2017 https://doi.org/10.5194/gmd-10-4405-2017-supplement .

Data from Zero Emissions Commitment Model Intercomparison Project (ZECMIP), http://terra.seos.uvic.ca/ZEC .

References

Amundson, R., 2001. The carbon budget in soils. *Annual Review of Earth and Planetary Sciences*, *29*, 535-562. https://www.annualreviews.org/doi/abs/10.1146/annurev.earth.29.1.535

Anav, A. et al., 2013. Evaluating the land and ocean components of the global carbon cycle in the CMIP5 Earth System Models. *Journal of Climate* **26**, 6801-6843.

Anav, A., Friedlingstein, P., Beer, C., Ciais, P., Harper, A., Jones, C., Murray-Tortarolo, G., Papale, D., Parazoo, N.C., Peylin, P. and Piao, S., 2015. Spatiotemporal patterns of terrestrial gross primary production: A review. *Revs. Geophys.*, **53**, 785-818. https://agupubs.onlinelibrary.wiley.com/doi/abs/10.1002/2015RG000483

Archer, D. 2005. Fate of fossil fuel CO_2 in geologic time. *J. Geophys. Res: Oceans*, 110 C09S05 https://agupubs.onlinelibrary.wiley.com/doi/abs/10.1029/2004JC002625

Archer, D., et al. (2009), Atmospheric Lifetime of Fossil Fuel Carbon Dioxide, *Annual Review of Earth and Planetary Sciences*, *37*, 117-134, doi:10.1146/annurev.earth.031208.100206.

Archer, D., H. Kheshgi, and E. Maier-Reimer (1997), Multiple timescales for neutralization of fossil fuel CO_2, *Geophysical Research Letters*, *24*(4), 405-408, doi:10.1029/97GL00168.

Arora, V. K., J. F. Scinocca, G. J. Boer, J. R. Christian, K. L. Denman, G. M. Flato, V. V. Kharin, W. G. Lee, and W. J. Merryfield (2011), Carbon emission limits required to satisfy future representative concentration pathways of greenhouse gases, *Geophys. Res. Lett.*, 38, L05805, doi:10.1029/2010GL046270

Bacastow R., and C. D. Keeling (1973), Atmospheric carbon dioxide and radiocarbon in the natural carbon cycle. II.
2610   Changes from AD 1700 to 2070 as deduced from a geochemical model. *In Carbon and the Biosphere*, Woodwell G. M. and
Pecan E. V., eds., pp. 86-135, U. S. Atomic Energy Commission Report CONF-720510-, OSTI Identifier, 4380392

Ballantyne, A. P., C. B. Alden, J. B. Miller, P. P. Tans, and J. W. C. White (2012), Increase in observed net carbon dioxide
uptake by land and oceans during the past 50 years, *Nature*, *488*, 70, doi:10.1038/nature11299.

Ballantyne, A., Smith, W., Anderegg, W., Kauppi, P., Sarmiento, J., Tans, P., Shevliakova, E., Pan, Y., Poulter, B., Anav, A.
2615   and Friedlingstein, P., 2017. Accelerating net terrestrial carbon uptake during the warming hiatus due to reduced respiration.
Nature Climate Change, **7**, 148-152. https://www.nature.com/articles/nclimate3204

Bastos, A., Ciais, P., Barichivich, J., Bopp, L., Brovkin, V., Gasser, T., Peng, S., Pongratz, J., Viovy, N. and Trudinger,
C.M., 2016. Re-evaluating the 1940s CO_2 plateau. *Biogeosciences*, **13**, 4877-4897. doi:10.5194/bg-13-4877-2016

Beer, C., et al. (2010), Terrestrial Gross Carbon Dioxide Uptake: Global Distribution and Covariation with Climate, *Science*,
2620   1184984, doi:10.1126/science.1184984.

Boden, T. A., R. J. Andres, and G. Marland (2017), *Global, Regional, and National Fossil-Fuel CO_2 Emissions (1751-2014)
(V. 2017)*, Carbon Dioxide Information Analysis Center (CDIAC), Oak Ridge, TN, doi:10.3334/CDIAC/00001_V2017.

Bolin, B., and E. Eriksson (1959), Changes in the carbon dioxide content of the atmosphere and sea due to fossil fuel
combustion, in *The atmosphere and the sea in motion (Scientific contributions to the Rossby memorial volume)*, edited by B.
2625   Bolin, pp. 30-142, Rockefeller Institute Press in association with Oxford University Press.

Bolin, B. and Rodhe, H., 1973. A note on the concepts of age distribution and transit time in natural reservoirs. *Tellus*, 25(1),
58-62. https://onlinelibrary.wiley.com/doi/abs/10.1111/j.2153-3490.1973.tb01594.x

Boucher, O., Halloran, P.R., Burke, E.J., Doutriaux-Boucher, M., Jones, C.D., Lowe, J., Ringer, M.A., Robertson, E. and
Wu, P., 2012. Reversibility in an Earth System model in response to CO2 concentration changes. *Environmental Research
2630   Letters*, *7*(2), p.024013. https://iopscience.iop.org/article/10.1088/1748-9326/7/2/024013/meta

Brasseur, G. P., and E. Roeckner (2005), Impact of improved air quality on the future evolution of climate, Geophys. Res.
Lett., 32, L23704, doi:10.1029/2005GL023902.

Broecker, W. S., and T. H. Peng (1974), Gas exchange rates between air and sea, *Tellus*, *26*(1-2), 21-35,
doi:10.3402/tellusa.v26i1-2.9733.

2635   Broecker, W. S. and T. Peng (1982), *Tracers in the sea*, 690 pp., Lamont-Doherty Geological Observatory, Columbia
University.

Broecker, W.S., Takahashi, T., Simpson, H.J. and Peng, T.H., 1979. Fate of fossil fuel carbon dioxide and the global carbon
budget. *Science*, **206**, 409-418.

Broecker, W. S., Sutherland, S., Smethie, W., Peng, T. H. and Ostlund, G., 1995. Oceanic radiocarbon: Separation of the
2640   natural   and   bomb   components.   *Global   Biogeochemical   Cycles*,   9,   263-288.
https://agupubs.onlinelibrary.wiley.com/doi/pdf/10.1029/95GB00208

Caldeira, K., Rau, G.H. and Duffy, P.B., 1998. Predicted net efflux of radiocarbon from the ocean and increase in atmospheric radiocarbon content. *Geophysical Research Letters*, **25**, 3811-3814. https://agupubs.onlinelibrary.wiley.com/doi/pdf/10.1029/1998GL900010

2645 Campbell, J.E., Berry, J.A., Seibt, U., Smith, S.J., Montzka, S.A., Launois, T., Belviso, S., Bopp, L. and Laine, M., 2017. Large historical growth in global terrestrial gross primary production. *Nature*, 544, 84-87. https://www.nature.com/articles/nature22030

Carvalhais, N. et al. (2014), Global covariation of carbon turnover times with climate in terrestrial ecosystems. *Nature*, 514, 213-217. https://www.nature.com/articles/nature13731.

2650 Cernusak, L.A., Haverd, V., Brendel, O., Le Thiec, D., Guehl, J.M. and Cuntz, M., 2019. Robust Response of Terrestrial Plants to Rising CO_2. 2019. *Trends in Plant Science*, **24**, 578-586 https://doi.org/10.1016/j.tplants.2019.04.003

Cheng, L., Zhang, L., Wang, Y.P., Canadell, J.G., Chiew, F.H., Beringer, J., Li, L., Miralles, D.G., Piao, S. and Zhang, Y., 2017. Recent increases in terrestrial carbon uptake at little cost to the water cycle. *Nature Communications*, **8**:110. https://www.nature.com/articles/s41467-017-00114-5

2655 Ciais, P., et al. (2014), Carbon and Other Biogeochemical Cycles, in *Climate Change 2013 – The Physical Science Basis: Working Group I Contribution to the Fifth Assessment Report of the Intergovernmental Panel on Climate Change*, edited by T. F. Stocker et al., pp. 465-570, Cambridge University Press, Cambridge, doi:10.1017/CBO9781107415324.015.

Craig, H. (1957), The Natural Distribution of Radiocarbon and the Exchange Time of Carbon Dioxide Between Atmosphere and Sea, *Tellus*, *9*(1), 1-17, doi:10.3402/tellusa.v9i1.9078.

2660 Del Giorgio, P. A., and C. M. Duarte (2002), Respiration in the open ocean, *Nature* **420**, 379-384, doi:10.1038/nature01165.

Denman, K. L., et al. (2007), Couplings between Changes in the Climate System and Biogeochemistry, in *Climate Change 2007: The Physical Science Basis, Contribution of Working Group I to the Fourth Assessment Report of the Intergovernmental Panel on Climate Change*, edited by S. Solomon, et al., pp. 500-587, Cambridge University Press, Cambridge, UK.

2665 DeVries, T., M. Holzer, and F. Primeau (2017), Recent increase in oceanic carbon uptake driven by weaker upper-ocean overturning, *Nature* **542**, 215-218, doi:10.1038/nature21068

Dlugokencky, E., and P. Tans (2018), *Trends in atmospheric carbon dioxide*, edited, NOAA/ESRL http://www.esrl.noaa.gov/gmd/ccgg/trends/global.html.

Eakins, B. W., and G. F. Sharman (2012), Hypsographic Curve of Earth's Surface from ETOPO1, Based on NOAA
2670 Technical Memorandum NESDIS NGDC-24, March 2009, NOAA National Geophysical Data Center. https://www.ngdc.noaa.gov/mgg/global/etopo1_surface_histogram.html. Based on Amante, C. and B. W. Eakins, ETOPO1 1 Arc-Minute Global Relief Model: Procedures, Data Sources and Analysis. NOAA Technical Memorandum NESDIS NGDC-24, 19 pp, March 2009, http://www.ngdc.noaa.gov/mgg/global/relief/ETOPO1/docs/ETOPO1.pdf.

Etheridge, D. M., L. P. Steele, R. L. Langenfelds, R. J. Francey, J. M. Barnola, and V. I. Morgan (1996), Natural and
2675 anthropogenic changes in atmospheric CO_2 over the last 1000 years from air in Antarctic ice and firn, *Journal of Geophysical Research: Atmospheres*, *101*, 4115-4128, doi:10.1029/95JD03410.

Fahey, T. J. et al. (2005). The biogeochemistry of carbon at Hubbard Brook. Biogeochemistry, 75, 109-176. https://link.springer.com/article/10.1007/s10533-004-6321-y

Falkowski, P. G., R. T. Barber, and V. Smetacek (1998), Biogeochemical Controls and Feedbacks on Ocean Primary Production, *Science*, *281*(5374), 200, doi:10.1126/science.281.5374.200.

Forkel, M., Carvalhais, N., Rödenbeck, C., Keeling, R., Heimann, M., Thonicke, K., Zaehle, S. and Reichstein, M., 2016. Enhanced seasonal CO_2 exchange caused by amplified plant productivity in northern ecosystems. *Science*, *351*, 696-699. https://science.sciencemag.org/content/351/6274/696

Friedlingstein, P., et al. (2006), Climate–Carbon Cycle Feedback Analysis: Results from the C4MIP Model Intercomparison, *Journal of Climate*, *19*(14), 3337-3353, doi:10.1175/JCLI3800.1.

Friedlingstein, P., M. Meinshausen, V. K. Arora, C. D. Jones, A. Anav, S. K. Liddicoat, and R. Knutti (2014), Uncertainties in CMIP5 Climate Projections due to Carbon Cycle Feedbacks, *Journal of Climate*, *27*(2), 511-526, doi:10.1175/JCLI-D-12-00579.1.

Friend, A. D. et al., 2014. Carbon residence time dominates uncertainty in terrestrial vegetation responses to future climate and atmospheric CO_2. *Proc. Nat. Acad. Sci.*, **111**, 3280-3285. https://www.pnas.org/content/111/9/3280

Gaffin, S. R., B. C. O'Neill, and M. Oppenheimer (1995), Comment on "The lifetime of excess atmospheric carbon dioxide" by Berrien Moore III and B. H. Braswell, *Global Biogeochemical Cycles*, *9*(1), 167-169, doi:10.1029/94GB03157.

Geoffroy, O., D. Saint-Martin, D. J. L. Olivié, A. Voldoire, G. Bellon, and S. Tytéca (2012), Transient Climate Response in a Two-Layer Energy-Balance Model. Part I: Analytical Solution and Parameter Calibration Using CMIP5 AOGCM Experiments, *Journal of Climate*, *26*, 1841-1857, doi:10.1175/JCLI-D-12-00195.1.

Gloor, M., J. L. Sarmiento, and N. Gruber (2010), What can be learned about carbon cycle climate feedbacks from the CO_2 airborne fraction?, *Atmos. Chem. Phys.*, *10*(16), 7739-7751, doi:10.5194/acp-10-7739-2010.

Graven, H.D., 2015. Impact of fossil fuel emissions on atmospheric radiocarbon and various applications of radiocarbon over this century. *Proc. Nat. Acad. Sci.*, **112** 9542-9545. https://www.pnas.org/content/112/31/9542

Graven, H. D., N. Gruber, R. Key, S. Khatiwala, and X. Giraud (2012), Changing controls on oceanic radiocarbon: New insights on shallow-to-deep ocean exchange and anthropogenic CO_2 uptake, *Journal of Geophysical Research: Oceans*, *117*(C10), doi:10.1029/2012JC008074.

Graven, H., Allison, C.E., Etheridge, D.M., Hammer, S., Keeling, R.F., Levin, I., Meijer, H.A., Rubino, M., Tans, P.P., Trudinger, C.M. and Vaughn, B.H., 2017. Compiled records of carbon isotopes in atmospheric CO_2 for historical simulations in CMIP6. Geosci. Model Dev., 10, 4405–4417, 2017 https://doi.org/10.5194/gmd-10-4405-2017

Gregory, J. M. (2000), Vertical heat transports in the ocean and their effect on time-dependent climate change, *Climate Dynamics*, *16*(7), 501-515, doi:10.1007/s003820000059.

Gruber, N., et al. (2009), Oceanic sources, sinks, and transport of atmospheric CO_2, *Global Biogeochem. Cycles*, 23, GB1005, doi:10.1029/2008GB003349.

2710 Gruber N., et al. (2019), The oceanic sink for anthropogenic CO_2 from 1994 to 2007. *Science* 363 (6432), 1193-1199. doi: 10.1126/science.aau5153

Hansis, E., S. J. Davis, and J. Pongratz (2015), Relevance of methodological choices for accounting of land use change carbon fluxes, *Global Biogeochemical Cycles*, *29*(8), 1230-1246, doi:10.1002/2014GB004997.

Hartmann, D. L., et al. (2014), Observations: Atmosphere and Surface, in *Climate Change 2013 – The Physical Science*
2715 *Basis: Working Group I Contribution to the Fifth Assessment Report of the Intergovernmental Panel on Climate Change*, edited by T. F. Stocker et al., Cambridge University Press, Cambridge.

Held, I. M., M. Winton, K. Takahashi, T. Delworth, F. Zeng, and G. K. Vallis (2010), Probing the Fast and Slow Components of Global Warming by Returning Abruptly to Preindustrial Forcing, *Journal of Climate*, *23*(9), 2418-2427, doi:10.1175/2009JCLI3466.1.

2720 Hellevang, H. and Aagaard, P., 2015. Constraints on natural global atmospheric CO_2 fluxes from 1860 to 2010 using a simplified explicit forward model. *Scientific Reports*, 5, 17352. https://www.nature.com/articles/srep17352

Henson, S. A., R. Sanders, E. Madsen, P. J. Morris, F. Le Moigne, and G. D. Quartly (2011), A reduced estimate of the strength of the ocean's biological carbon pump, *Geophysical Research Letters*, *38*(4), doi:10.1029/2011GL046735.

Houghton, R. A., and A. A. Nassikas (2017), Global and regional fluxes of carbon from land use and land cover change
2725 1850-2015, *Global Biogeochemical Cycles*, *31*(3), 456-472, doi:10.1002/2016GB005546.

Jacobson, M. Z. (2005), Correction to "Control of fossil-fuel particulate black carbon and organic matter, possibly the most effective method of slowing global warming", *Journal of Geophysical Research: Atmospheres*, *110*(D14), doi:10.1029/2005JD005888.

Joiner, J., Yoshida, Y., Zhang, Y., Duveiller, G., Jung, M., Lyapustin, A., Wang, Y. and Tucker, C.J., 2018. Estimation of
2730 terrestrial global gross primary production (GPP) with satellite data-driven models and eddy covariance flux data. Remote Sensing, 10, 1346. https://www.mdpi.com/2072-4292/10/9/1346

Joos, F., et al. (2013*a*), Carbon dioxide and climate impulse response functions for the computation of greenhouse gas metrics: a multi-model analysis, *Atmos. Chem. Phys.*, *13*(5), 2793-2825, doi:10.5194/acp-13-2793-2013.

Joos, F. et al. (2013*b*), Interactive comment on "Carbon dioxide and climate impulse response functions for the computation
2735 of greenhouse gas metrics: a multi-model analysis" by F. Joos et al., *Atmos. Chem. Phys. Discuss.*, *12*, C11514-C11514. https://www.atmos-chem-phys-discuss.net/12/C11514/2013/acpd-12-C11514-2013.pdf; http://www.atmos-chem-phys-discuss.net/12/C11514/2013/acpd-12-C11514-2013-supplement.pdf

Jung, M., Reichstein, M., Margolis, H.A., Cescatti, A., Richardson, A.D., Arain, M.A., Arneth, A., Bernhofer, C., Bonal, D., Chen, J. and Gianelle, D., 2011. Global patterns of land-atmosphere fluxes of carbon dioxide, latent heat, and sensible heat
2740 derived from eddy covariance, satellite, and meteorological observations. *J. Geophys. Res.: Biogeosciences*, **116** G00J07. https://agupubs.onlinelibrary.wiley.com/doi/abs/10.1029/2010JG001566

Karl, D. M., J. R. Christian, J. E. Dore, D. V. Hebel, R. M. Letelier, L. M. Tupas, and C. D. Winn (1996), Seasonal and interannual variability in primary production and particle flux at Station ALOHA, *Deep Sea Research Part II: Topical Studies in Oceanography*, *43*(2), 539-568, doi:10.1016/0967-0645(96)00002-1.

2745   Keeling, C.D., 1979. The Suess effect: ^{13}Carbon-^{14}Carbon interrelations. *Environment International*, 2, 229-300. https://www.sciencedirect.com/science/article/pii/0160412079900059

Keeling, C. D., R. B. Bacastow, A. E. Bainbridge, C. A. Ekdahl Jr, P. R. Guenther, L. S. Waterman, and J. F. S. Chin (1976), Atmospheric carbon dioxide variations at Mauna Loa Observatory, Hawaii, *Tellus*, *28*(6), 538-551, doi:10.1111/j.2153-3490.1976.tb00701.x.

2750   Keeling, C. D., S. C. Piper, R. B. Bacastow, M. Wahlen, T. P. Whorf, M. Heimann, and H. A. Meijer (2001), Exchanges of atmospheric CO_2 and $^{13}CO_2$ with the terrestrial biosphere and oceans from 1978 to 2000. I. Global aspects, *SIO REFERENCE NO. 01-06*, *Scripps Institution of Oceanography, San Diego*, 88 pp.

Keeling, C. D., Piper, S. C., Whorf, T. P., & Keeling, R. F. (2011). Evolution of natural and anthropogenic fluxes of atmospheric CO_2 from 1957 to 2003. *Tellus* B: Chemical and Physical Meteorology, 63(1), 1-22.
2755   https://www.tandfonline.com/doi/abs/10.1111/j.1600-0889.2010.00507.x

Keenan, T.F., Prentice, I.C., Canadell, J.G., Williams, C.A., Wang, H., Raupach, M. and Collatz, G.J., 2016. Recent pause in the growth rate of atmospheric CO_2 due to enhanced terrestrial carbon uptake. *Nature communications*, 7, p.13428. https://www.nature.com/articles/ncomms13428

Key, R. M., A. Kozyr, C. L. Sabine, K. Lee, R. Wanninkhof, J. L. Bullister, R. A. Feely, F. J. Millero, C. Mordy, and T. H.
2760   Peng (2004), A global ocean carbon climatology: Results from Global Data Analysis Project (GLODAP), *Global Biogeochemical Cycles*, *18*(4), doi:10.1029/2004GB002247.

Kondo, M. et al., 2018. Land use change and El Niño-Southern Oscillation drive decadal carbon balance shifts in Southeast Asia. *Nature Communications*, 9, 1-11. https://www.nature.com/articles/s41467-018-03374-x

Landschützer, P., N. Gruber, D. C. E. Bakker, and U. Schuster (2014), Recent variability of the global ocean carbon sink,
2765   *Global Biogeochemical Cycles*, *28*(9), 927-949, doi:10.1002/2014GB004853.

Landschützer, P., et al. (2015), The reinvigoration of the Southern Ocean carbon sink, *Science*, *349*(6253), 1221, doi:10.1126/science.aab2620.

Laws, E. A., P. G. Falkowski, W. O. Smith Jr, H. Ducklow, and J. J. McCarthy (2000), Temperature effects on export production in the open ocean, *Global Biogeochemical Cycles*, *14*(4), 1231-1246, doi:10.1029/1999GB001229.

2770   Le Quéré, C., et al. 2018*a*, Global Carbon Budget 2017, *Earth Syst. Sci. Data*, 10, 405-448, doi:10.5194/essd-10-405-2018.

Le Quéré, C. et al., 2018*b*. Global carbon budget 2018. *Earth System Science Data*, 10, 2141-2194. https://doi.org/10.5194/essd-10-2141-2018

Levin, I. and Hesshaimer, V., 2000. Radiocarbon–a unique tracer of global carbon cycle dynamics. *Radiocarbon*, 42, 69-80. https://doi.org/10.1017/S0033822200053066

2775   Lee, J. Y. et al. 2021, Future Global Climate: Scenario-Based Projections and Near-Term Information. In: *Climate Change 2021: The Physical Science Basis. Contribution of Working Group I to the Sixth Assessment Report of the Intergovernmental Panel on ClimateChang*e [Masson-Delmotte, V. et al. (eds.)]. Cambridge University Press. In Press. https://www.ipcc.ch/report/ar6/wg1/#FullReport

2780 Levin, I., Naegler, T., Kromer, B., Diehl, M., Francey, R., Gomez-Pelaez, A., Steele, P., Wagenbach, D., Weller, R. and Worthy, D., 2010. Observations and modelling of the global distribution and long-term trend of atmospheric $^{14}CO_2$. *Tellus B: Chemical and Physical Meteorology*, 62, 26-46. https://www.tandfonline.com/doi/abs/10.1111/j.1600-0889.2009.00446.x

Lewis, E., and D. Wallace (1998), Program developed for CO_2 System Calculations, *Rep.*, 38 pp. https://www.nodc.noaa.gov/ocads/oceans/CO2SYS/cdiac105.pdf. Version 01.05, https://data.ess-dive.lbl.gov/view/doi:10.15485/1464255

2785 Liss, P. S. and Slater P. G. (1974), Flux of gases across the air-sea interface, *Nature*, *247*, 181-184, doi:10.1038/247181a0.

Liss, P. S., and L. Merlivat (1986), Air-Sea Gas Exchange Rates: Introduction and Synthesis, in *The Role of Air-Sea Exchange in Geochemical Cycling*, edited by P. Buat-Ménard, pp. 113-127, Springer Netherlands, Dordrecht, doi:10.1007/978-94-009-4738-2_5.

Los, S. O. (2013), Analysis of trends in fused AVHRR and MODIS NDVI data for 1982–2006: Indication for a CO_2
2790 fertilization effect in global vegetation, *Global Biogeochem. Cycles*, 27, 318–330, doi:10.1002/gbc.20027.

MacDougall, A.H. et al., 2020. Is there warming in the pipeline? A multi-model analysis of the Zero Emissions Commitment from CO_2. *Biogeosciences*, *17*(11), pp.2987-3016. https://bg.copernicus.org/articles/17/2987/2020/

Martin, J. H., G. A. Knauer, D. M. Karl, and W. W. Broenkow (1987), VERTEX: carbon cycling in the northeast Pacific, *Deep Sea Research Part A. Oceanographic Research Papers*, *34*(2), 267-285, doi:https://doi.org/10.1016/0198-
2795 0149(87)90086-0.

McKinley, G. A., A. R. Fay, N. S. Lovenduski, and D. J. Pilcher (2017), Natural Variability and Anthropogenic Trends in the Ocean Carbon Sink, *Annual Review of Marine Science*, *9*(1), 125-150, doi:10.1146/annurev-marine-010816-060529.

Moore III, B., and B. H. Braswell (1994), The lifetime of excess atmospheric carbon dioxide, *Global Biogeochemical Cycles*, *8*(1), 23-38, doi:10.1029/93GB03392.

2800 Mouchet, A., 2013. The ocean bomb radiocarbon inventory revisited. *Radiocarbon* **55**, 1580-1594. DOI: 10.2458/azu_js_rc.55.16402

Myhre, G., D. Shindell, F. Bréon, W. Collins, J. Fuglestvedt, J. Huang, D. Koch, J. Lamarque, D. Lee, and B. Mendoza (2013), Anthropogenic and natural radiative forcing, in *Climate Change 2013: The Physical Science Basis*, edited by T. F. Stocker et al., pp. 659-740, Cambridge University Press.

2805 Naegler, T., and I. Levin (2006), Closing the global radiocarbon budget 1945–2005, *J. Geophys. Res.*, 111, D12311, doi:10.1029/2005JD006758.

Naegler T. and I. Levin (2009*a*) Biosphere-atmosphere gross carbon exchange flux and the$^{13}CO_2$ and $^{14}CO_2$ disequilibria constrained by the biospheric excess radiocarbon inventory. *J. Geophys. Res*. 114, D17303. doi:10.1029/2008JD011116.

Naegler, T., and I. Levin (2009*b*), Observation-based global biospheric excess radiocarbon inventory 1963–2005, *J.*
2810 *Geophys. Res*., 114, D17302, doi:10.1029/2008JD011100.

Neftel, A., Moor, E., Oeschger, H. and Stauffer, B., 1985. Evidence from polar ice cores for the increase in atmospheric CO_2 in the past two centuries. *Nature*, **315**, 45-47. https://www.nature.com/articles/315045a0

Oeschger, H., Siegenthaler, U., Schotterer, U. and Gugelmann, A., 1975. A box diffusion model to study the carbon dioxide exchange in nature. *Tellus*, 27, 168-192. https://doi.org/10.1111/j.2153-3490.1975.tb01671.x

2815   O'Neill, B. C., S. R. Gaffin, F. N. Tubiello, and M. Oppenheimer (1994), Reservoir timescales for anthropogenic CO_2 in the atmosphere, *Tellus B*, *46*(5), 378-389, doi:10.1034/j.1600-0889.1994.t01-4-00004.x.

O'Neill, B.C., Oppenheimer, M. and Gaffin, S.R., 1997. Measuring time in the greenhouse; an editorial essay. Climatic change, 37, 491-505. https://link.springer.com/article/10.1023/A:1005335816806

Pan, Y., et al., 2011. A large and persistent carbon sink in the world's forests. *Science*, **333**, 988-993.
2820   https://science.sciencemag.org/content/333/6045/988.abstract

Peacock, S. (2004), Debate over the ocean bomb radiocarbon sink: Closing the gap, Global Biogeochem. Cycles, 18, GB2022, doi:10.1029/2003GB002211

Piao, S., Luyssaert, S., Ciais, P., Janssens, I.A., Chen, A., Cao, C., Fang, J., Friedlingstein, P., Luo, Y. and Wang, S., 2010. Forest annual carbon cost: A global-scale analysis of autotrophic respiration. *Ecology*, 91(3), pp.652-661.
2825   https://besjournals.onlinelibrary.wiley.com/doi/abs/10.1890/08-2176.1

Piao, S., Wang, X., Park, T., Chen, C., Lian, X., He, Y., Bjerke, J.W., Chen, A., Ciais, P., Tømmervik, H. and Nemani, R.R., 2019. Characteristics, drivers and feedbacks of global greening. *Nature Reviews Earth & Environment*, 1-14. https://www.nature.com/articles/s43017-019-0001-x

Pierrot, D. E. Lewis, and D. W. R. Wallace. 2006. MS Excel Program Developed for CO_2 System Calculations.
2830   ORNL/CDIAC-105a. Carbon Dioxide Information Analysis Center, Oak Ridge National Laboratory, U.S. Department of Energy, Oak Ridge, Tennessee. https://data.ess-dive.lbl.gov/catalog/d1/mn/v2/object/ess-dive-71ca85ad228b1ad-20180716T150109005535.

Planton, S. (2013), Glossary, in *Climate Change 2013: The Physical Science Basis*, edited by T. F. Stocker et al., pp. 1447-1481, Cambridge Univ. Press.

2835   Popper, K.R., 1963. *Conjectures and Refutations: The Growth of Scientific Knowledge*. Routledge and Keagan Paul (London); 5th Edition, 1989, p. 36; ISBN-13: 978-0415043182.

Prather, M. J., C. D. Holmes, and J. Hsu (2012), Reactive greenhouse gas scenarios: Systematic exploration of uncertainties and the role of atmospheric chemistry, *Geophysical Research Letters*, *39*(9), doi:10.1029/2012GL051440.

Pregitzer, K.S. and Euskirchen, E.S. (2004). Carbon cycling and storage in world forests: biome patterns related to forest
2840   age. *Global Change Biology* **10**, 2052-2077. https://onlinelibrary.wiley.com/doi/abs/10.1111/j.1365-2486.2004.00866.x

Prentice, I. C. et al. (2001), The Carbon Cycle and Atmospheric Carbon Dioxide, in *Climate Change 2001: The Scientific Basis. Contributions of Working Group I to the Third Assessment Report of the Intergovernmental Panel on Climate Change*, edited by J. T. Houghton et al., pp. 185-237, Cambridge University Press, Cambridge, UK.

Raich, J.W. and Schlesinger, W.H., 1992. The global carbon dioxide flux in soil respiration and its relationship to vegetation
2845   and climate. Tellus B, 44(2), pp.81-99. https://onlinelibrary.wiley.com/doi/abs/10.1034/j.1600-0889.1992.t01-1-00001.x

Ramanathan, V., 1988. The greenhouse theory of climate change: a test by an inadvertent global experiment. *Science* **240**, 293-299 https://science.sciencemag.org/content/240/4850/293.abstract

Raupach, M. R. (2013), The exponential eigenmodes of the carbon-climate system, and their implications for ratios of responses to forcings, *Earth Syst. Dynam.*, *4*(1), 31-49, doi:10.5194/esd-4-31-2013.

2850 Raupach, M. R., M. Gloor, J. L. Sarmiento, J. G. Canadell, T. L. Frölicher, T. Gasser, R. A. Houghton, C. Le Quéré, and C. M. Trudinger (2014), The declining uptake rate of atmospheric CO_2 by land and ocean sinks, *Biogeosciences*, *11*(13), 3453-3475, doi:10.5194/bg-11-3453-2014.

Revelle, R. and Suess, H.E., 1957. Carbon dioxide exchange between atmosphere and ocean and the question of an increase of atmospheric CO_2 during the past decades. *Tellus*, 9, 18-27.
2855 https://www.tandfonline.com/doi/pdf/10.3402/tellusa.v9i1.9075?needAcc

Rhein, M., et al. (2013), Observations: Ocean, in *Climate Change 2013 – The Physical Science Basis: Working Group I Contribution to the Fifth Assessment Report of the Intergovernmental Panel on Climate Change*, edited by T. F. Stocker et al., Cambridge University Press, Cambridge.

Rödenbeck, C., D. C. E. Bakker, N. Metzl, A. Olsen, C. Sabine, N. Cassar, F. Reum, R. F. Keeling, and M. Heimann (2014),
2860 Interannual sea–air CO_2 flux variability from an observation-driven ocean mixed-layer scheme, *Biogeosciences*, *11*(17), 4599-4613, doi:10.5194/bg-11-4599-2014.

Rodhe, H. and A. Björkström (1979). Some consequences of non-proportionality between fluxes and reservoir contents in natural systems. *Tellus*, 31(3), 269-278. https://onlinelibrary.wiley.com/doi/abs/10.1111/j.2153-3490.1979.tb00905.x

Roth, R. and Joos, F., 2013. A reconstruction of radiocarbon production and total solar irradiance from the Holocene ^{14}C
2865 and CO_2 records: implications of data and model uncertainties. *Climate of the Past*, 9, 1879-1909. doi:10.5194/cp-9-1879-2013

Rubino, M., Etheridge, D.M., Thornton, D.P., Howden, R., Allison, C.E., Francey, R.J., Langenfelds, R.L., Steele, L.P., Trudinger, C.M., Spencer, D.A. and Curran, M.A.J., 2019. Revised records of atmospheric trace gases CO_2, CH4, N2O, and δ13C-CO_2 over the last 2000 years from Law Dome, Antarctica, Earth Syst. Sci. Data, 11, 473–492. doi:10.5194/essd-11-
2870 473-2019

Running, S.W., Nemani, R.R., Heinsch, F.A., Zhao, M., Reeves, M. and Hashimoto, H., 2004. A continuous satellite-derived measure of global terrestrial primary production. *Bioscience*, 54, 547-560. https://academic.oup.com/bioscience/article/54/6/547/294347

Sander R., Acree Jr. W. E., De Visscher A., Schwartz S. E., and Wallington T. J. (2021). Henry's law constants. *Pure Appl.*
2875 *Chem*. 2021. In press. https://doi.org/10.1515/pac-2020-????

Sarmiento, J. L., and N. Gruber (2002), Sinks for anthropogenic carbon, *Physics Today*, *55*(8), 30-36, doi:10.1063/1.1510279

Sarmiento, J. L., and N. Gruber (2013), *Ocean biogeochemical dynamics*, Princeton University Press.

Sarmiento, J.L. and Sundquist, E.T., 1992. Revised budget for the oceanic uptake of anthropogenic carbon dioxide. *Nature*,
2880 356, 589-593. https://link.springer.com/content/pdf/10.1038/356589a0.pdf

Sarmiento, J. L., J. C. Orr, and U. Siegenthaler (1992), A perturbation simulation of CO_2 uptake in an ocean general circulation model, *Journal of Geophysical Research: Oceans*, *97*(C3), 3621-3645, doi:10.1029/91JC02849.

Schimel, D., Stephens, B. B., and Fisher, J. B. (2015). Effect of increasing CO_2 on the terrestrial carbon cycle. *Proceedings of the National Academy of Sciences*, 112(2), 436-441. https://www.pnas.org/content/112/2/436.

2885 Schlitzer, R. (2000), Applying the Adjoint Method for Biogeochemical Modeling: Export of Participate Organic Matter in the World Ocean, *Inverse Methods in Global Biogeochemical Cycles*, doi:10.1029/GM114p0107.

Schneider, S. H., and S. L. Thompson (1981), Atmospheric CO_2 and climate: Importance of the transient response, *Journal of Geophysical Research: Oceans*, *86*(C4), 3135-3147, doi:10.1029/JC086iC04p03135.

Schwartz, S. E. (1979), Residence times in reservoirs under non-steady-state conditions: Application to atmospheric SO_2
2890 and aerosol sulfate, *Tellus*, *31*, 530-547. https://onlinelibrary.wiley.com/doi/abs/10.1111/j.2153-3490.1979.tb00935.x

Schwartz, S. E. (1992), Factors governing dry deposition of gases to surface water, in *Precipitation Scavenging and Atmospheric-Surface Exchange*, edited by S. E. Schwartz and W. G. N. Slinn, pp. 789-801, Hemisphere Publishing Corp., Washington, DC.

Schwartz SE (2008) Reply to comments by G. Foster et al., R. Knutti et al., and N. Scafetta on ''Heat capacity, time
2895 constant, and sensitivity of Earth's climate system''. J Geophys Res 113:D15105. doi: 10.1029/2008JD009872

Schwartz, S. E. (2012), Interactive comment on "Carbon dioxide and climate impulse response functions for the computation of greenhouse gas metrics: a multi-model analysis" by F. Joos et al., *Atmos. Chem. Phys. Discuss.*, *12*, C5982-C5984. http://www.atmos-chem-phys-discuss.net/12/C5982/2012/acpd-12-C5982-2012-supplement.pdf

Schwartz, S. E. (2018), Unrealized Global Temperature Increase: Implications of Current Uncertainties, *J. Geophys. Res.*
2900 *Atmos.*, *123*, 3462-3482, doi:10.1002/2017JD028121.

Shine, K.P., Derwent, R.G., Wuebbles, D.J. and Morcrette, J.J., 1990. Radiative forcing of climate. In *Climate change: The IPCC scientific assessment*, J. T. Houghton, G. J. Jenkins and J. J. Ephraums Eds. Cambridge University Press, Cambridge UK, pp. 41-68. https://core.ac.uk/download/pdf/42811043.pdf

Sierra, C. A., Müller, M., Metzler, H., Manzoni, S., and Trumbore, S. E. (2017). The muddle of ages, turnover, transit, and
2905 residence times in the carbon cycle. Global Change Biology, 23:1763–1773. doi: 10.1111/gcb.13556

Sitch, S., et al. (2015), Recent trends and drivers of regional sources and sinks of carbon dioxide, *Biogeosciences*, *12*(3), 653-679, www.biogeosciences.net/12/653/2015/doi:10.5194/bg-12-653-2015.

Six, K. D., and E. Maier-Reimer (1996), Effects of plankton dynamics on seasonal carbon fluxes in an ocean general circulation model, *Global Biogeochemical Cycles*, *10*, 559-583, doi:10.1029/96GB02561.

2910 Stephenson, N. L. et al., 2014. Rate of tree carbon accumulation increases continuously with tree size. Nature **507**, 90-93. https://www.nature.com/articles/nature12914

Stuiver, M. and Polach, H.A., 1977. Discussion. Reporting of ^{14}C data. *Radiocarbon*, 19, 355-363. https://journals.uair.arizona.edu/index.php/radiocarbon/article/viewFile/4183/3608

2915 Stuiver, M., Reimer, P.J. and Braziunas, T.F., 1998. High-precision radiocarbon age calibration for terrestrial and marine samples. radiocarbon, 40, 1127-1151. https://www.cambridge.org/core/journals/radiocarbon/article/highprecision-radiocarbon-age-calibration-for-terrestrial-and-marine-samples/1660E9D7A43772ACBB56614C1DD09D46

Takahashi, T., et al. (2009), Climatological mean and decadal change in surface ocean pCO_2, and net sea–air CO_2 flux over the global oceans, *Deep Sea Research Part II: Topical Studies in Oceanography*, *56*, 554-577, doi:https://doi.org/10.1016/j.dsr2.2008.12.009.

2920 Tans, P. P. (1997). The CO_2 lifetime concept should be banished. *Climatic Change*, **37**, 487-490. https://link.springer.com/article/10.1023%2FA%3A1005373006194?LI=true

Torn, M.S., Swanston, C.W., Castanha, C. and Trumbore, S.E., 2009. Storage and turnover of organic matter in soil. In *Biophysico-chemical processes involving natural nonliving organic matter in environmental system*s. Senesi, N., Xing, B. and Huang, P.M., Eds. Wiley, Hoboken, pp. 219-272. https://onlinelibrary.wiley.com/doi/abs/10.1002/9780470494950.ch6

2925 Tramontana, G., Jung, M., Schwalm, C.R., Ichii, K., Camps-Valls, G., Ráduly, B., Reichstein, M., Arain, M.A., Cescatti, A., Kiely, G. and Merbold, L., 2016. Predicting carbon dioxide and energy fluxes across global FLUXNET sites with regression algorithms. Biogeosciences, 13, 4291-4313. www.biogeosciences.net/13/4291/2016/ doi:10.5194/bg-13-4291-2016

Trudinger, C. M., I. G. Enting, P. J. Rayner, and R. J. Francey (2002), Kalman filter analysis of ice core data 2. Double deconvolution of CO_2 and $\delta^{13}C$ measurements, *J. Geophys. Res.: Atmospheres*, 107, ACH 5-1-ACH 5-24,
2930 doi:10.1029/2001JD001112.

Volk, T., and M. I. Hoffert (1985), Ocean Carbon Pumps: Analysis of Relative Strengths and Efficiencies in Ocean-Driven Atmospheric CO_2 Changes, In *The Carbon Cycle and Atmospheric CO_2: Natural Variations Archean to Present*, E. T. Sundquist and W. S. Broecker, Eds. Amer. Geophys. Un., Washington DC, https://agupubs.onlinelibrary.wiley.com/doi/abs/10.1029/GM032p0099.

2935 Wang, L., J. Huang, Y. Luo, and Z. Zhao (2016), Narrowing the spread in CMIP5 model projections of air-sea CO2 fluxes, Scientific Reports, 6, 37548, doi:10.1038/srep37548.

Wang, Y. P., Lu, X. J., Wright, I. J., Dai, Y. J., Rayner, P. J. and Reich, P. B., 2012. Correlations among leaf traits provide a significant constraint on the estimate of global gross primary production. *Geophys. Res. Lett.*, 39. https://agupubs.onlinelibrary.wiley.com/doi/abs/10.1029/2012GL053461

2940 Wanninkhof, R., et al. (2013), Global ocean carbon uptake: magnitude, variability and trends, *Biogeosciences*, 10, 1983-2000, doi:10.5194/bg-10-1983-2013.

Weiss, R. F. 1974. Carbon dioxide in water and seawater: The solubility of a non-ideal gas. *Marine Chemistry* 2:203-15. https://www.sciencedirect.com/science/article/pii/0304420374900152

Welp, L.R., Keeling, R.F., Meijer, H.A., Bollenbacher, A.F., Piper, S.C., Yoshimura, K., Francey, R.J., Allison, C.E. and
2945 Wahlen, M., 2011. Interannual variability in the oxygen isotopes of atmospheric CO_2 driven by El Niño. Nature, 477, 579-582. https://www.nature.com/articles/nature10421

Yan, Y., Zhou, X., Jiang, L. and Luo, Y., 2017. Effects of carbon turnover time on terrestrial ecosystem carbon storage. Biogeosciences, 14. doi: 10.5194/bg-14-5441-2017.

Zhang, Y., Xiao, X., Guanter, L., Zhou, S., Ciais, P., Joiner, J., Sitch, S., Wu, X., Nabel, J., Dong, J. and Kato, E., 2016. Precipitation and carbon-water coupling jointly control the interannual variability of global land gross primary production. Sci. Rep. 6, 39748; doi: 10.1038/srep39748

Zhang, Y., Xiao, X., Wu, X., Zhou, S., Zhang, G., Qin, Y. and Dong, J., 2017. A global moderate resolution dataset of gross primary production of vegetation for 2000–2016. *Scientific Data*, 4, 170165. https://www.nature.com/articles/sdata2017165

Zhu, Z. et al., 2016. Greening of the Earth and its drivers. *Nature Climate Change*, 6, 791-795. https://www.nature.com/articles/doi%3A10.1038/nclimate3004

Zhu, Z., Piao, S., Yan, T., Ciais, P., Bastos, A., Zhang, X., & Wang, Z. (2018). The accelerating land carbon sink of the 2000s may not be driven predominantly by the warming hiatus. Geophysi. Res. Lett., 45, 1402–1409. https://doi.org/10.1002/2017GL075808

Zickfeld, K., Eby, M., Weaver, A.J., Alexander, K., Crespin, E., Edwards, N.R., Eliseev, A. V., Feulner, G., Fichefet, T., Forest, C. E. and Friedlingstein, P., 2013. Long-term climate change commitment and reversibility: an EMIC intercomparison. *J. Climate*, 26, 5782-5809. https://doi.org/10.1175/JCLI-D-12-00584.1

2950

2955

2960

2965

Table 1. Stocks and fluxes comprising preindustrial CO_2 budget and present (2016) anthropogenic perturbation (present minus preindustrial), and associated uncertainties, as developed here and as presented in AR5, pertinent to 2000-2009 (Ciais et al., 2013) where available, upright type, or otherwise in AR4, pertinent to the 1990s, (Denman et al., 2007), *italic*. Unc denotes 1-sigma uncertainty estimate; minus sign on uncertainty denotes anticorrelation with uncertainty in flux in opposite direction. Uncertainties do not include uncertainties in emissions except where indicated by bold.

Category Unit	Quantity	Pre-industrial	Unc	*AR4* *AR5*	Anthro (2016)	Unc	*AR4* *AR5*	Unc
Emission Pg yr^{-1}	Q_{ff}				9.9	0.5	7.8	0.6
	Q_{lu}				1.4	0.7	1.1	0.8
	Q_{ant}				11.2	0.9	8.9	1
Integrated Emission Pg	Ω_{ff}				422	**21**	375	19
	Ω_{lu}				228	**114**	180	50
	Ω_{ant}				649	**116**	555	
Mixing ratio, ppm	x_{CO2}	278	2	278	127	2	113	4.7
Stocks Pg	S_a	589.4	4.2	589	269.2	4.2	240	10
	S_m	900	0.7	900	32.2	0.6	}155	19
	S_d	35915		37100	[100, 124]	12		
	S_{lo}	2800	+430, -280	2500	[-1, 33]	17	-30	28
	S_l	[200, 700]			[143, 24]	60		
	S_o	[2600, 2100]			[-139,4]	72		
	$\int F_{a\text{-}lo,net}^{ant}$				[227, 261]	17	160	56
Fluxes Pg yr^{-1}	F_{am}	70.0	21	*70*	32.0	9.7	20.0	
	F_{ma}	70.6	-21	*70.6*	29.8	-9.7	17.7	
	$F_{am,}$	-0.6	0.2	*-0.7*	2.2	0.6	2.3	0.4
	F_{pc}	5.6	1.8	*11*				
	F_{md}	49.5	16.3	*90.2*	1.8	0.6		
	F_{dm}	55.1	-16.3	*101*	0.2	0.1		
	$F_{md,}$	5.6	-1.8	*11*	1.6	0.6	*1.6*	
	F_{al}	120			[19, 48]			
	F_{la}	120			[17, 46]			
	$F_{al.net}^{ant}$	0			[0.5, 2.5]			
	F_{ao}	[4.6, 21.6]			[1.1, 3.2]			
	F_{oa}	[4.0, 21.0]			[0, -0.3]			
	$F_{ao,net}^{ant}$	0.6			[3.2, 1.4]			
	$F_{a\text{-}lo}$	120.0		*120.0*	[20, 51]		11.6	
	$F_{lo\text{-}a}$	119.4		*119.6*	[17, 46]		14.1	
	$F_{a\text{-}lo,net}^{ant}$	0.6		*0.4*	4.0	**1.1**	2.6	0.8
	F_{om}	0.6		*0.9*				
Annual changes in stocks Pg yr^{-1}	ΔS_a				5.2	0.40	4.3	0.1
	ΔS_m				0.5	0.06	}2.3	0.4
	ΔS_d				1.6	0.60		0.4
	ΔS_{lo}				4.0	**1.1**	1.6	0.6
	ΔS_l				[2.5, 0.5]	1.0		
	ΔS_o				[1.4, 3.4]	1.0		
	$\Delta S_d + \Delta S_o$				[3.0, 5.0]	**1.1**		

2970

Table 2. Model parameters and related quantities (stocks, S_i; fluxes, F_{ij}, transfer coefficients, k_{ij}) characterizing evolution of CO_2 over the Anthropocene. Primary model parameters are denoted by boxes. Ranges in curly brackets for K'_{ma}, k'_{ma}, K_{ma}, and k_{ma}, characterizing equilibria and kinetics governing exchange of CO_2 between ML and atmosphere are for range of CO_2 over the Anthropocene, $x_{CO2} = \{278, 405\}$ ppm. Ranges in square brackets for primary parameters S_l^{pi} (PI LB stock) and b (exponent describing growth of GPP) and derived PI and PD quantities are constrained by comparison of model with observations.

2975

Quantity	Unit	Relation	Value [Range]	Uncertainty
$\boxed{k_{am}}$	yr^{-1}	F_{am}^{pi} / S_a^{pi}	0.119	0.036
K'_{ma}	–	$(dS_a / dS_m)_{eq}$	$\{6.1, 9.9\}$	
k'_{ma}	yr^{-1}	$K'_{ma} k_{am}$	$\{0.73, 1.17\}$	
K_{ma}	–	$(S_a / S_m)_{eq}$	$\{0.66, 0.92\}$	
k_{ma}^*	yr^{-1}	$K_{ma} k_{am}$	$\{0.078, 0.109\}$	
$\boxed{v_p}$	$m\ yr^{-1}$		5.5	1.8
z_m	m		100	
z_d	m	$3683 - z_m$	3583	
k_{md}	yr^{-1}	v_p/z_m	0.055	
k_{dm}	yr^{-1}	v_p/z_d	0.00153	
$F_{GPP}^{pi} \equiv F_{al}^{pi}$	$Pg\ yr^{-1}$		120	
F_{om}^{pi}	$Pg\ yr^{-1}$		0.6	
$\Delta S_{lo} \equiv dS_{lo}^{pd} / dt$	$Pg\ yr^{-1}$		4.0	1.1
S_{lo}^{pi}	Pg		2800	
$\boxed{S_l^{pi}}$	Pg		$[200, 700]$	
S_o^{pi}	Pg	$S_{lo}^{pi} - S_l^{pi}$	$[2600, 2100]$	
$\boxed{b}$	–		$[0.4, 0.9]$	
$F_{GPP}^{pd} = F_{al}^{pd}$	$Pg\ yr^{-1}$	$F_{GPP}^{pi}\left(S_a^{pd} / S_a^{pi}\right)^b$	$[139, 168]$	
F_{ao}^{pi}	$Pg\ yr^{-1}$	$\dfrac{\Delta S_o^{pd} - F_{om}^{pi}\left(S_o^{pd} - S_o^{pi}\right)/S_o^{pi}}{\left(S_a^{pd} / S_a^{pi}\right)^b - S_o^{pd}/S_o^{pi}}$	$[5, 20]$	
F_{ao}^{pd}	$Pg\ yr^{-1}$	$F_{ao}^{pi}\left(S_a^{pd}/S_a^{pi}\right)^b$	$[6, 25]$	
k_{al}^{pd}	yr^{-1}	F_{al}^{pd}/S_a^{pd}	$[0.16, 0.193]$	
k_{la}	yr^{-1}	F_{GPP}^{pi}/S_l^{pi}	$[0.8, 0.17]$	
k_{ao}^{pd}	yr^{-1}	$k_{ao}^{pd} F_{ao}^{pd}/S_a^{pd}$	$[0.007, 0.028]$	
k_{oa}	yr^{-1}	$\left(F_{ao}^{pi} - F_{om}^{pi}\right)/S_o^{pi}$	$[0.0015, 0.008]$	

Table 3. Evaluation of observationally based turnover time for Anthropogenic CO_2 in the combined atmosphere–labile-biosphere–mixed-layer-ocean (alm) compartment by **Eq 5.8**. Central estimate is for best estimate anthropogenic emissions Q_{ant} together with ($S_{l,ant}^{pd}$, ΔS_l) corresponding to central estimate for (S_l^{pi}, b), (400 Pg, 0.6). For low and high (S_l^{pi}, b) turnover times are calculated also for values of Q_{ant} at high and low ends of uncertainty range, with uncertainties propagated in quadrature.

$S_{l,ant}^{pd}$		Low	Low	Low	Central	**Central**	Central	High	High	High
Q_{ant}^{pd}		High	Central	Low	High	**Central**	Low	High	Central	Low
Quantity	Unit									
$S_{a,ant}^{pd}$	Pg	269.2	269.2	269.2	269.2	**269.2**	269.2	269.2	269.2	269.2
$S_{m,ant}^{pd}$	Pg	32.2	32.2	32.2	32.2	**32.2**	32.2	32.2	32.2	32.2
S_l^{pi}	Pg	200	200	200	400	**400**	400	700	700	700
b	–	0.4	0.4	0.4	0.6	**0.6**	0.6	0.5	0.5	0.5
$S_{l,ant}^{pd}$	Pg	25	25	25	99	**99**	99	140	140	140
$S_{alm,ant}^{pd}$	Pg	336	336	336	391.4	**391.4**	391.4	441	441	441
ΔS_a	Pg yr^{-1}	5.2	5.2	5.2	5.2	**5.2**	5.2	5.2	5.2	5.2
ΔS_m	Pg yr^{-1}	0.5	0.5	0.5	0.5	**0.5**	0.5	0.5	0.5	0.5
ΔS_l	Pg yr^{-1}	0.5	0.5	0.5	1.8	**1.8**	1.8	2.7	2.7	2.7
ΔS_{alm}	Pg yr^{-1}	6.2	6.2	6.2	6.2	**7.4**	8.4	8.4	8.4	8.4
Q_{ant}	Pg yr^{-1}	12.3	11.2	10.1	11.2	**11.2**	11.2	12.3	11.2	10.1
$Q_{ant}^{pd} - \Delta S_{alm,ant}^{pd}$	Pg yr^{-1}	5.4	5.0	2.2	4.9	**3.8**	2.7	5.3	2.8	2.3
$\tau_{alm}^{to,obs}$	yr	62	67	155	80	**103**	145	83	158	191

Figure 1 (*caption on following page*)
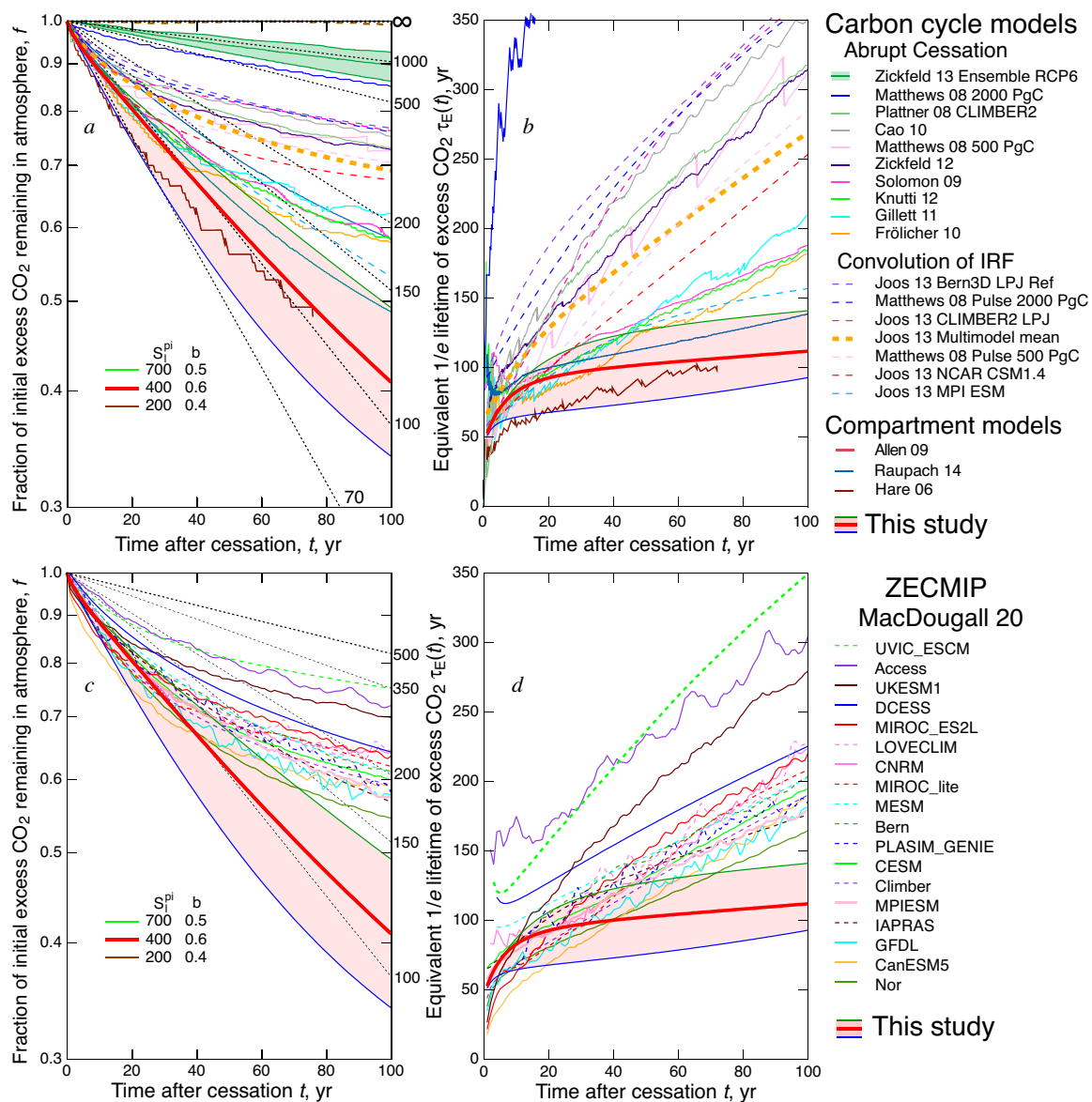
Figure 1 (*preceding page*). Decay of excess atmospheric CO_2 and corresponding adjustment times over the initial 100 years following abrupt cessation of emissions as determined from prior publications and present study. *a*, CO_2 amounts are plotted as fraction *f* of initial amount in excess of preindustrial amount on a logarithmic scale versus time *t* subsequent to cessation. Thin curves show results from published model studies identified by first author and publication year. Solid curves denote results of direct calculations using carbon cycle models or compartment models; dashed curves are results of convolution of impulse response functions (IRFs) with historical emissions; thicker dashed ochre curve shows multimodel mean of Joos et al. (2013*a*). Calculations were conducted for a variety of initial conditions, importantly amount of CO_2 in atmosphere at time of cessation, summarized, with citations, in **Table S1.1** of Supporting Information **SI Text Sect. S1**. Jags in curves result mainly from digitization of published figures. Dotted black lines denote exponential decay with $1/e$ time constant in years. Modified from Schwartz (2018) with addition of best estimate (bold red) and range (light red) as calculated with the model developed here, **Sect. 7.6**; S_1^{pi} and *b* denote parameters of present model, preindustrial stock in the labile biosphere and fertilization exponent characterizing dependence of gross primary production on mixing ratio of atmospheric CO_2, respectively. *b*, Adjustment time (equivalent $1/e$ lifetime, **Sect. 2**) τ_E over time horizon *t* subsequent to cessation of emissions for decay curves in *a*. *c*. As in *a*, calculated from results presented by the Zero Emissions Commitment Model Intercomparison Project (ZECMIP; MacDougall et al., 2020); models are identified in legend; model descriptions and citations are given in MacDougall et al.. *d*, As in *b*, for ZECMIP results. Results from present study are given in **SI data table, sheet 6**.

3010
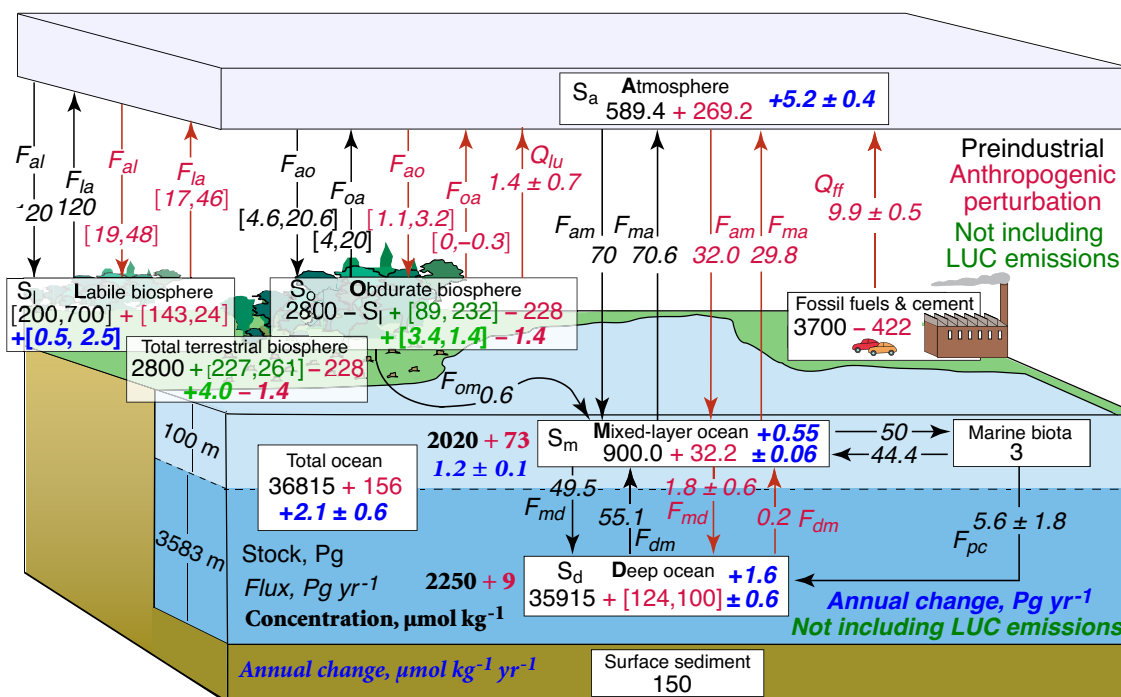
Figure 2. Stocks S_i of carbon in principal compartments pertinent to atmospheric CO_2 and fluxes between compartments F_{ij}; Q_{ff} and Q_{lu} denote anthropogenic emissions from fossil-fuel combustion (including cement production) and from net

3015   land use change, respectively. Stocks (Pg C) are indicated by upright type; fluxes and annual changes in stocks (Pg C yr^{-1}) are indicated by slant type; concentrations of dissolved CO_2 (dissolved inorganic carbon, DIC, μmol kg$_{sw}^{-1}$) are shown in bold serif typeface. Preindustrial quantities are given in black; perturbations resulting from anthropogenic emissions in red; annual changes in stocks (Pg C yr^{-1}) or concentration in the ML in blue; or, excluding land-use change (LUC) emissions, in green. Square brackets reflect ranges of preindustrial stock in labile biosphere S_l^{pi} and fertilization exponent b but not

3020   uncertainties of emissions. Depths of the ocean mixed layer and of the deep ocean are shown at left. The figure is adapted and substantially modified from AR4 (Denman et al., 2007), with quantities updated to the 2016 time frame and other changes, as discussed in the text. Uncertainties are one-sigma estimates. Quantities are shown with more precision than is justified by the accuracy with which they are known to permit differencing.
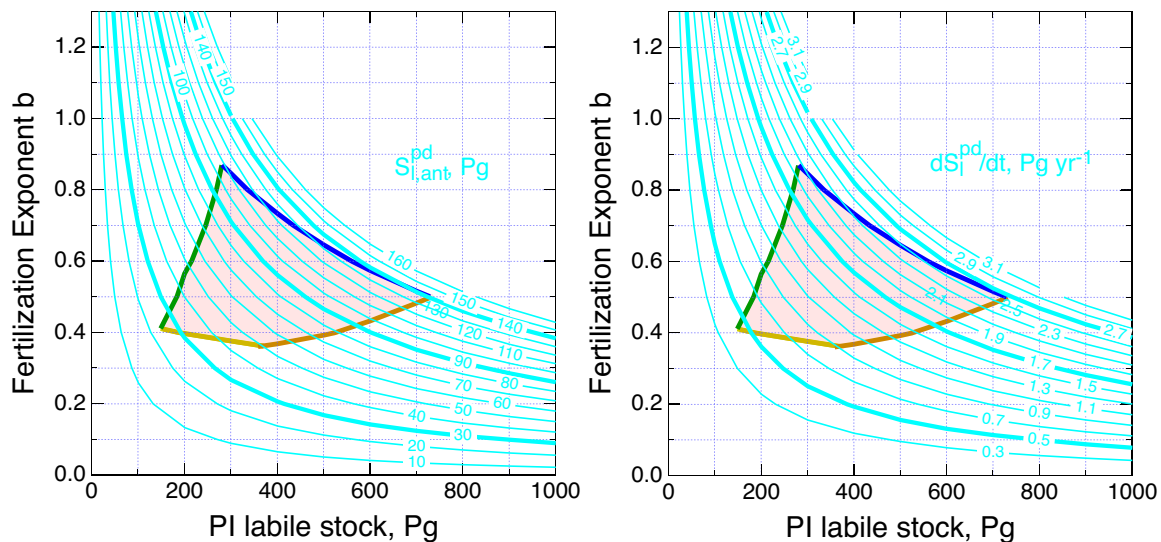
3025

Figure 3. *a*., PD anthropogenic stock in LB, and *b*, PD rate of increase in LB stock as function of fertilization exponent *b* and PI stock in LB; ; absence of contours at upper right denotes regions of (S_l^{pi}, *b*) that are excluded because the rate of increase in stocks would exceed emissions. Thick contours denote algebraically determined best estimate and bounds, **Table 3**. All evaluations are for best estimate PD anthropogenic emissions, Q_{ant} = 11.2 Pg yr^{-1}. Light red quadrilateral denotes region of (S_l^{pi}, *b*) domain that is consistent with observations; colored boundaries denote limits of satisfaction of model results with specific observations, **Sect. 7,2, Sect. 7.3**. **SI data table, sheet 5**.

3030
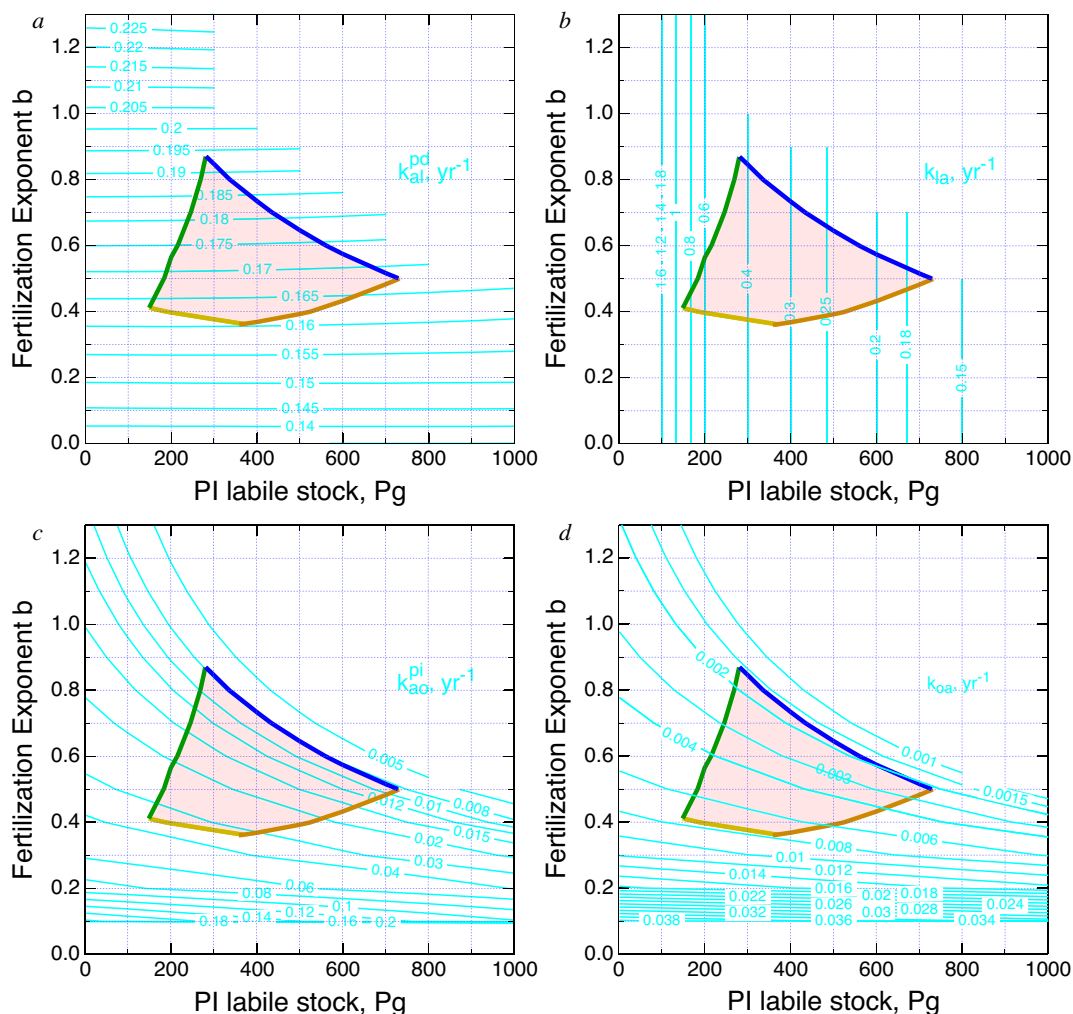
3035 **Figure 4**. *a*. Transfer coefficients between the atmosphere and the two terrestrial biosphere compartments calculated algebraically (**Eqs. 4.8, 4.10, 4.12, 4.13; Appendix A12**) as functions of PI stock in the LB S_l^{pi} and fertilization exponent *b*. Contours show values for entire range of (S_l^{pi}, *b*) examined; absence of contours at upper right denotes regions of (S_l^{pi}, *b*) that are excluded because the rate of increase in stocks would exceed emissions. Light red quadrilateral denotes region of (S_l^{pi}, *b*) domain that is consistent with observations based on comparison of model results with observations; colored

3040 boundaries denote limits of satisfaction of model results with specific observations, **Sect. 7.2, Sect. 7.3**. *a*, Present-day k_{al}; *b*, k_{la}; *c*, preindustrial k_{ao}; *d*, k_{oa}. **SI data table, sheet 5**.
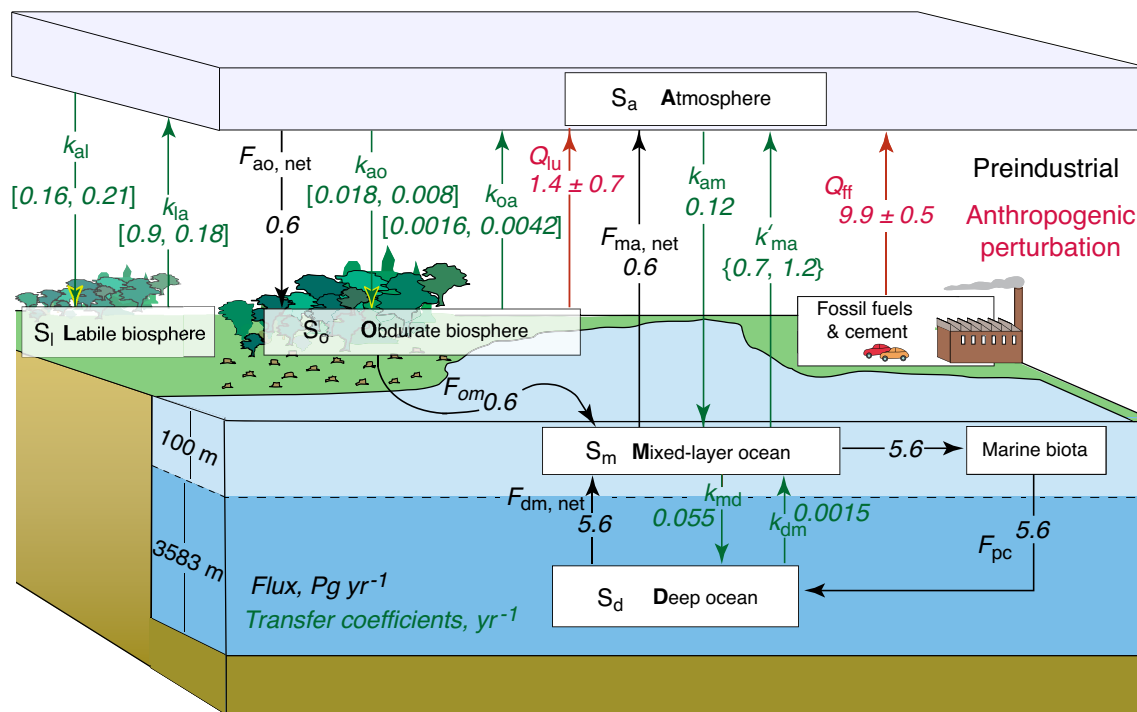
Figure 5. Transfer coefficients k_{ij} (green), yr^{-1}, describing the rate of transfer of anthropogenic CO_2 (or of dissolved inorganic carbon DIC) from stock S_i to stock S_j and other quantities required to model the budget of excess CO_2 (above preindustrial) over the Anthropocene. Square brackets denote ranges propagated from ranges in fertilization exponent b and preindustrial LB stock S_l^{pi}, consistent with observations. Curly brackets denote range arising from increase in CO_2 over the Anthropocene. Red denotes present (2016) annual anthropogenic emissions from fossil fuel combustion and cement production Q_{ff} and from land-use change Q_{lu}, Pg yr^{-1}. Preindustrial steady-state fluxes responsible for departure from equilibrium in the preindustrial budget are shown in black. Depths of the ocean mixed layer and of the deep ocean are shown at left.
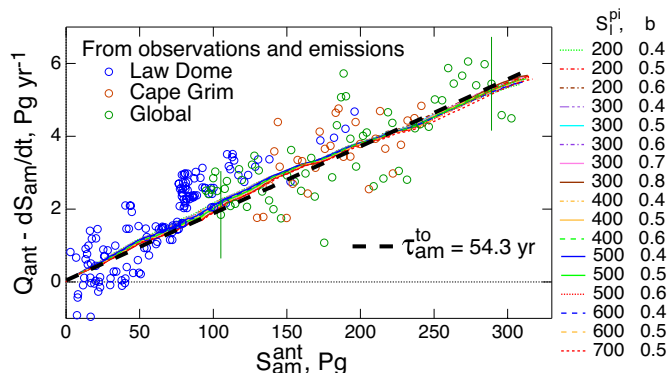
Figure 6. Rate of uptake of CO_2 from AC and the ML combined, S_{am}, into the TB and DO obtained as difference between emissions and observed annual increase in stock in the AC $\triangle S_a$, augmented by annual increase in stock in the ML $\triangle S_m$ calculated for assumed equilibrium between S_a and S_m, versus sum of anthropogenic stocks in the AC and the ML S_{am}^{ant}, also calculated for assumed equilibrium between S_a and S_m. Emissions data from Boden et al. (2017) and Houghton and Nassikas (2017) as tabulated by Le Quéré et al., (2018a). S_a obtained from measurements of CO_2 in glacial ice cores at Law Dome, Antarctica and air at Cape Grim, Tasmania (Etheridge et al., 1996) and from measurements in air (Keeling et al., 1976, 2001 as updated; Ballantyne et al., 2012 as updated by Dlugokencky and Tans, 2018) as tabulated by Le Quéré et al., (2018a) with representative uncertainties. Colored curves denote net flux from AC and ML into TB and DO calculated by model over the time period 1750–2016 for indicated pairs of values of preindustrial stock in LB S_l^{pi} and fertilization exponent b for range (S_l^{pi}, b), indicated in legend, consistent with observations, **Sect. 7**. Dashed black straight line through the origin with slope 0.0184 yr^{-1} corresponds to turnover time for the combined AC-ML compartments τ_{AM}^{to} = 54.3 yr. Observation-derived data, **SI data table, sheet 4**, **sheet 6**.
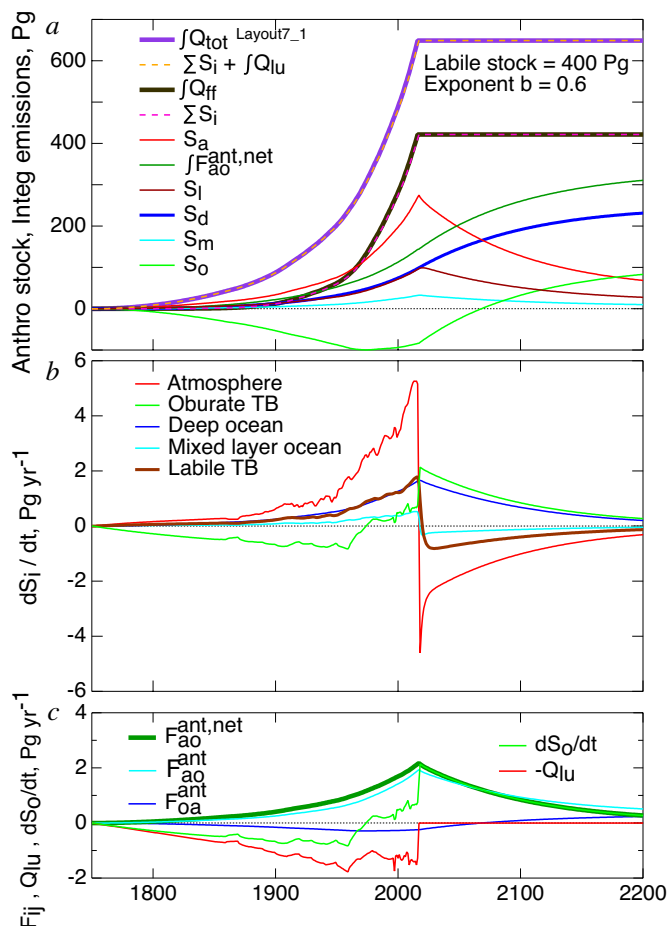
Figure 7. Anthropogenic stocks and related quantities during historical run and subsequent to hypothetical abrupt cessation of emissions in 2017 for (S_l^{pi}, b) = (400 Pg, 0.6). *a*, Stocks of anthropogenic carbon in the several compartments, and total, and running integral of total fossil fuel emissions; OB uptake denotes integrated net transfer from AC; Obdurate biosphere stock includes decrease from LUC emissions. *b*, Rates of change of the several stocks dS_i/dt, and net anthropogenic flux from AC to ML. *c*, Gross and net anthropogenic fluxes between the AC and the OB, rate of change of stock in the OB, dS_O/dt as in *b*, and negative of land use change emissions, on same vertical scale as *b*. **SI, Data table, sheet 6.**
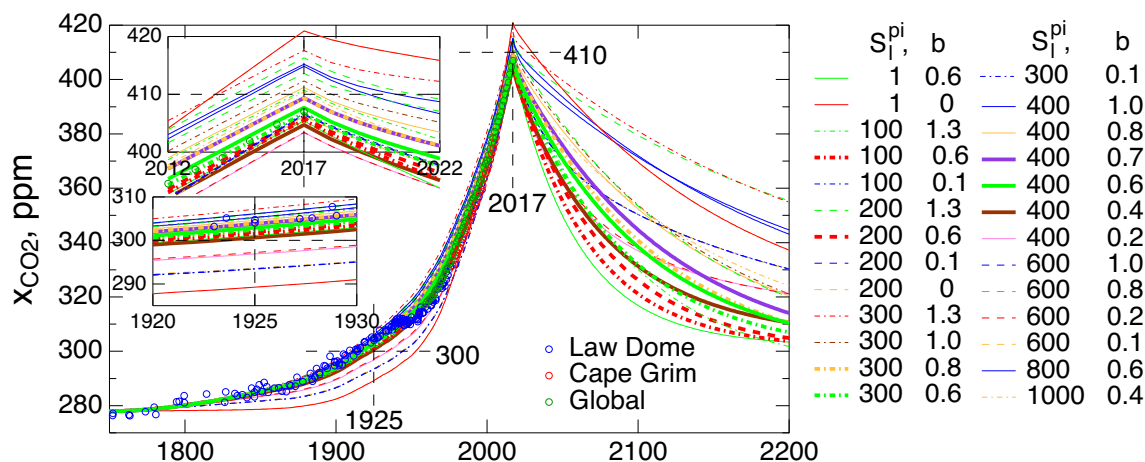
3075

Fig. 8. Consistency of model variants with observed atmospheric CO_2. Curves denote modeled mixing ratio of atmospheric CO_2 x_{CO2} for multiple model variants indicated by values of parameters S_l^{pi} (Pg), preindustrial stock in labile biosphere; and b, exponent characterizing growth of GPP, for anthropogenic emissions given by historical inventories to 2016 (data sources as in **Fig. 5**) and set to zero commencing in 2017. Circles denote observations (data sources as in **Fig. 5**). Insets show

3080   time periods examined to assess consistency with observations: 1925, $x_{CO2} > 300$ ppm; 2017, $x_{CO2} < 410$ ppm, indicated by dashed black lines. Curve colors denote values of S_l^{pi}; styles (e.g. solid, dashed) denote values of b. Bold curves denote consistency with both criteria. **SI Data table, sheets 4, 6.**
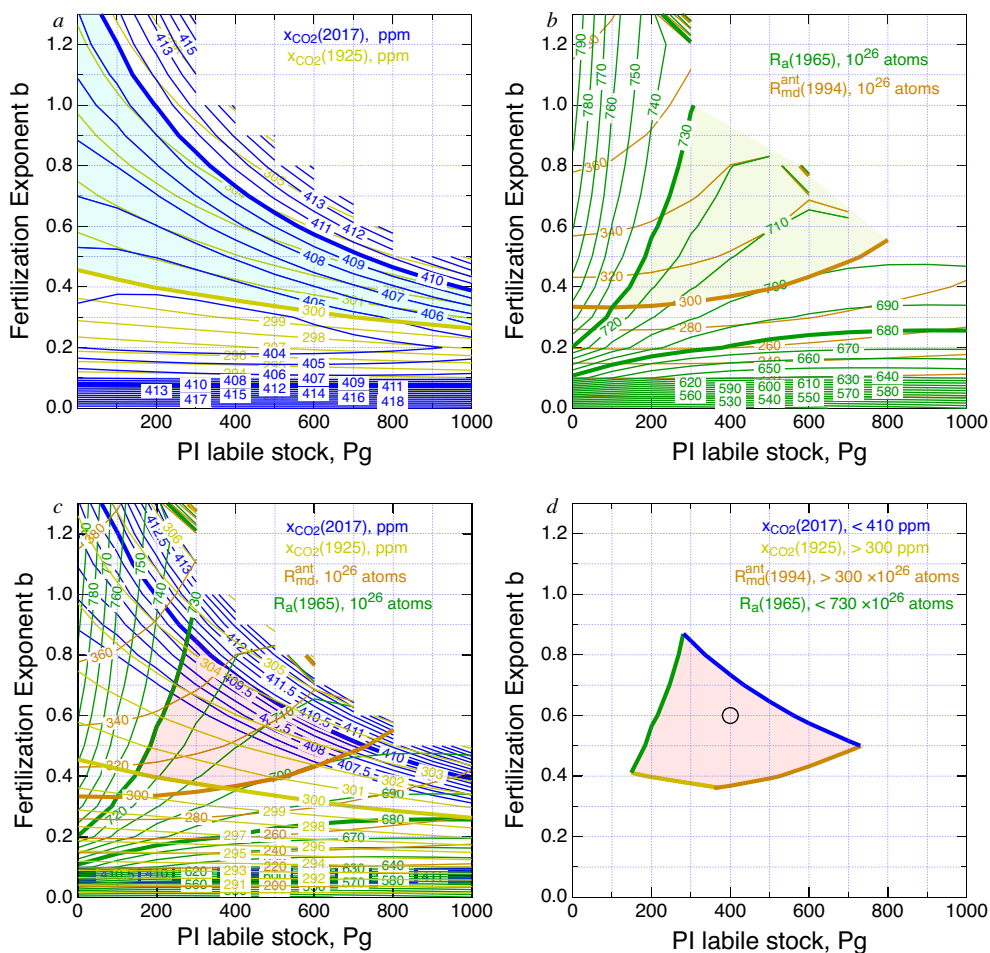
8085 **Figure 9**. Contour diagrams of modeled amounts of CO_2 and of radiocarbon as function of S_l^{pi} and b showing observational constraints on values of (S_l^{pi}, b) pairs. *a*, Mixing ratio of atmospheric CO_2 in 1925 (ochre) and 2017 (blue); bold contours denote lower limit of observed $x_{CO2}(1925)$, 300 ppm, and upper limit of observed $x_{CO2}(2017)$, 410 ppm. *b*, Stock of atmospheric radiocarbon in 1965 (green) and oceanic radiocarbon (ML + DO) in 1994 (tan); bold contours denote lower and upper limits of observed $R_a(1965)$, 680 and 730×10^{26} atoms, respectively, and lower limit of observed R_{md}^{ant}, 300×10^{26}

8090 atoms. Shadings in *a* and *b* denote subdomains of (S_l^{pi}, b) consistent with the respective bounds. *c*, Superposition of panels *a* and *b*; shading denotes intersection of shaded regions in *a* and *b*. *d*, Shaded region in *c*, with controlling observational bounds. Marker at (S_l^{pi}, b) = (400 Pg, 0.6) denotes values of (S_l^{pi}, b) used as an example in subsequent analyses. **SI data table, sheet 5**.
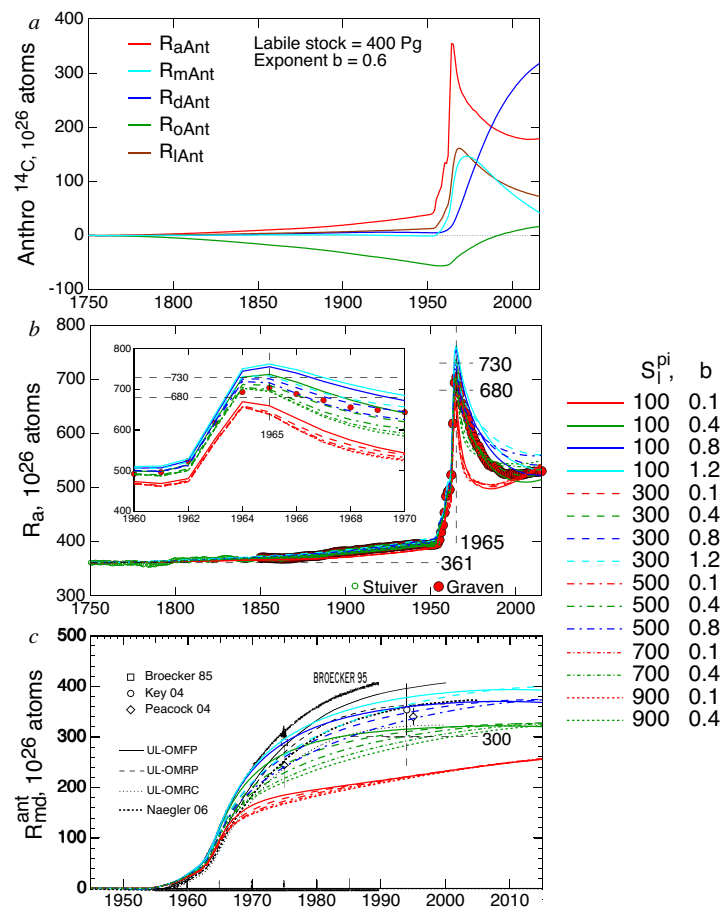
3095

Figure 10. Modeled and measured radiocarbon stocks over the Anthropocene. *a*, Anthropogenic stocks in the several compartments calculated with the present model for S_l^{pi} and $b = 0.6$. *b*, Atmospheric $^{14}CO_2$ in observations and as calculated with several (S_l^{pi} , *b*) pairs; inset shows time range centered about peak value in 1965; dashed lines at 680 and 730 $\times 10^{26}$ atoms denotes limits for which modeled $^{14}CO_2$ at year 1965 is considered consistent with observations. *c*,

3100   Anthropogenic dissolved inorganic radiocarbon [DI^{14}C] in the world ocean in observations and as calculated with several (S_l^{pi} , *b*) pairs as in *b*; dashed line at 300×10^{26} atoms is below which variants are considered inconsistent with observations. Measured atmospheric radiocarbon stocks are from dendrochronologically dated tree rings (Stuiver et al., 1998) and direct measurements in air (as tabulated by Graven et al., 2017). Ocean measurements are from Broecker et al. (1995), Key et al. (2004), and Peacock (2004). Also shown in *c* are model results of Naegler and Levin (2006) and several model variants

3105   denoted UL from Mouchet (2013). **SI Data table, sheet 6**.
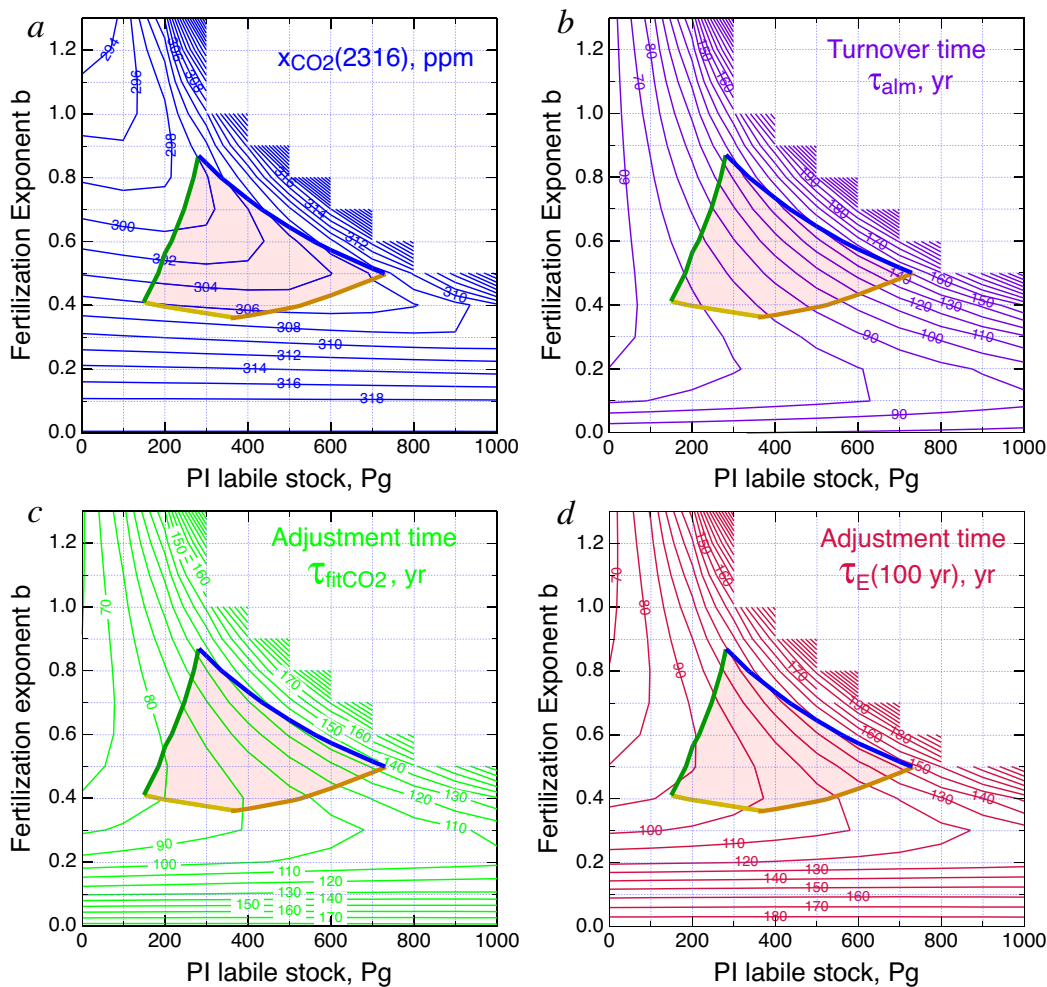
Figure 11. *a*, Mixing ratio of atmospheric CO2 300 years after cessation of emissions as a function of model parameters S_l^{pi} and *b*. *b-d*, several measures of lifetime of excess CO2; *b*, present-day turnover time of stock in combined atmosphere-LB-ML compartment, **Eq 2.2**; *c*, time constant τ_{Fit} characterizing exponential decay from fit to atmospheric CO2 over initial 100 years subsequent to cessation of emissions; *d*, equivalent 1/*e* lifetime of excess CO2, **Eq 2.6b**, evaluated at time horizon $T =$ 100 yr subsequent to cessation. Light red quadrangle denotes region of (S_l^{pi}, *b*) that is consistent with observations the colors of boundaries denoting the several observational constraints, as in **Fig. 9**. **SI data table, sheet 5**.

3110
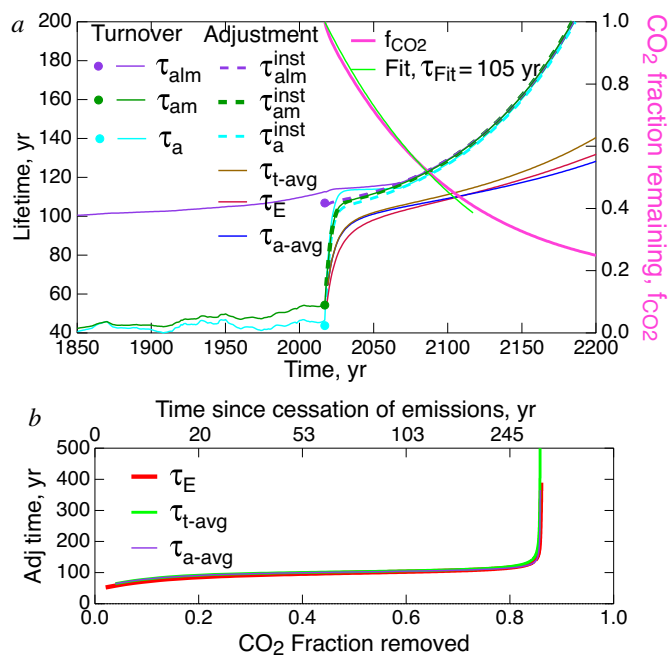
3115

Figure 12. Multiple measures of the lifetime of excess CO_2. *a*, As a function of time for preindustrial LB stock S_l^{pi}, 400 Pg and fertilization exponent *b*, 0.6. Turnover times are evaluated for anthropogenic atmospheric stock S_a^{ant} and for combined anthropogenic stocks in AC and ML, S_{am}^{ant}, and in AC, LB, and ML, S_{alm}^{ant}, by **Eq 2.1** for present-day observational data (markers) and model output using net leaving flux. Adjustment times are evaluated following abrupt cessation of

3120 anthropogenic emissions in 2017. Instantaneous adjustment times τ^{inst} for the three stock quantities are evaluated by **Eq 2.3**. Time-average adjustment time $\tau_{t\text{-avg}}$ is evaluated by **Eq 2.4**; amount-weighted–average lifetime $\tau_{a\text{-avg}}$, **Eq. 2.5**; equivalent $1/e$ lifetime, τ_E, **Eq. 2.6b**; all for S_a. Fraction of excess CO_2 mixing ratio at time of cessation remaining as function of time and fit to exponential decay function for initial 100 yr, with baseline zero, yielding time constant $\tau_{CO2Fit} = 105$ yr, are shown on right axis. *b*, $\tau_{t\text{-avg}}$, $\tau_{a\text{-avg}}$, and τ_E as in *a*, but plotted versus fraction of CO_2 remaining; top axis shows time subsequent

3125 to cessation of emissions corresponding to fraction removed on bottom axis. **SI Data table, sheet 6.**
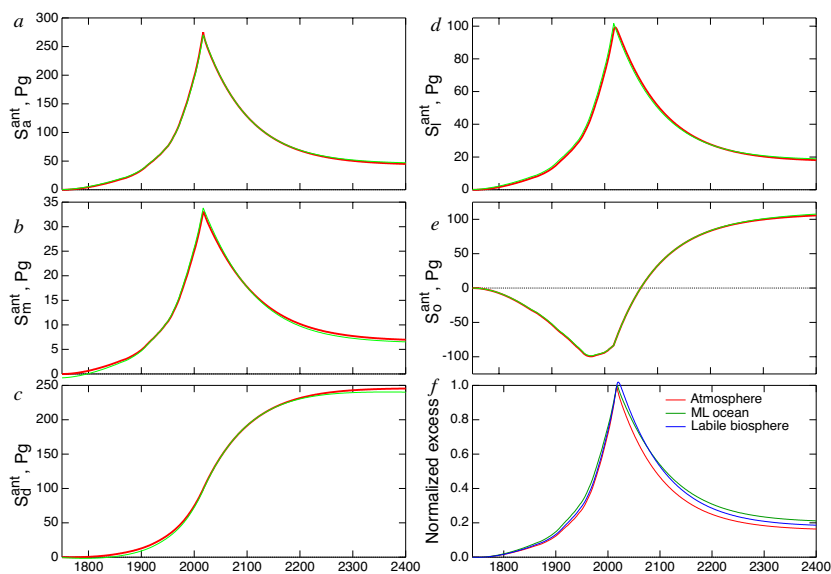
Figure 13. Examination of equilibrium–steady-state (ESS) assumption. *a-e*, Anthropogenic perturbation to stocks in AC, ML, DO, LB, and OB; results from exact model, red, and from ESS model, green. Anthropogenic perturbation to OB stock includes loss from LUC emissions. *f*, Anthropogenic enhancement to stocks in AC, ML, and LB, for exact model, normalized to their values in 2017 prior to cessation of emissions. All results are for $S_{\mathrm{alm}}^{\mathrm{ant}}$ = 400 Pg and *b* = 0.6. **SI Data table, sheet 6.**

Figure 14 (*caption on following page*)
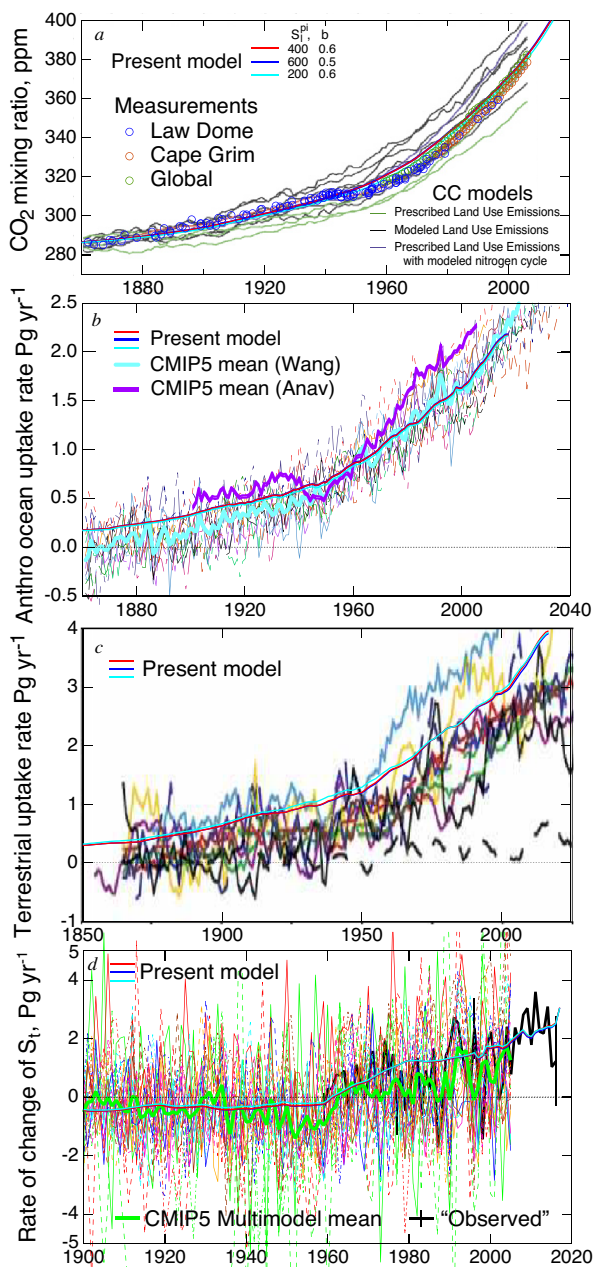
Figure 14 (*preceding page*). CO_2 mixing ratio and net rates of transfer of anthropogenic CO_2 as determined with the present model, as presented by several investigators based on global CC models, and from observations. *a*, Global CO_2 mixing ratio from 11 Earth system models that participated in the CMIP5 intercomparison, adapted from Friedlingstein et al., (2014, Figure 1*a*); observations from Law Dome, Cape Grim and measurements in air as in **Fig. 8**. *b*, Rate of ocean uptake of anthropogenic CO_2 from present model and from 13 CMIP5 models (adapted from Wang et al. 2016, Figure 1*a*), with multimodel means presented by Wang et al. (2016) and by Anav et al. (2013). *c*, Net flux from AC to TB (*i.e.*, not including change due to LUC emissions) from 7 coupled ocean atmosphere GCMs and 4 models of intermediate complexity, modified from Friedlingstein et al. (2006, Figure 1*c*). *d*, Net rate of change of stock in TB (*i.e.*, difference between net uptake rate and LUC emissions); present model, results and multimodel mean from 18 CMIP5 models (data courtesy of Alessandro Anav). "Observed" denotes difference between emissions from fossil fuel and cement manufacture minus observed atmospheric growth and modeled ocean uptake (multimodel mean from Le Quéré et al., (2018*a*) and representative associated uncertainties. Results from present model are shown for three (S_1^{pi}, *b*) pairs indicated in *a*;; cf. **Fig. 8, Fig. 9*d***. Present model results, **SI Data table, sheet 6.**

Figure 15 (*following page*). Comparison of present model results with measurements and other models (Global Carbon Budget GCB17, Le Quéré et al., 2018*a*) over the period of contemporaneous in-situ measurements of atmospheric CO_2. *a*) Rate of uptake of anthropogenic CO_2 by the combined ML + DO, equivalent to net flux from AC to ML minus PI flux: eight CC model calculations from GCB 2017 (thicker lines), and multimodel mean (Le Quéré et al., 2018*a*); 13 CC model calculations from CMIP5 (thinner lines), and multimodel mean (data from Wang et al., 2016, Fig. 1*a*); observation-based studies (Takahashi et al., 2009; Rödenbeck et al., 2014 (data from Le Quéré et al., 2018*a*); Landschützer et al., 2015 (data from Le Quéré et al., 2018*a*, incremented by 0.6 Pg yr^{-1}); Wang et al., 2016 (incremented by 0.6 Pg yr^{-1}); Gruber et al., 2019, mean and uncertainty over indicated time range), and inferred from analysis of radiocarbon data (Graven et al., 2012, mean and uncertainty over indicated time range). *b*) Net anthropogenic flux from atmosphere to combined LB and OB compartments: 15 CC model calculations from GCB17 (data from Le Quéré et al., 2018*a*) and multimodel mean; and as inferred by difference from emissions, atmospheric growth, and ocean uptake, (Gruber et al., 2019). *c*) "Observed" denotes sum of uptake from atmosphere to ocean and TB evaluated as difference between annual emissions and atmospheric growth; multimodel means and observation-derived data tabulated by Le Quéré et al. (2018*a*) as in **Fig. 8**. *d*) Residual of sum of uptake from atmosphere to ocean and TB (model minus observations) for present model and multimodel mean from panel *c*, with average and standard deviation at right. Results from present model are shown for three (S_1^{pi}, *b*) pairs indicated in *c*; only a single instance (400 Pg, 0.6) is shown in *d*. Present model results, **SI Data table, sheet 6.**; cf. **Fig. 8*d***.

Figure 15 *(caption on peceding page)*
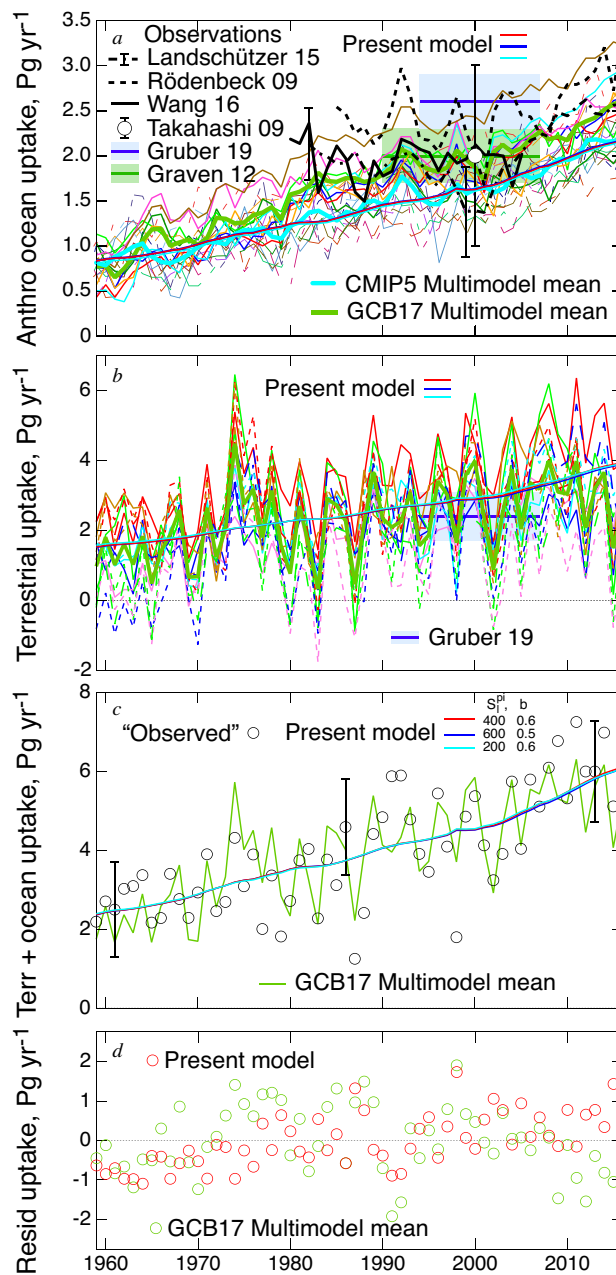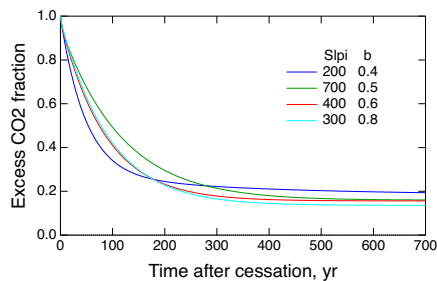
3170 **Figure 16**. Model results for fraction of CO_2 remaining in atmosphere as a function of time, 0 to 700 yr, subsequent to cessation of emissions for indicated values of (S_I^{pi}, b). **SI Data table, sheet 6.**
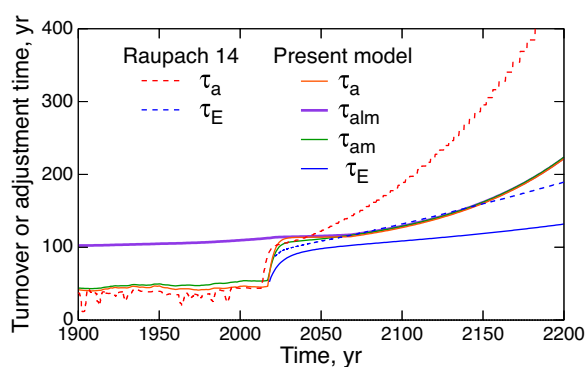
3175 **Figure 17**. Model results for turnover time referenced to excess stock in the AC, evaluated as inverse of transfer coefficient from AC to the ML, DO, and TB, combined, presented by Raupach et al. (2014, their Figure 5) for historical emissions with abrupt cessation in 2013; jags result from digitization. Shown for comparison are turnover times evaluated with present model, with (S_I^{pi}, b) = (400 Pg, 0.6) for excess stock in AC, AC+ML, and AC+ML+LB, for historical emissions with abrupt cessation of emissions in 2017, as in **Fig. 8**. Present model results, **SI Data table, sheet 6.**
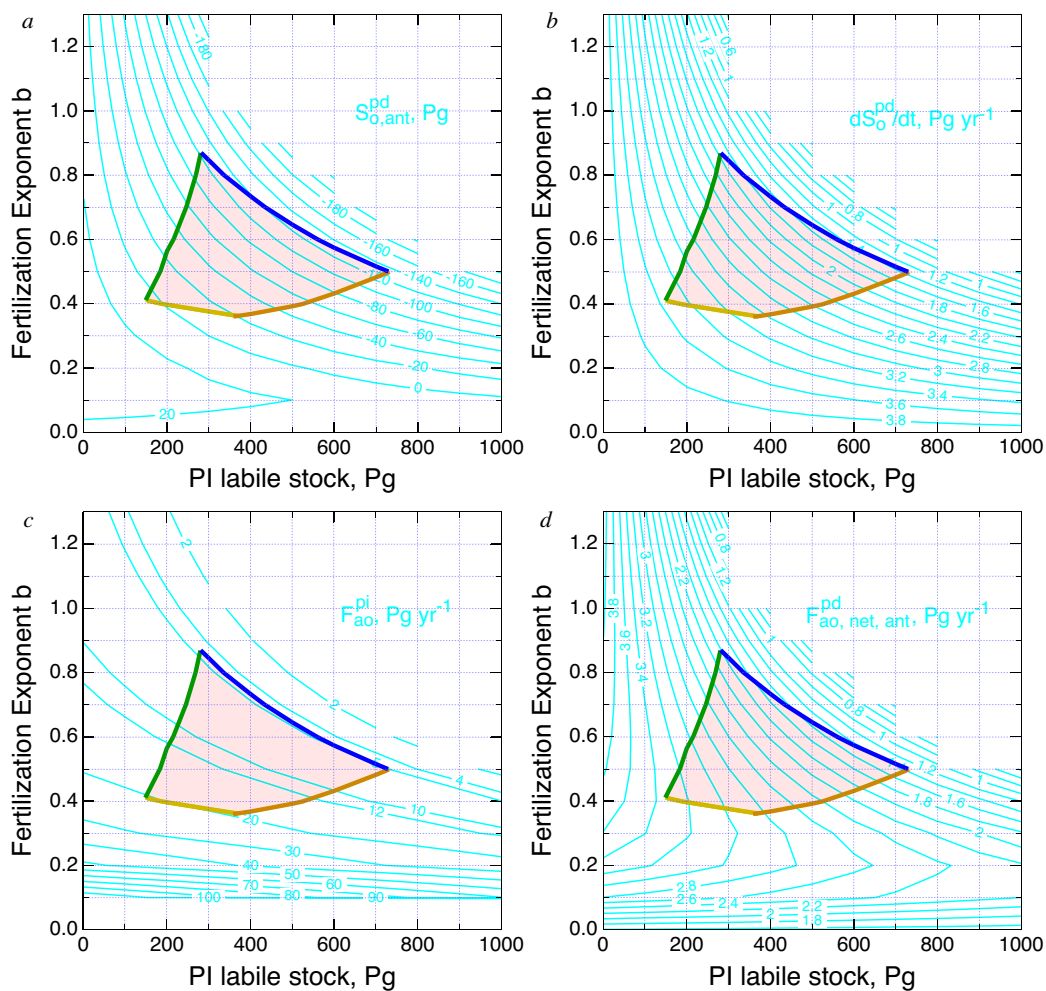
Figure A1. Dependence of quantities characterizing exchange of material between the atmosphere and the obdurate biosphere on preindustrial (PI) stock in the labile biosphere S_l^{pi} and exponent b characterizing rate of increase of GPP with increasing atmospheric CO_2 stock. a, PD stock of anthropogenic carbon in the OB, $S_{o}^{Ant,pd}$ b, Present-day (PD) annual rate of increase of stock in the OB due to transfer between the atmosphere and the OB, $\triangle S_o^{tr,pd}$. c, PI flux from the atmosphere to the OB F_{ao}^{pi}. d., PD net anthropogenic flux from the atmosphere and the OB. Contours show values for entire range of [S_l^{pi}, b] examined; light red quadrilateral denotes region in (S_l^{pi}, b) domain that is consistent with observations, as in **Fig. 3**. **SI data table, sheet 5**.
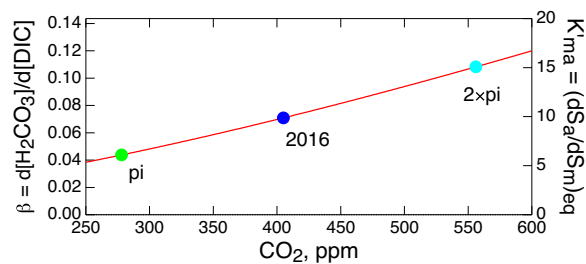
3190

Figure B1. Differential equilibrium constant $\beta = d[H_2CO_3]/d[DIC]$ (left axis) denoting equilibrium change in H_2CO_3 concentration per change in DIC concentration as a function of CO_2 mixing ratio (in dry air) evaluated for seawater alkalinity 2349 μmol kg_{sw}^{-1}, salinity 35, and temperature 18°C; and (right axis) differential equilibrium constant $K'_{ma} = dS_a / dS_m$, the corresponding change in S_a per change in S_m evaluated for depth of mixed layer $z_m = 100$ m. Shown

3195   for reference are mixing ratios of preindustrial, present (2016), and twice preindustrial CO_2. **SI Data table, sheet 2**.
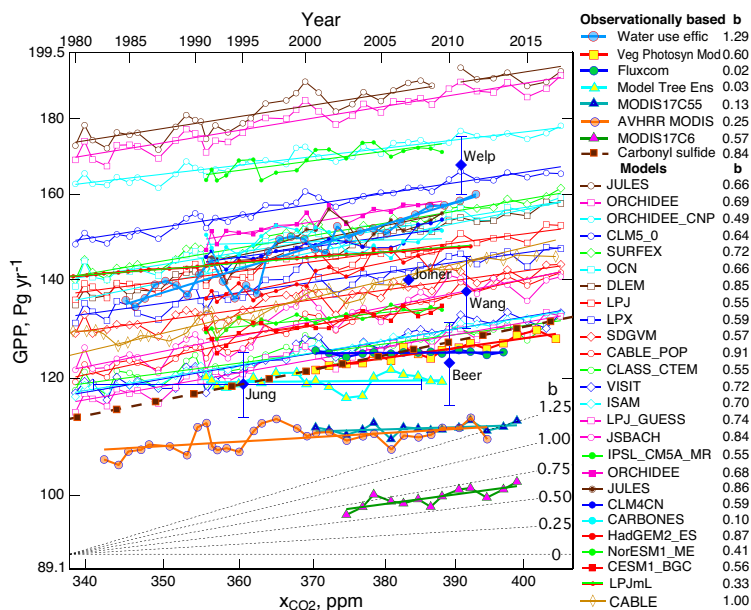
Figure C1. Double logarithmic plot of recent observationally based determinations and model-based estimates of global gross primary production GPP, versus global CO_2 mixing ratio, lower axis, together with fits to the expression $\log F_{GPP} = \log a + b \log x_{CO2}$ (straight lines without markers), corresponding to $F_{GPP} = a x_{CO2}^{b}$, with slope coefficient b given at right; black dotted lines at lower part of figure show slope corresponding to indicated value of b. Date corresponding to CO_2 mixing ratio is shown on top axis. Observationally based determinations (thick lines with markers): two Moderate Resolution Imaging Spectroradiometer MODIS products, data from Zhang et al, 2017; a hybrid MODIS-AVHRR (Advanced Very High Resolution Radiometer) product as determined by the Running et al. (2004) procedure; data from Ballantyne et al., 2017; Model Tree Ensemble MTE product, Jung et al., 2011, data from Anav et al., 2015; Fluxcom, Tramontana et al., 2016, data from Zhang et al., 2017; Vegetation Photosynthesis Model VPM product, Zhang et al., 2017; as inferred from water use and water use efficiency, Cheng et al. (2017); and as inferred from carbonyl sulfide budget (slope only; Campbell et al., 2017). Model based estimates (thin lines with markers) are from the TRENDY project (Sitch et al., 2015 as summarized by Anav et al., 2015, smaller, filled markers, *circa* 2014, data provided by A. Anav; and as summarized by Piao et al., 2019, smaller open markers, *circa* 2018; data provided by S. Piao); additional model based estimates LPJmL (Forkel et al., 2016) and CABLE (Cernusak et al, 2019). Additional assessments (blue diamonds, with uncertainties if provided) plotted against year if specified (Joiner et al., 2018), with pertinent time range (Jung et al., 2011), or year of publication (Beer et al., 2010; Welp et al., 2011, Wang et al., 2012). For identification of model-based and satellite-based products see cited publications, Sitch et al. (2015), and Le Quéré et al. (2018*a*).
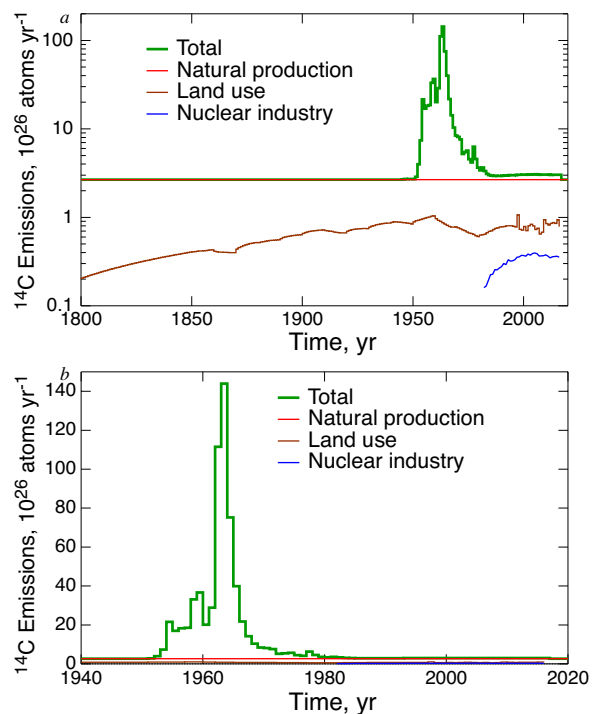
Figure E1. Radiocarbon emissions. *a*, Logarithmic scale and *b*, linear scale. Land-use change emissions, which are slightly dependent on parameters are shown for (S_I^{pi} , *b*) = (500 Pg, 0.3). **SI Data table, sheet 3**.

3220
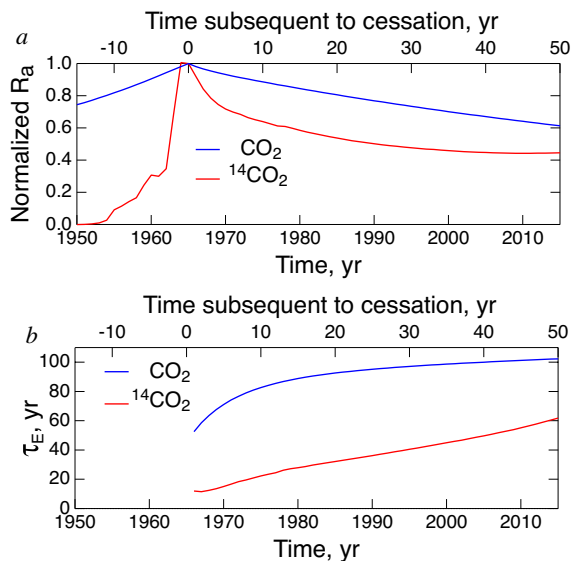
Figure E2. *a*, Normalized fractional excess of atmospheric $^{14}CO_2$ as a function of time, red, lower axis, and, for comparison of ordinary CO_2 as a function of time relative to time of cessation, blue, upper axis. *b*, Equivalent 1/*e* lifetimes corresponding to fractional excess amounts in *a*. For (S_l^{pi}, *b*) = (400 Pg, 0.6). **SI Data table, sheet 6**.
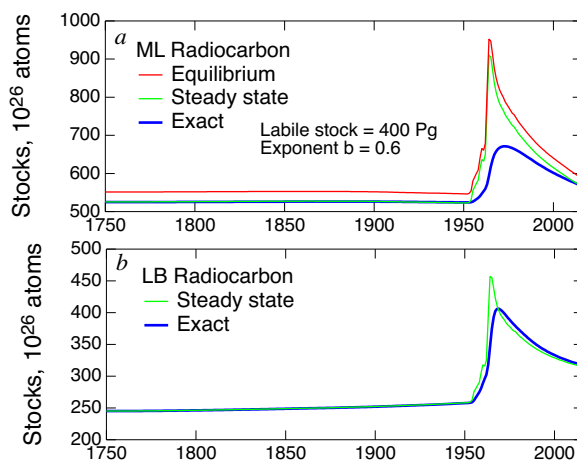
Figure E3. Examination of equilibrium and steady-state approximations for radiocarbon in ML and LB, for (S_l^{pi}, *b*) = (400 Pg, 0.6). **SI Data table, sheet 6**.
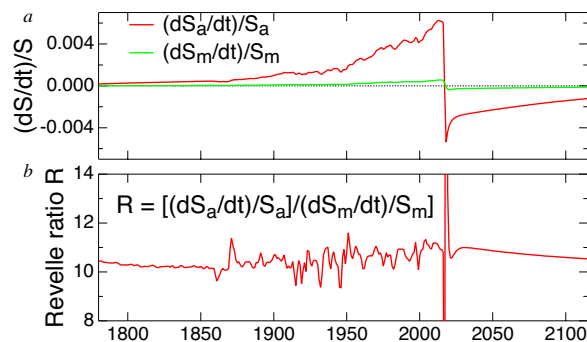
Figure F1. *a*. Fractional changes in stocks in atmosphere and ML in output from the present model, and *b*. Revelle factor evaluated as ratio of those fractional changes, red, and for equilibrium conditions, **Eq B19**, green. Both evaluated

8235 for (S_l^{pi} , *b*) = (400 Pg, 0.6). Transition from smooth to noisy curve evident in *b* between 1850 and 2016 results from using emissions obtained by inventory methods. **SI Data table, sheet 6**.